JAERI-M
83-114

EFFECT OF UPPER PLENUM WATER ACCUMULATION ON REFLOODING PHENOMENA UNDER FORCED-FEED FLOODING IN SCTF CORE-I TESTS

July 1983

Yukio SUDO, Makoto SOBAJIMA, Takamichi IWAMURA,
Masahiro OSAKABE, Akira OHNUKI, Yutaka ABE
and Hiromichi ADACHI

日本原子力研究所
Japan Atomic Energy Research Institute

JAERI-M レポートは，日本原子力研究所が不定期に公刊している研究報告書です。

入手の問合わせは，日本原子力研究所技術情報部情報資料課（〒319—11 茨城県那珂郡東海村）あて，お申しこしください。なお，このほかに財団法人原子力弘済会資料センター（〒319—11 茨城県那珂郡東海村日本原子力研究所内）で複写による実費頒布をおこなっております。

JAERI-M reports are issued irregularly.

Inquiries about availability of the reports should be addressed to Information Section, Division of Technical Information, Japan Atomic Energy Research Institute, Tokai-mura, Naka-gun, Ibaraki-ken 319--11, Japan.

編集兼発行　日本原子力研究所
印　　刷　日立高速印刷株式会社

JAERI-M 83-114

EFFECT OF UPPER PLENUM WATER ACCUMURATION ON REFLOODING PHENOMENA UNDER FORCED-FEED FLOODING IN SCTF CORE-I TESTS

Yukio SUDO, Makoto SOBAJIMA, Takamichi IWAMURA,
Masahiro OSAKABE, Akira OHNUKI, Yutaka ABE
and Hiromichi ADACHI
Department of Nuclear Safety Research,
Tokai Research Establishment, JAERI

(Received July 1, 1983)

Large Scale Reflood Test Program has been performed under contract with the Atomic Energy Bureau of Science and Technology Agency of Japan since 1976. The Slab Core Test Program is a part of the Large Scale Reflood Test Program along with the Cylindrical Core Test Program.

Major purpose of the Slab Core Test Program is to investigate two-dimensional, thermo-hydrodynamic behavior in the core and the effect of fluid communication between the core and the upper plenum on the reflood phenomena in a postulated loss-of-coolant accident of a PWR.

A significant upper plenum water accumulation was observed in the Base Case Test S1-01 which was carried out under forced-feed flooding condition. To investigate the effects of upper plenum water accumulation on reflooding phenomena, accumulated water is extracted out of the upper plenum in Test S1-03 by full opening of valves for extraction lines located just above the upper core support plate.

This report presents this effect of upper plenum water accumulation on reflooding phenomena through the comparison of Tests S1-01 and S1-03. In spite of full opening of valves for upper plenum water extraction in Test S1-03, a little water accumulation was observed which is of the same magnitude as in Test S1-01 for about 200 s after the beginning of reflood.

The work was performed under contract with the Atomic Energy Bureau of Science and Technology Agency of Japan.

From 200 s after the beginning of reflood, however, the upper plenum water accumulation is much less in Test S1-03 than in Test S1-01, showing the following effects of upper plenum water accumulation.

In Test S1-03, (1) the two-dimensionality of horizontal fluid distribution is much less both above and in the core, (2) water carryover through hot leg and water accumulation in the core are less, (3) quench time is rather delayed in the upper part of the core by less water fall back from the upper plenum, and (4) difference in the core thermal behavior and core heat transfer are not significant in the middle and lower part of the core.

KEYWORDS: Reactor Safety, PWR-LOCA, Reflood, Large Scale Reflood Test, Slab Core Test, Two-dimensional Core Behavior, Forced-feed Flooding, Upper Plenum Water Accumulation.

強制注入条件における再冠水現象に及ぼす上部プレナム蓄水の影響
―― ＳＣＴＦ第一次炉心再冠水試験 ――

日本原子力研究所東海研究所安全工学部
数土　幸夫・傍島　　真・岩村　公道
刑部　真弘・大貫　　晃・阿部　　豊
安達　公道

（1983年7月1日受理）

大型再冠水効果実証試験は，科学技術庁からの受託研究として，１９７６年から実施されている。平板炉心再冠水試験は円筒炉心再冠水試験と共にその一部をなすもので，加圧水型原子炉の冷却材喪失事故時の再冠水過程において炉心部の二次元的熱水力挙動や，炉心と上部プレナム間の流体挙動の再冠水現象に及ぼす影響の解明を目的としている。

本報告書は，強制注入条件下で行なわれた基準試験Ｓ１－０１で観測された上部プレナム蓄水が，再冠水現象にどんな影響を及ぼすかを調べるために，上部プレナム蓄水を上部炉心支持板直上にある抽水ラインのバルブを全開して抽出する実験Ｓ１－０３を行い，Ｓ１－０１と比較検討したものである。

ＢＯＣＲＥＣ後約２００秒間は，実験Ｓ１－０３では抽水用のバルブを全開したが，実験Ｓ１－０１と同程度の僅かな蓄水が観測された。しかしながら，それ以後ではＳ１－０３の蓄水はＳ１－０１より小さく，次の影響が見受けられた。Ｓ１－０３では，(1)炉心より上方及び炉心内の流体挙動の２次元性が平担化される。(2)ホットレグへのキャリーオーバ水量及び炉心内蓄水が小さくなる。(3)炉心上部でクエンチ時間がフォールバック水量の減少によって長くなる。(4)一方，炉心中央及び下部では炉心内熱的挙動，熱伝達にはその影響がほとんど現われていない。

本報告書は，電源開発促進対策特別会計法に基づき，科学技術庁からの受託によって行なった研究の成果である。

CONTENTS

目　　次

List of Tables and Figures

1. Introduction

1.1 SCTF Program

The Slab Core Test Facility is one of the facilities of the Large Scale Reflood Test Program which has been carried out at Japan Atomic Energy Research Institute (JAERI) under the trilateral cooperation among Japan, U.S. and FRG.[1]

The objectives of the Large Scale Reflood Test Program are:

(1) Demonstration of the safety margin in the current safety evaluation Analysis on the effectiveness of the Emergency Core Cooling System (ECCS) during the refill and reflood phases of a PWR-LOCA.

(2) Provision of information for analytical modeling of thermo-hydrodynamic phenomena during the refill and reflood phases of a PWR LOCA.

(3) Verification of an integral reflood analysis code, "REFLA"[2], and a US-developed reactor transient analysis code, "TRAC"[3].

For this program were constructed two test facilities, Cylindrical Core Test Facility (CCTF)[4] and Slab Core Test Facility (SCTF).[5] The objectives of CCTF are to achieve the above mentioned task with the integral simulation of all crucial components for a PWR.

The objectives of the SCTF test are to study two-dimensional hydrodynamics and heat transfer in the core and performance of the emergency core cooling system (ECCS) during the last part of blowdown, refill and reflood phases of a PWR LOCA by the use of a full height and full radius electrically heated core but with a simple simulation for the primary coolant loops.

1.2 Objectives of This Study

A significant upper plenum water accumulation was observed in the Base Case Test S1-01, which was carried out under the forced-feed flooding with the system pressure of 0.2 MPa. The SCTF simulates the upper plenum internals of the new Westinghouse 17 × 17 array fuel assemblies. It is considered that much larger flow area in the upper plenum than in the core causes accumulation of water in the upper plenum which is carried over from the core by steam generated in the core. Upper plenum water accumulation should have significant effects on the cooling of fuel rods and two-dimensional thermo-hydrodynamics in the core.

When more water is accumulated in the upper plenum, it is considered that upper part of core should be cooled earlier by more intense fall

back of water from the upper plenum into the core and that the two-dimensionality of core thermo-hydrodynamics should be dependent on the fall back intensity at each bundle.

Therefore, this study aims to investigate the effects of water accumulated in the upper plenum on the core heat transfer and hydrodynamics. As a method for making clear the effect of upper plenum water accumulation on the reflooding phenomena, water accumulated in the upper plenum was extracted out of the upper plenum as much as possible by the actuation of the upper plenum water extraction system with full opening of valves at the nozzles just above the upper core support plates in Test S1-03 under the same conditions for other parameters as Test S1-01.

Through the comparison of Tests S1-01 and S1-03 the effects of upper plenum water accumulation are investigated in this report.

1.3 Constitution of This Report

In Chapter 2, the test conditions and test sequence for Tests S1-01 and S1-03 are presented, and compared.

In Chapter 3, mass balance in the system is discussed. This investigation is important not only to well understand the overall fluid behavior in the system but also to confirm the good quality of the measured data. Characteristics of carryover water from the upper plenum to the hot leg and water distribution behavior in the pressure vessel are also discussed.

In Chapter 4, the core thermal behavior is discussed. Major items of this investigation are time and temperature of the turnaround and the quench at the respective measuring point. The quench propagation velocity is also discussed.

In Chapter 5, heat transfer coefficient on the surface of the simulated fuel rods is discussed as a function of the location and time. This investigation gives important information about the heat transfer mechanism in the reflooding phase. For this study, heat transfer analysis code HEATQ[6] was used, which has taken into account the effect of axial heat conduction.

In Chapter 6, two-dimensional hydrodynamic behavior in the core and the upper plenum is discussed. Two-dimensional thermo-hydrodynamics in the pressure vessel including the core is the major objective of the SCTF program to be studied.

Major conclusions of each chapter are given in the last part of the respective chapter and summarized in Chapter 7.

Selected data for Test S1-03 are given in Appendix.

2. Test Description

2.1 Test Facility

The SCTF was designed to study the two-dimensional, thermo-hydraulic flow behavior in the pressure vessel during the end of blowdown, refill and reflood phases of a simulated LOCA for a pressurized water reactor.

The overall schematic diagram of the SCTF is shown in Fig. 2.1. The principal dimensions of the facility is shown in Table 2.1, and the comparison of dimensions between the SCTF and the referred PWR is shown in Fig. 2.2.

2.1.1 Pressure Vessel and Internals

The pressure vessel is of slab geometry as shown in Fig. 2.3. The height of the components in the pressure vessel is almost the same as the reference reactor's, and the flow area and the fluid volume of each component are scaled down based on the nominal core flow area scaling.

The core consists of 8 bundles in a row and each bundle includes simulated fuel rods and non-heated rods with 16×16 array. The core arrangement for the SCTF Core-I is shown in Fig. 2.4, which includes 6 normal bundles and 2 blocked bundles. The core is enveloped by the honeycomb thermal insulator which is attached on the barrel.

The downcomer is located at one end of the pressure vessel which corresponds to the periphery of the actual PWR. The core baffle region is, on the other hand, located between the core and the downcomer. For better understanding, the cross section of the pressure vessel at the elevation of midplane of the core is shown in Fig. 2.5.

The design of upper plenum internals is based on that of the new Westinghouse 17×17 array fuel assemblies. The internals consist of control rod guide tubes, support columns, orifice plates and open holes and the arrangement is shown in Fig. 2.6. The radius of each internal is scaled down by factor 8/15 from that of an actual reactor. Flow resistance baffles are inserted into the guide tubes. The elevation and the configuration of baffles plate are shown in Fig. 2.7 and 2.8.

The height of the hot leg and cold legs are designed as close to the actual PWR as possible. However, in order to avoid the interference of the nozzles in the downcomer, the heights of nozzles for the broken cold leg and the intact cold leg are shifted down compared to that of the hot leg as shown in Fig. 2.3.

2.1.2 Heater Rod Assembly

The heater rod assembly for the SCTF Core-I consists of 8 bundles arranged in a row. These bundles are composed of 6 normal unblocked bundles which are located at the 1st, 2nd and 5th to 8th bundles and 2 blocked bundles which are 3rd and 4th bundles as shown in Fig. 2.4. Each bundle has 234 electrically heated rods and 22 non-heated rods. The dimensions of the heater rods are based on a 15×15 fuel rod bundle, and the heated length and the outer diameter of each heater rod are 3.66 m and 10.7 mm, respectively. A heater rod consists of a nichrome heater element, magnesium oxide (MgO) and Nichrofer-7216 sheath (equialent to Inconel 600). The sheath wall thickness is about 1.0 mm and is thicker than the actual fuel cladding because of the requirements for thermocouple installation. The heating element is a helical coil and has a 17 step chopped cosine axial power profile as shown in Fig. 2.9. The peaking factor is 1.4.

Non-heated rods are either stainless steel pipes or solid rods of 13.8 mm O.D. The heater rods and non-heated rods are fixed at the top of the core allowing the rods to move downward when the thermal expansion occurs. In Fig. 2.10 the axial position where blockage sleeves for simulating the ballooned fuel rod are equipped is shown. The blockage sleeves consist of three types of sleeve, one is used for the rods at the corner adjacent to the adjacent blocked bundle, another for the rods adjacent to the side walls and the third for the rods except for the periphery of the blocked bundle. These are named A, B and C respectively in the Fig. 2.11 and the configurations for these are shown in Fig. 2.12.

For better simulation for flow resistance in the lower plenum the simulated rods do not penetrate through the bottom plate of the lower plenum as shown in Fig. 2.10.

2.1.3 Primary Loops and ECCS

Primary loops consist of a hot leg equivalent to the four actual hot legs, a steam/water separator for measuring the flow rate of carry over water, an intact cold leg equivalent to the three actual intact loops, a broken cold leg on the pressure vessel side and a broken cold leg on the steam water separator side. These two broken cold legs are connected with two containment tanks through break valves, respectively. The arrangement of the primary loops is shown in Fig. 2.13. The flow area of each loop is scaled down based on the core flow area scaling. It should be emphasized

that the cross section of the hot leg is an elongated circle to realize the proper flow pattern in the hot leg. The steam/water separator has a steam generator inlet plenum simulator to realize the flow characteristics of carryover water. The cross section of the hot leg and the configuration of the steam generator inlet plenum simulator are shown in Fig. 2.14.

A pump simulator and a loop seal part are provided for the intact cold leg. The arrangement of the intact cold leg is shown in Fig. 2.15. The pump simulator consists of the casing, duct simulators and an orifice plate as shown in Fig. 2.16. The loop resistance is adjusted with the orifice plate.

In principle, ECCS consists of an accumulator and a low pressure injection system. The injection port is located as already described in the design criteria. Besides, the Upper Core Support Plate (UCSP) extraction system is provided and the UCSP water injection and extraction system will be used for combined injection tests.

2.1.4 Containment Tanks and Auxiliary System

Two containment tanks are provided to the SCTF. The containment tank-I is connected with the downcomer through the pressure vessel side broken cold leg and the containment tank-II is connected with the steam/water separator through the steam/water separator side broken cold leg. Especially in the containment tank-I, carryover water from the downcomer is measured by phase separation.

As auxiliary systems, UCSP water injection and extraction systems are provided to the SCTF. These systems are used to investigate the effects of fluid condition just above the UCSP on the reflooding phenomena by injecting water at specified temperature and flow rate with or without water extraction out of upper plenum. In Test S1-03, the UCSP water extraction system was used and upper plenum water was extracted out of the upper plenum for investigating the effects of water accumulation on core thermal-hydrodynamics. The schematic of the UCSP water extraction system is shown in Fig. 2.17 and the detail of nozzles installed just above the UCSP for UCSP water injection and extraction is shown in Fig. 2.18.

2.1.5 Instrumentation

The instrumentation in the SCTF has been provided both by JAERI and the USNRC. The JAERI-provided instrumentation includes the measurement of temperatures, pressures, differential pressures, liquid levels, flow

velocities, and heating powers. The USNRC has provided film probes, impedance probes, string probes, liquid level detectors (LLDs), fluid distribution grids (FDGs), turbine meters, drag disks, γ-densitometers, spool pieces and video optical probes.[7] The measurement items of the JAERI- and USNRC-provided instruments are listed in Tables 2.2 and 2.3, respectively.

2.2 Test Conditions and Test Sequences for Test S1-03 and S1-01

The only difference in test conditions and test sequence between Tests S1-01 and S1-03 is if the upper plenum water is extracted out of the upper plenum or not. In Test S1-01 upper plenum water is not extracted, but in Test S1-03 water accumulated on UCSP in the upper plenum is extracted during the test, by full opening of valves at nozzles located just above the UCSP.

The test conditions common to these two tests are as follows.

Tests S1-03 and S1-01 were performed under forced-feed flooding, that is, the lower plenum and the downcomer were isolated from each other with a blocking plate and the emergency core cooling (ECC) water was directly injected into the lower plenum. The vent valve simulation line connecting the upper plenum with the downcomer was blocked by inserting a blind plate. To give proper flow resistances, orifices were installed at each loop simulating primary loops. Orifice diameters for steam/water separator side broken cold leg, the intact cold leg and the pump simulator were 87.7, 191.1 and 173.7 mm, respectively, and no orifice was attached to the pressure vessel side broken cold leg (See Fig. 2.13). Radial power profile simulated that of the Westinghouse initial core and the initial bundle power for each bundle was:

No.1, 2 bundles	:	887	KW/bundle
No.3, 4 "	:	944	"
No.6, 6 "	:	900	"
No.7, 8 "	:	815	"

Table 2.4 gives the comparison of major pretest and measured test conditions for Tests S1-03 and S1-01. Test conditions are basically the same for the two tests except for condition of upper plenum water extraction system.

Test sequences for both tests were as follows. First, the pressure vessel (including the core), steam/water separator, pump simulator,

containment tanks-I and -II and pipings connecting these components with each other were heated up and pressurized up to the near saturation condition at the specified system pressure by external heating with electric heaters and by supplying saturated steam to the system.

Next, core temperature was adjusted gradually so as to set the initial maximum rod surface temperature in the core at 523 K.

Cold water which initially occupied the accumulator (Acc) injection piping was replaced with hot water in the Acc tank by repeating four times to supply hot water through the piping into the lower plenum and to drain it.

Water temperature in the low pressure coolant injection (LPCI) piping was kept at the near saturation temperature corresponding to the system pressure by circulating the water through the LPCI tank.

Next, near saturated water at the system pressure made up in the saturated water tank was supplied in the lower plenum upto 1.3 m from the bottom of the lower plenum.

Core heating was then initiated and reached a constant specified rate of core heating after about 6 s. In the present report, time "zero" is defined as the time when core heating is initiated unless it is indicated as the time after the bottom-of-core recovery (BOCREC), that is, the time when water level reaches the bottom of core.

When four cladding temperature exceeded 926 K, power decay simulation was initiated following core power decay curve from 30 s after scram with the core power kept at the constant for the first 5 s.

Figure for the decay heat curve was based on the "ANS Standard + Actinides + Delayed Neutron Effect for Voided Core".

Simultaneously with the beginning of the decay heat simulation, Acc injection into the lower plenum was initiated. The maximum Acc injection rate was about 22 kg/s, which corresponds to the nominal flooding speed of about 5 cm/s in the core. Here, the nominal flooding speed is defined based on the core area including the core baffle region and the gap between core barrel and vessel wall, etc..

At 20 s after the initiation of the Acc injection, Acc injection was switched to LPCI. The LPCI injection rate was about 11 kg/sec, which corresponds to the nominal flooding speed of about 2.5 cm/s.

Pressure in the containment tank-II was controlled by a regulating valves so as to keep the pressure at the constant. However, the pressure showed a small overshoot in both tests due to delay of the valve action.

Since core pressure showed an overshoot and core inlet temperature varied slightly, core inlet subcooling varied during the tests. The water subcooling at the core inlet was depending on the time but the maximum value was about 15 K in both tests.

At 900 s after the initiation of LPCI injection, the tests were terminated.

2.3 Chronologies of Major Events in Tests S1-03 and S1-01

Table 2.5 gives comparison of the chronologies of jajor events in Tests S1-03 and S1-01. The chronologies of major events in both tests are almost the same and are as follows. Whole core quench which means quench of all rods in the core occurred at 307 s after the BOCREC in Test S1-03 and at 292 s after the BOCREC in Test S1-01. Maximum core pressure was 0.218 MPa at 48 seconds after the BOCREC in Test S1-03 and was 0.233 MPa at 48 seconds after the BOCREC in Test S1-01. Maximum core inlet subcooling was 15.5 at about 138 seconds after the BOCREC in Test S1-03 and was 15.4 K at 53 seconds after the BOCREC in Test S1-01.

Figs. 2.19 and 2.20 show the comparison of transients of pressures at the top of pressure vessel, at the center of the core, at the core inlet and at the upper downcomer and pressures at the containment tanks I and II. Fig. 2.21 shows the comparison of ECC water inejction rates. There is no significant difference in these transients between the two tests as intended. Fig. 2.22 shows the transient of integrated mass of water extracted from the upper plenum for Test S1-03, and Fig. 2.23 shows the comparison of transients of water level in the upper plenum. From Figs. 2.22 and 2.23 it is known that water was effectively extracted from the upper plenum after about 200 s from the BOCREC. No significant difference is observed until 200 s after the BOCREC in spite of full opening of valves at the nozzles for upper plenum water extraction. However, much difference in water level is observed between Tests S1-03 and S1-01 from about 200 s after the BOCREC. Therefore, the effect of water accumulation on reflood phenomena should be recognized from that time. Fig. 2.24 shows the comparison of heating bundle power. The power was also the same in both tests.

Table 2.1 Principal Dimensions of Test Facility

1. Core Dimension		
(1) Quantity of Bundle	8	Bundles
(2) Bundle Array	1×8	
(3) Bundle Pitch	230	mm
(4) Rod Array in a Bundle	16×16	
(5) Rod Pitch in a Bundle	14.3	mm
(6) Quantity of Heater Rod in a Bundle	234	rods
(7) Quantity of Non-Heated Rod in a Bundle	22	rods
(8) Total Quantity of Heater Rods	234×8=1872	rods
(9) Total Quantity of Non-Heated Rods	22×8=176	rods
(10) Effective Heated Length of Heater Rod	3660	mm
(11) Diameter of Heater Rod	10.7	mm
(12) Diameter of Non-Heated Rod	13.8	mm
2. Flow Area & Fluid Volume		
(1) Core Flow Area* (nominal)	0.227	m^2
(2) Core Fluid Volume	0.92	m^3
(3) Baffle Region Flow Area	0.10	m^2
(4) Baffle Region Fluid Volume	0.36	m^3
(5) Downcomer Flow Area	0.121	m^2
(6) Upper Annulus Flow Area	0.158	m^2
(7) Upper Plenum Horizontal Flow Area	0.525	m^2
(8) Upper Plenum Fluid Volume	1.16	m^3
(9) Upper Head Fluid Volume	0.86	m^3
(10) Lower Plenum Fluid Volume	1.38	m^3
(11) Steam Generator Inlet Plenum Simulator Flow Area	0.626	m^2
(12) Steam Generator Inlet Plenum Simulator Fluid Volume	0.931	m^3
(13) Steam Water Separator Fluid Volume	5.3	m^3
(14) Flow Area at the Top Plate of Steam Generator Inlet Plenum Simulator	0.195	m^2
(15) Hot Leg Flow Area	0.0826	m^2

* Flow area in the core is 0.35 m^2, including the excess flow area of gaps between the bundle and surface of thermal insulator and between the core barrel and the pressure vessel wall.

(Continued)

(16)	Intact Cold Leg Flow Area (Diameter = 297.9 mm)	0.0697 m^2
(17)	Broken Cold Leg Flow Area (Diameter = 151.0 mm)	0.0179 m^2
(18)	Containment Tank I Fluid Volume	30 m^3
(19)	Containment Tank II Fluid Volume	50 m^3

3. Elevation & Height

(1)	Top Surface of Upper Core Support Plate (UCSP)	0 mm
(2)	Bottom Surface of UCSP	- 76 mm
(3)	Top of the Effective Heated Length of Heater Rod	- 393 mm
(4)	Bottom of the Skirt in the Lower Plenum	-5270 mm
(5)	Bottom of Intact Cold Leg	+ 724 mm
(6)	Bottom of Hot Leg	+1050 mm
(7)	Top of Upper Plenum	+2200 mm
(8)	Bottom of Steam Generator Inlet Plenum Simulator	+1933 mm
(9)	Centerline of Loop Seal Bottom	-2281 mm
(10)	Bottom Surface of End Box	- 185.1mm
(11)	Top of the Upper Annulus	+2234 mm
(12)	Height of Steam Generator Inlet Plenum Simulator	1595 mm
(13)	Height of Loop Seal	3140 mm
(14)	Inner Height of Hot Leg Pipe	737 mm
(15)	Bottom of Lower Plenum	-5770 mm
(16)	Top of Upper Head	+2887 mm

Table 2.2 Measurement Items of SCTF (JAERI-provided instruments)

LOCATION	ITEM	PROBE	QUANTITY
1. CORE			
center	pressure	DP cell	1
short range of core	diff. press.	DP cell	22
half length of core	diff. press.	DP cell	16
full length of core	diff. press.	DP cell	8
across spacers	diff. press.	DP cell	7
across end box	diff. press.	DP cell	8
across 4 assemblies	diff. press.	DP cell	3
across 8 assemblies	diff. press.	DP cell	3
below and above end box	steam velocity	Pitot-tube	3
sub channel	steam velocity	Pitot-tube	13
below end box hole	fluid temp.	T/C	16
above end box hole	fluid temp.	T/C	16
core baffle	fluid temp.	T/C	6
non-heating rods	fluid temp.	T/C	96
	steam temp.	SSP	16
	clad temp.	T/C	108
heater rods	clad temp.	T/C	640
side walls	wall temp.	T/C	36
core baffle	wall temp.	T/C	6
core baffle	liquid level	DP cell	1
short range of core baffle	liquid level	DP cell	6
heated rod	power		8 sum(1039)
2. UPPER PLENUM			
centre	pressure	DP cell	1
across end box tie plate	diff. press.	DP cell	8
core outlet-hot leg inlet	diff. press.	DP cell	4
periphery of UCSP hole	fluid temp.	T/C	8
centre of UCSP hole	fluid temp.	T/C	8
250mm & 1000mm above UCSP	fluid temp.	T/C	8
surface of UCSP	fluid temp.	T/C	8
above UCSP hole	steam temp.	SSP	8

(Continued)

LOCATION	ITEM	PROBE	QUANTITY
surface of structure	wall temp.	T/C	15
side walls	wall temp.	T/C	8
above end box tie plate	liquid level	DP cell	8
above UCSP	liquid level	DP cell	9
above UCSP (v.)	steam velocity	Pitot-tube	2
inter-structures (h.)	steam velocity	Pitot-tube	2
			sum(97)
3. LOWER PLENUM			
below bottom spacer	pressure	DP cell	1
lower plenum - upper plenum	diff. press.	DP cell	1
core inlet	fluid temp.	T/C	8
inlet from downcomer	fluid temp.	T/C	2
side & bottom walls	wall temp.	T/C	4
below bottom spacer	liquid level	DP cell	1
			sum(17)
4. DOWNCOMER			
upper position	pressure	DP cell	1
horizontal direction	diff. press.	DP cell	1
four levels	fluid temp.	T/C	8
side wall	wall temp.	T/C	2
inner wall	wall temp.	T/C	2
below cold leg level	liquid level	DP cell	1
above cold leg level	liquid level	DP cell	1
below core inlet level	liquid level	DP cell	1
bottom	momentum flux	Drag disk	2
			sum(19)
5. HOT LEG			
full length	diff. press.	DP cell	1
multiple points	fluid temp.	T/C	3
	steam temp.	SSP	3
	wall temp.	T/C	1
	liquid level	DP cell	2
			sum(10)

(Continued)

LOCATION	ITEM	PROBE	QUANTITY
6. S/W SEPARATOR SIDE BROKEN COLD LEG			
across resistance simulator	diff. press.	DP cell	1
S/W separator to containment tank II	flow rate	venturi	1
multiple points	fluid temp.	T/C	1
	steam temp.	SSP	1
	wall temp.	T/C	1
			sum(5)
7. INTACT COLD LEG			
full length	diff. press.	DP cell	1
across resistance simulator	diff. press.	DP cell	1
across pump simulator	diff. press.	DP cell	1
	flow rate	venturi	1
near resistance simulator	fluid temp.	T/C	1
pump simulator	fluid temp.	T/C	3
	wall temp.	T/C	1
			sum(9)
8. PV SIDE BROKEN COLD-LEG	pressure	DP cell	1
full length	diff. press.	DP cell	1
across resistance simulator	diff. press.	DP cell	1
multiple points	fluid temp.	T/C	4
	wall temp.	T/C	2
	liquid level	DP cell	2
			sum(11)
9. VENT LINE			
across the length	diff. pres.	DP cell	1
			sum(1)

(Continued)

LOCATION	ITEM	PROBE	QUANTITY
10. S/W SEPARATOR			
	pressure	DP cell	1
between inlet and outlet	diff. press.	DP cell	1
SG plenum simulator	diff. press.	DP cell	1
SG plenum simulator	fluid temp.	T/C	2
top and bottom	fluid temp.	T/C	2
wall	wall temp.	T/C	2
full height	liquid level	DP cell	1
liquid extraction	flow rate	DP cell	1
			sum(11)
11. CONTAINMENT TANK-I			
	pressure	DP cell	1
downcomer-CT-I	diff. press.	DP cell	1
CT-I - CT-II	diff. press.	DP cell	1
	flow rate	DP cell	1
full height	liquid level	DP cell	1
		float	1
top, middle & bottom	fluid temp.	T/C	3
wall	wall temp.	T/C	1
			sum(10)
12. CONTAINMENT TANK-II			
	pressure	DP cell	1
upper plenum - CT-II	diff. press.	DP cell	1
separator - CT-II	diff. press.	DP cell	1
steam blow line	flow rate	DP cell	1
full height	liquid level	DP cell	1
top, middle & bottom	fluid temp.	T/C	3
			sum(8)
13. ECC INJECTION SYSTEM			
ACC tank	pressure	DP cell	1
total and LPCI	flow rate	E-M flow meter	2
			1
ACC tank	fluid temp.	T/C	1

(Continued)

LOCATION	ITEM	PROBE	QUANTITY
13. ECC INJECTION SYSTEM			
header	fluid temp.	T/C	2
ACC tank	liquid level	DP cell	1
			sum(8)
14. UCSP WATER EXTRACTION SYSTEM			
extraction line	flow rate	E-M flow meter	4
steam line	flow rate	DP cell	4
extraction line	fluid temp.	T/C	5
steam line	fluid temp.	T/C	1
extraction line	liquid level	DP cell	4
			sum(18)
15. SATURATED WATER TANK			
	fluid temp	T/C	1
	liquid level	DP cell	1
			sum(2)
16. NITROGEN GAS SYSTEM			
	flow rate	DP cell	1
injection port	fluid temp.	T/C	1
			sum(2)

Total 1267

Table 2.3 Measurement Items of SCTF (USNRC-provided instruments)

LOCATION	ITEM	PROBE	QUANTITY
1. CORE			
non-heated rods	liquid level	LLD	20×4 = 80
non-heated rods	film thickness and velocity	film probe	6
non-heated rods	void fraction and droplet velocity	flag probe	8
side walls	film thickness and velocity	film probe	8
sub-channel	fluid density	γ-densitometer	10
end box	fluid density	γ-densitometer	5
end box	flow pattern	video optical probe	1
2. UPPER PLENUM			
full height	liquid level	FDG	8×8 = 64
structure surface	film thickness and velocity	film probe	6
side walls	film thickness and velocity	film probe	6
inter structure	void fraction	prong probe	8
above UCSP hole	velocity	turbine	8
inter structure	velocity	turbine	4
inter structure	fluid density	γ-densitometer	4
hot leg inlet	flow pattern	video optical probe	1
3. LOWER PLENUM			
core inlet	velocity	turbine	4
bottom	reference conductivity	reference probe	1
4. DOWNCOMER			
full height	liquid level	FDG	2×3×7 = 42
two levels	velocity	drag disk	3
two levels	void fraction	string probe	3

(Continued)

LOCATION	ITEM	PROBE	QUANTITY
5. HOT LEG	mass flow rate fluid density void fraction	spool piece	1
6. PV SIDE BROKEN COLD-LEG	mass flow rate fluid density void fraction	spool piece	1
7. VENT LINE	mass flow rate void fraction	spool piece	1

Table 2.4 Comparison of Test Conditions between Test S1-03 and Test S1-01

TEST CONDITIONS FOR TEST S1-03

	PRETEST CONDITION	MEASURED CONDITION
TEST TYPE	FORCED FLOODING	FORCED FLOODING
INITIAL PRESSURE (CORE CENTER)	0.2 MPA	0.202 MPA
PRESSURE (CONTAINMENT - II)	0.2 MPA (INITIAL)	0.202 MPA (INITIAL) 0.219 MPA (MAX)
MAX CORE TEMP (AT BOCREC)	973 K	970 K
POWER HOLDING AFTER ACC INITIATION	5 SEC	——
DECAY CURVE	ANS + ACTINIDES + D.N. FROM 30 SEC (REAC. TIME)	SEE FIG. 2-5
MAX ACC INJ. RATE	22 KG/SEC	22 KG/SEC
LPCI INJ. RATE	11 KG/SEC	11 KG/SEC
MAX CORE INLET SUBCOOLING	AS LOW AS POSSIBLE	15.4 K
UCSP WATER EXTRACTION	MAXIMUM	SEE FIG. 2-4

TEST CONDITIONS FOR TEST S1-01

	PRETEST CONDITION	MEASURED CONDITION
TEST TYPE	FORCED FLOODING	FORCED FLOODING
INITIAL PRESSURE (CORE CENTER)	0.2 MPA	0.198 MPA
PRESSURE (CONTAINMENT - II)	0.2 MPA	0.195 MPA (INITIAL) 0.218 MPA (MAX)
MAX CORE TEMP (AT BOCREC)	973 K	970 K
POWER HOLDING AFTER ACC INITIATION	5 SEC	——
DECAY CURVE	ANS + ACTINIDES + D.N. FROM 30 SEC (REAC. TIME)	SEE FIG. 2-10
MAX ACC INJ. RATE	22 KG/SEC	22 KG/SEC
LPCI INJ. RATE	11.4 KG/SEC	11.4 KG/SEC
MAX CORE INLET SUBCOOLING	AS LOW AS POSSIBLE	15.5 K
UCSP WATER EXTRACTION	NONE	NONE (SEE FIG. 2-9)

Table 2.5 Comparison of Chronology between Test S1-03 and Test S1-01

CHRONOLOGY OF TEST S1-03	TIME AFTER CORE POWER "ON"	TIME AFTER BOCREC	CHRONOLOGY OF TEST S1-01	TIME AFTER CORE POWER "ON"	TIME AFTER BOCREC
CORE POWER "ON"	0 SEC.	-106 SEC.	CORE POWER "ON"	0 SEC.	-107 SEC.
ACC INJ. INITIATION	97	-9	ACC INJ. INITIATION	97	-10
CORE POWER DECAY INITIATION	102	-4	CORE POWER DECAY INITIATION	102	-5
BOCREC	106	0	BOCREC	107	0
SWITCH ACC TO LPCI	117	11	SWITCH ACC TO LPCI	117	10
MAXIMUM ECC INJ. RATE (24 KG/SEC)	118	12	MAXIMUM ECC INJ. RATE (23 KG/SEC)	118	11
MAXIMUM CONT - II PRESSURE (0.219 MPA)	127	21	MAXIMUM CONT - II PRESSURE (0.218 MPA)	127	20
MAXIMUM CORE TEMPERATURE (1010 K)	140	34	MAXIMUM CORE TEMPERATURE (1012 K)	140	33
MAXIMUM CORE PRESSURE (0.218 MPA)	154	48	MAXIMUM CORE PRESSURE (0.233 MPA)	155	48
MAXIMUM CORE INLET SUBCOOLING (15.4 K)	∿244	∿138	MAXIMUM CORE INLET SUBCOOLING (15.5 K)	160	53
WHOLE CORE QUENCHED	413	307	WHOLE CORE QUENCHED	399	292

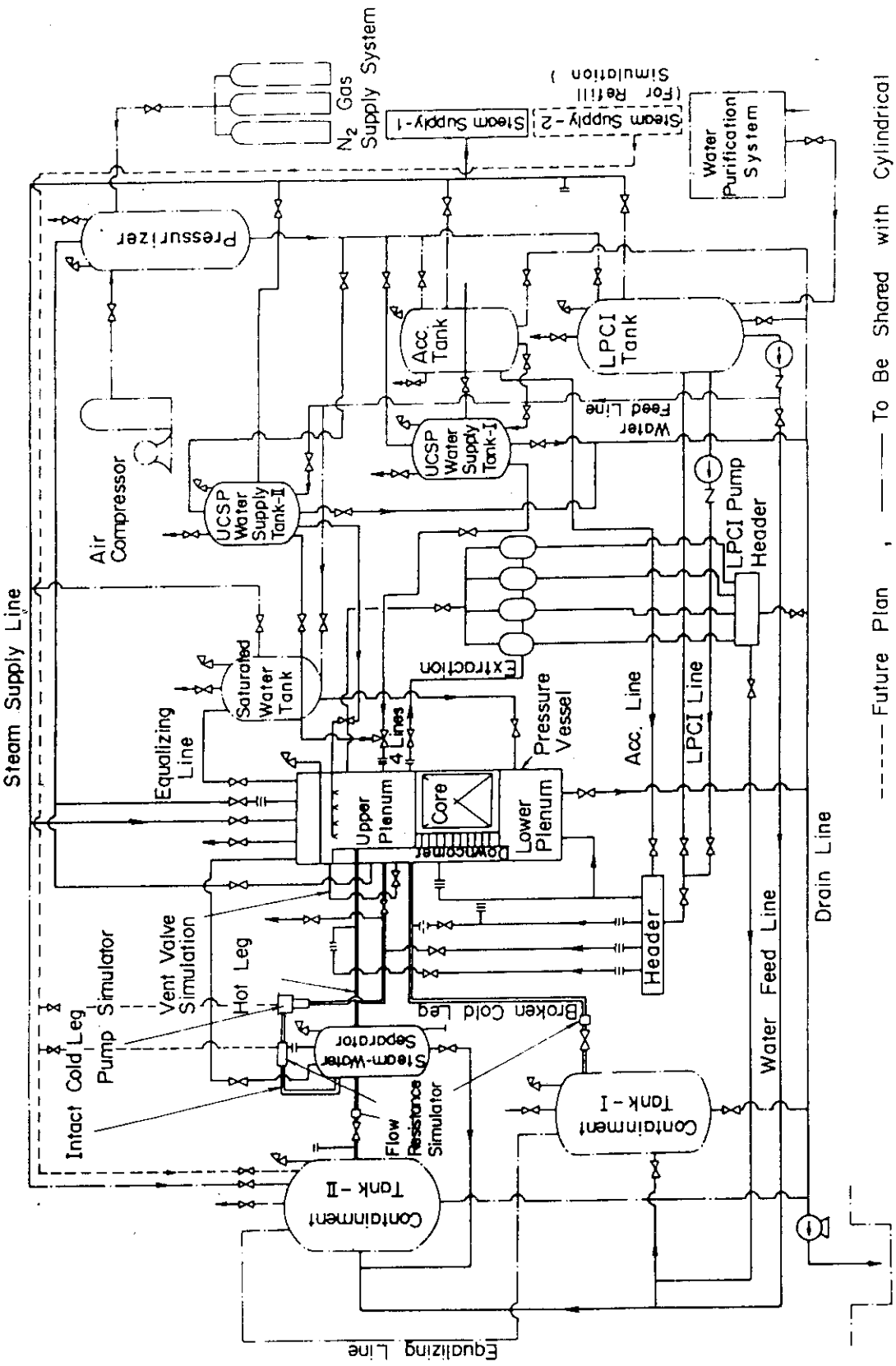

Fig.2.1 Schematic Diagram of Slab Core Test Facility

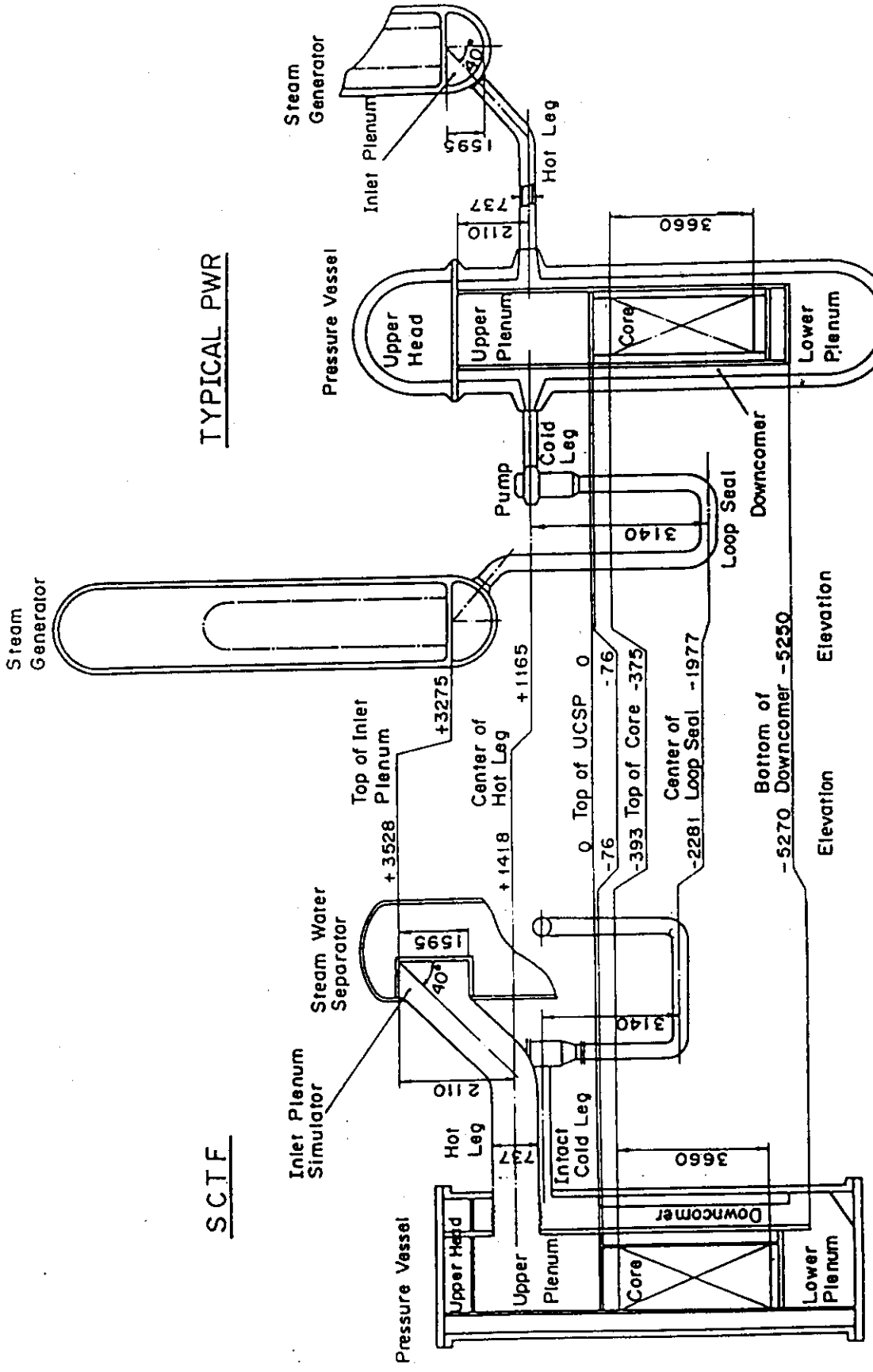

Fig.2.2 Comparison of Dimensions between SCTF and a Reference PWR

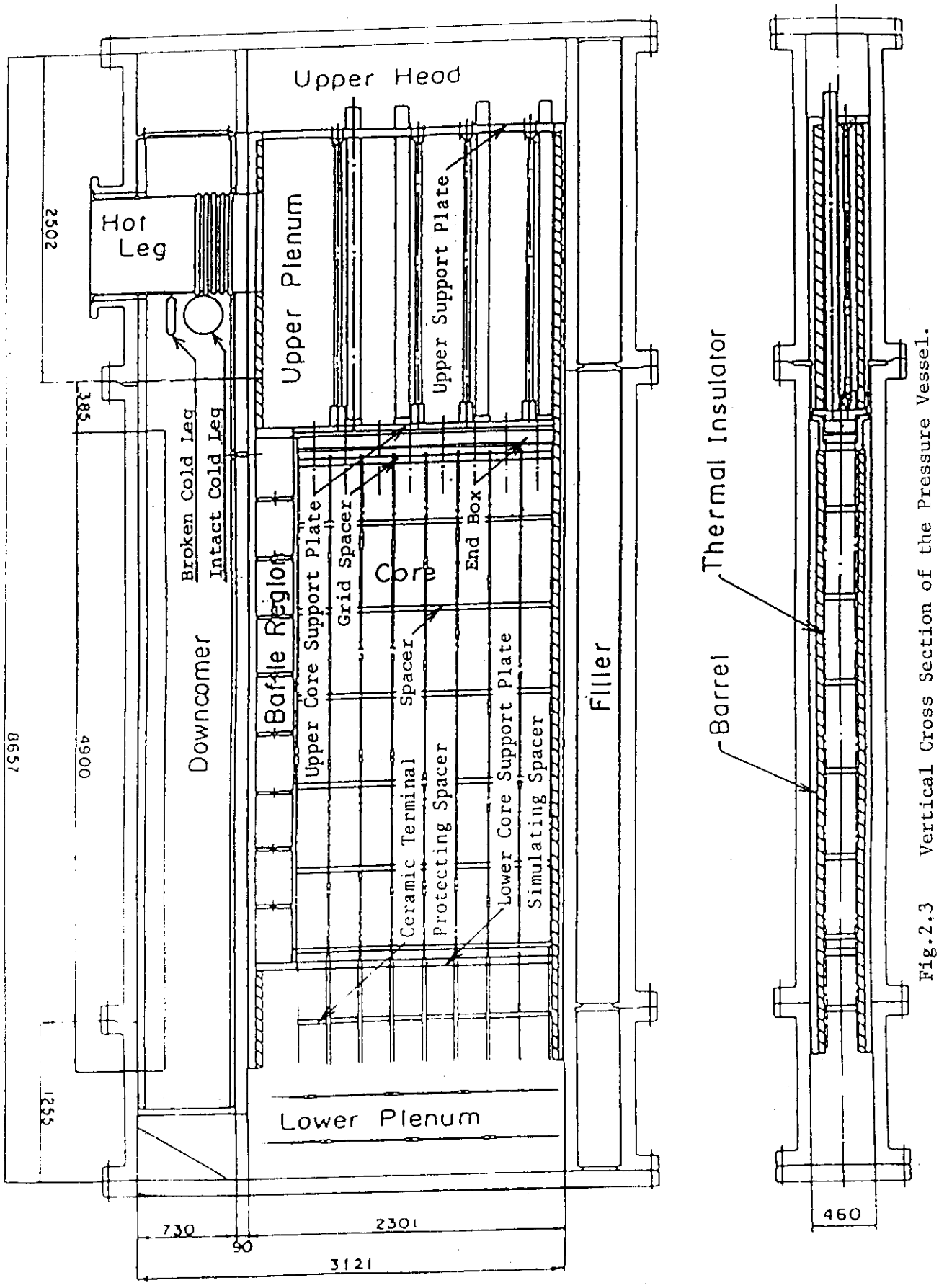

Fig.2.3 Vertical Cross Section of the Pressure Vessel.

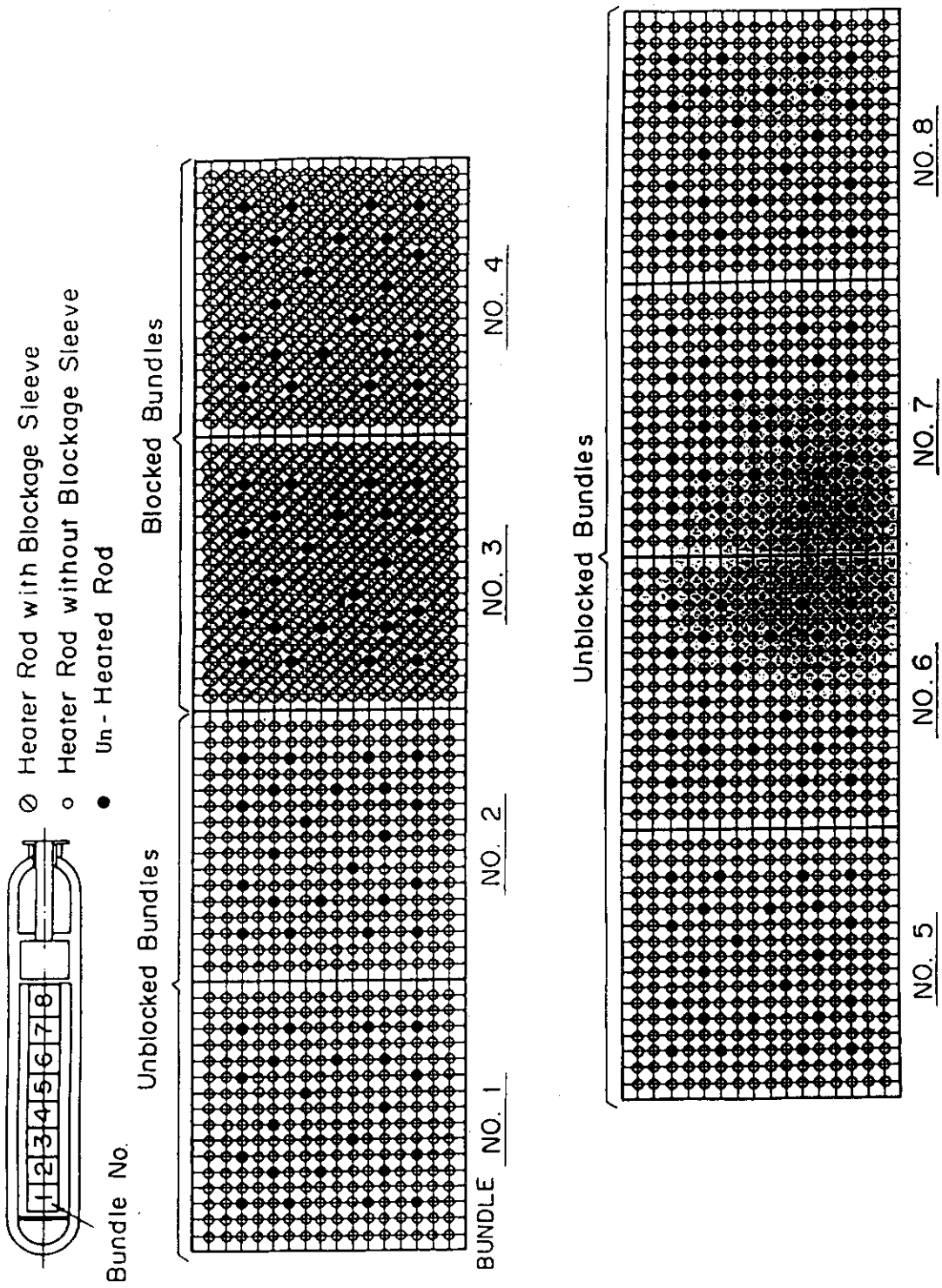

Fig.2.4 Arrangement of Heater Bundles

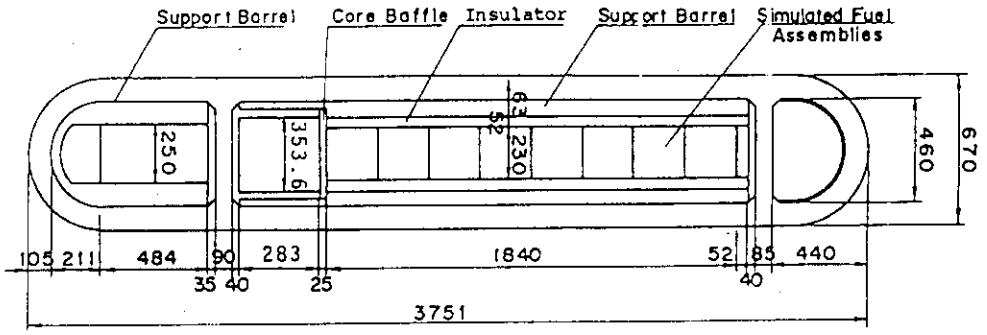

Fig.2.5 Horizontal Cross Section of the Pressure Vessel (1)

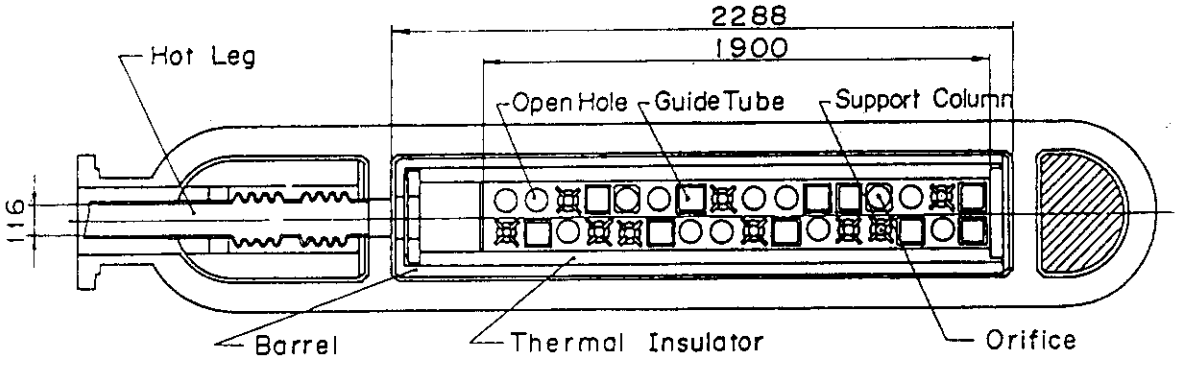

Upper Plenum Cross Section

Fig.2.6 Horizontal Cross Section of the Pressure Vessel (2)

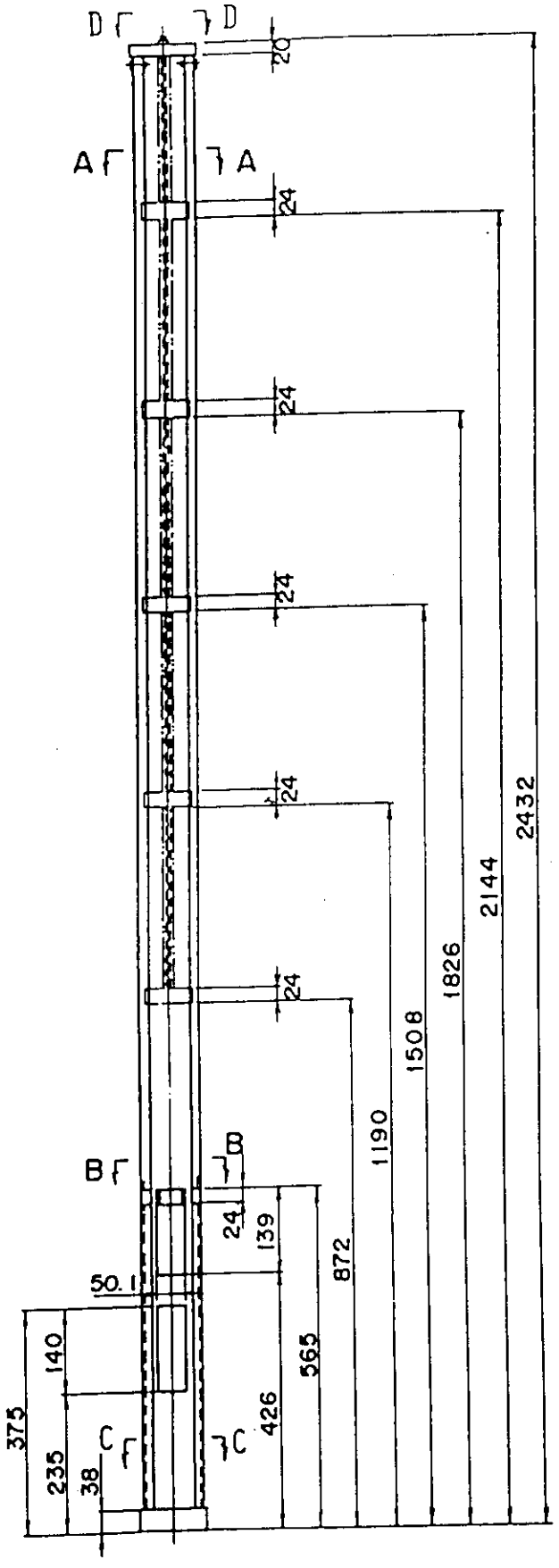

Fig.2.7 Dimension of Guide Tube (1)

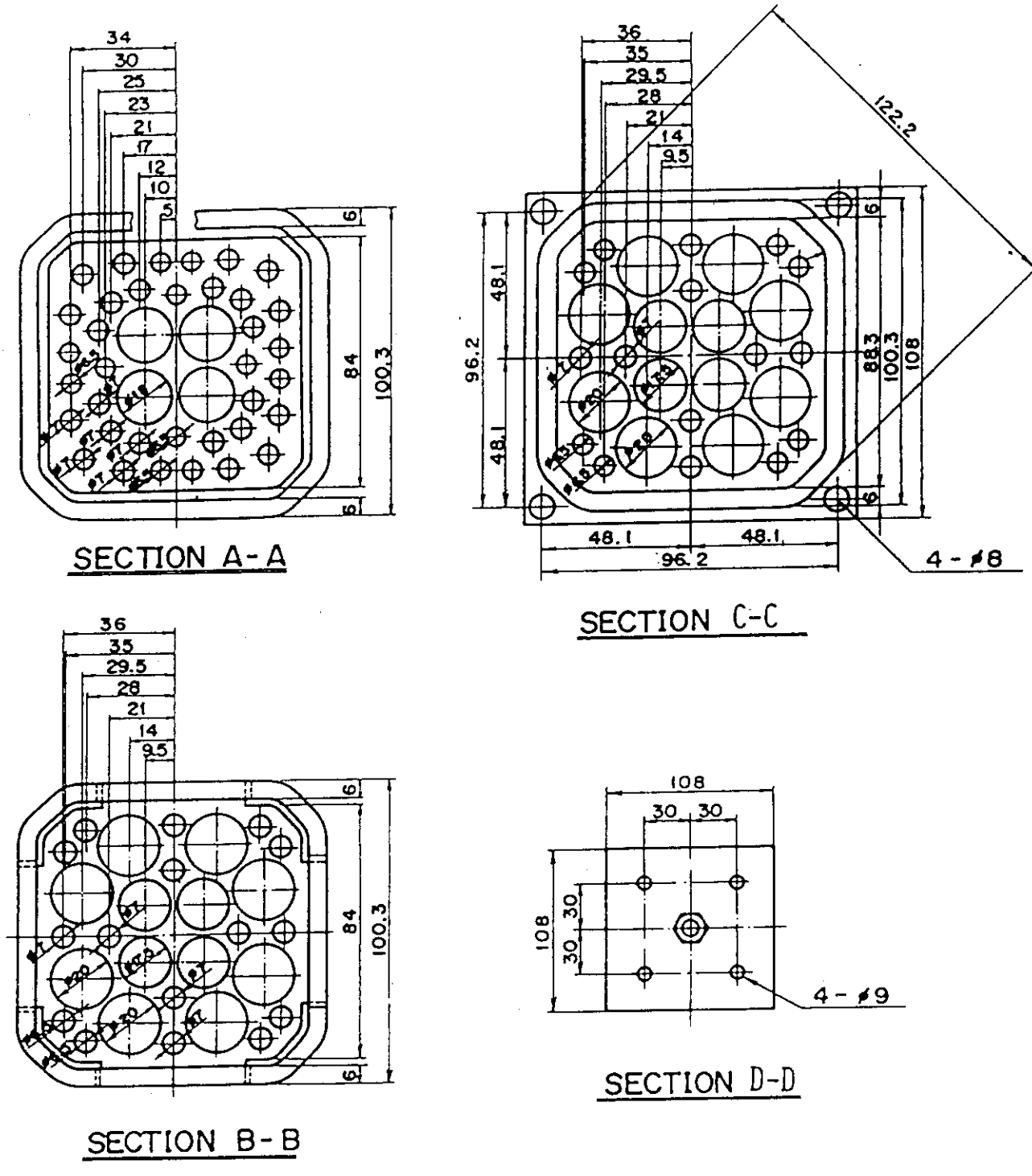

Fig.2.8 Dimension of Guide Tube (2)

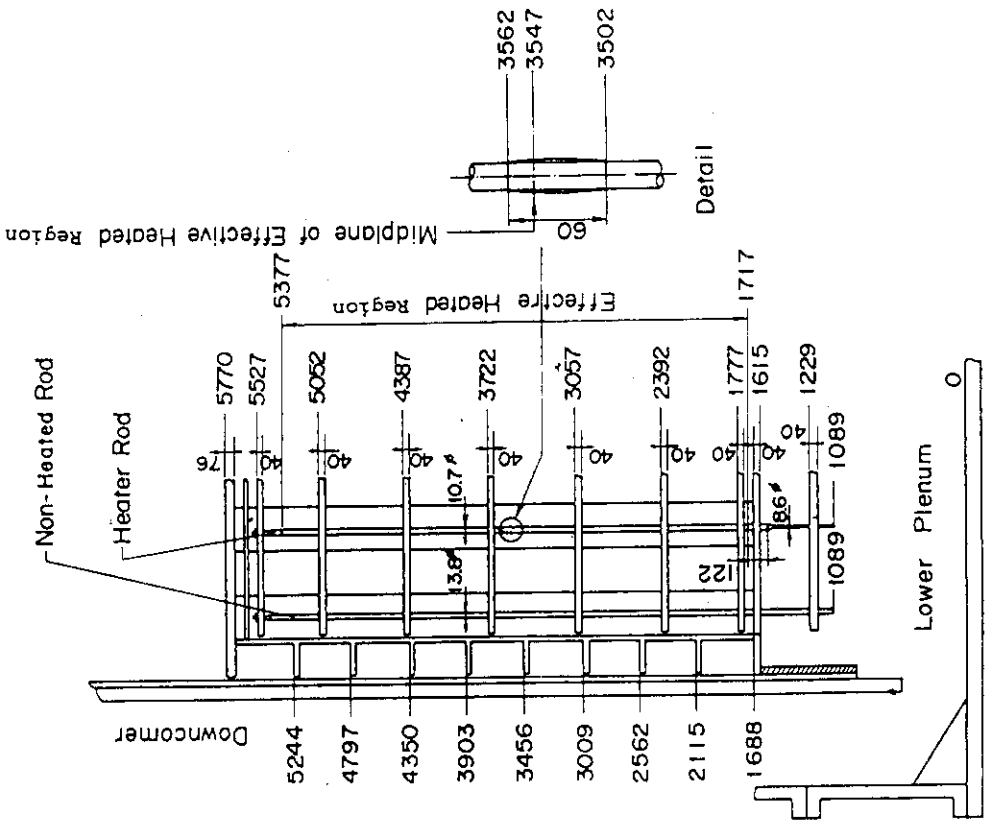

Fig.2.10 Relative Elevation and Dimension of the Core in SCTF

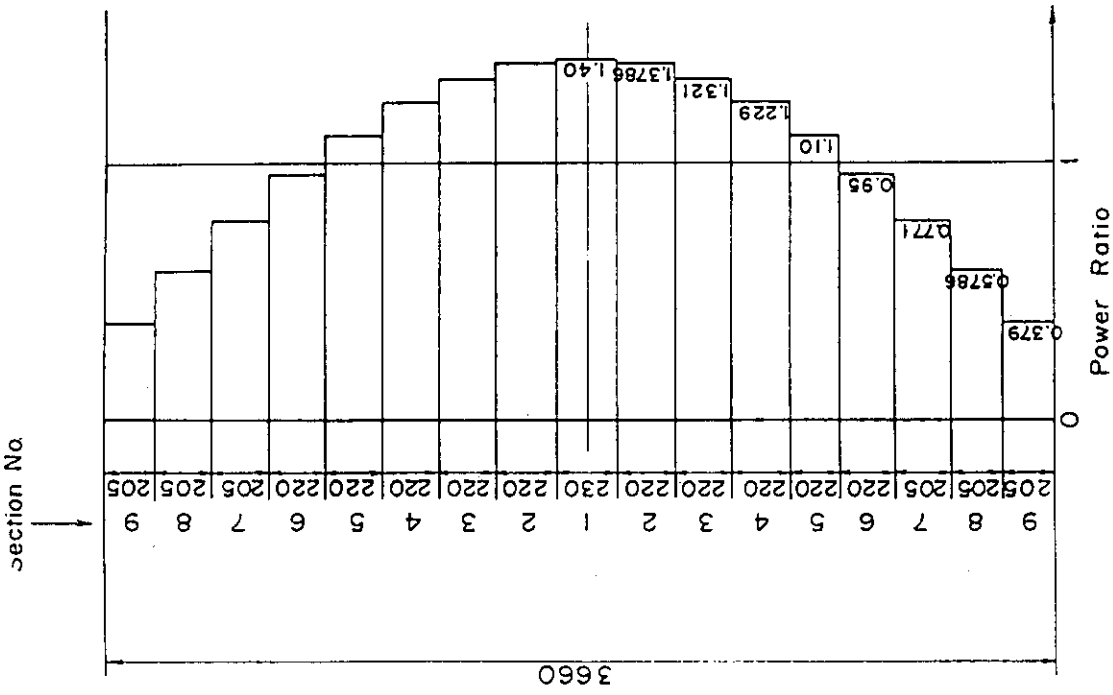

Fig.2.9 Axial Power Distribution of Heater Rod

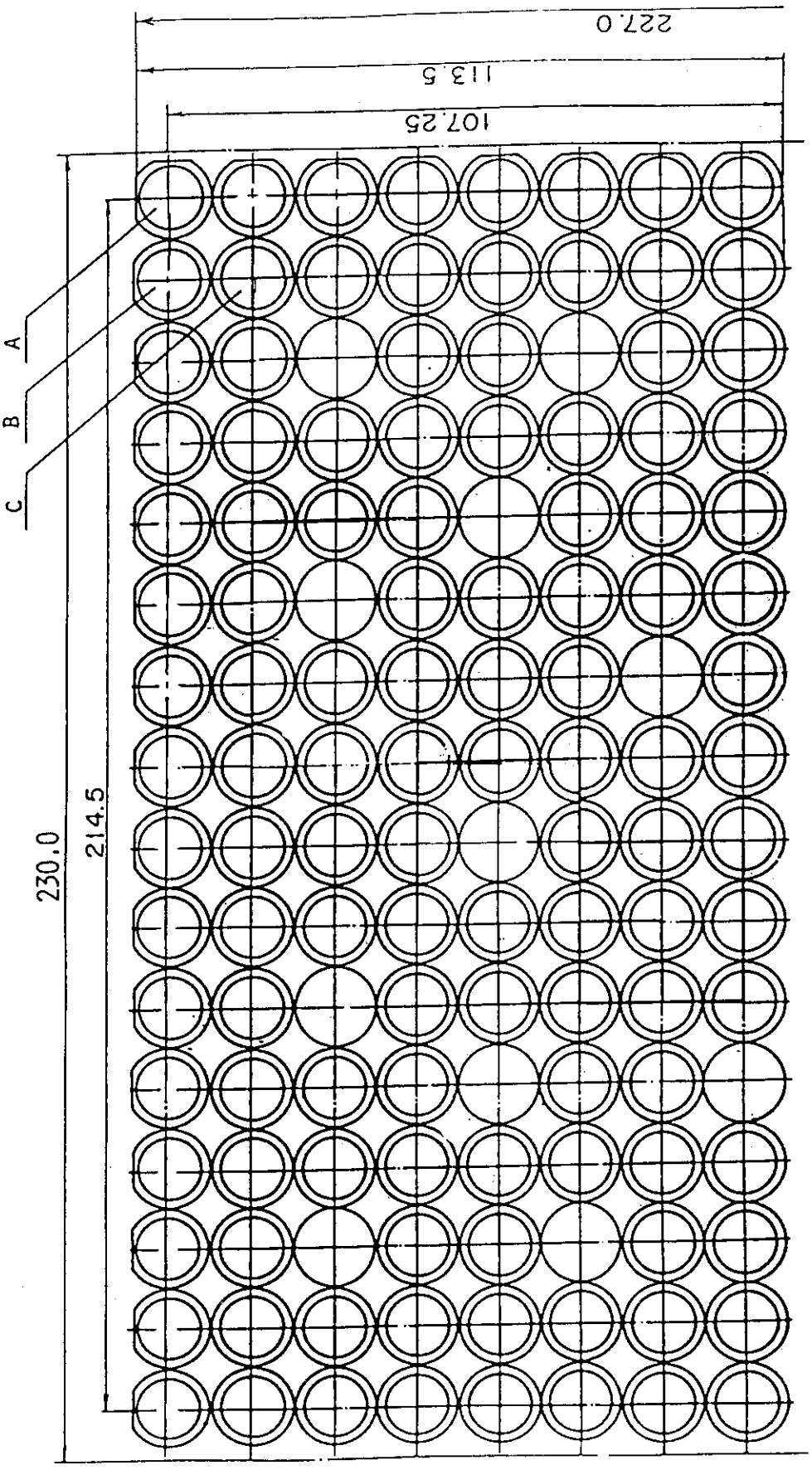

Fig.2.11 Arrangement of the Heater Rods with three kinds of Blockage Sleeve

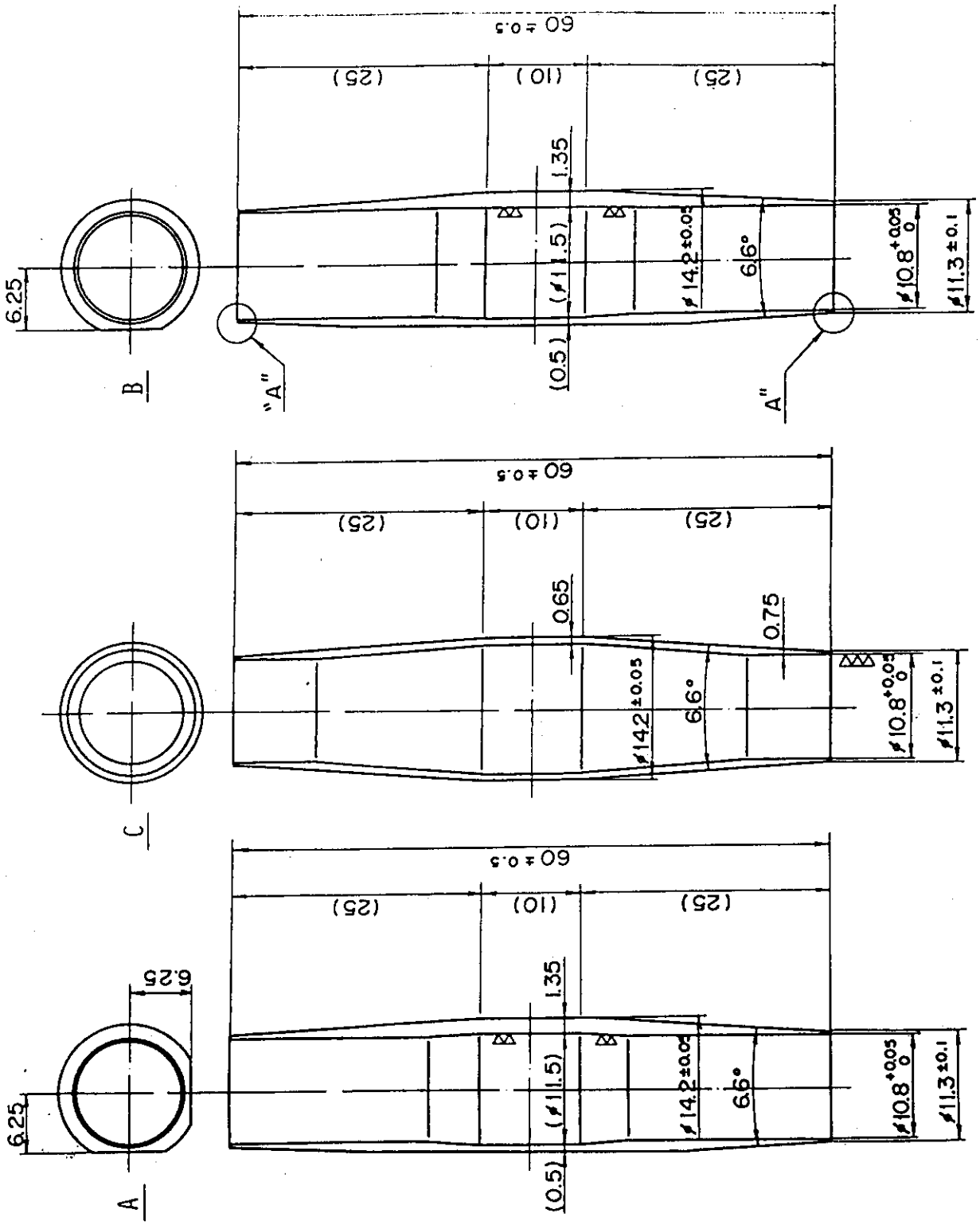

Fig.2.12 Configuration and Dimension of the three Blockage Sleeve

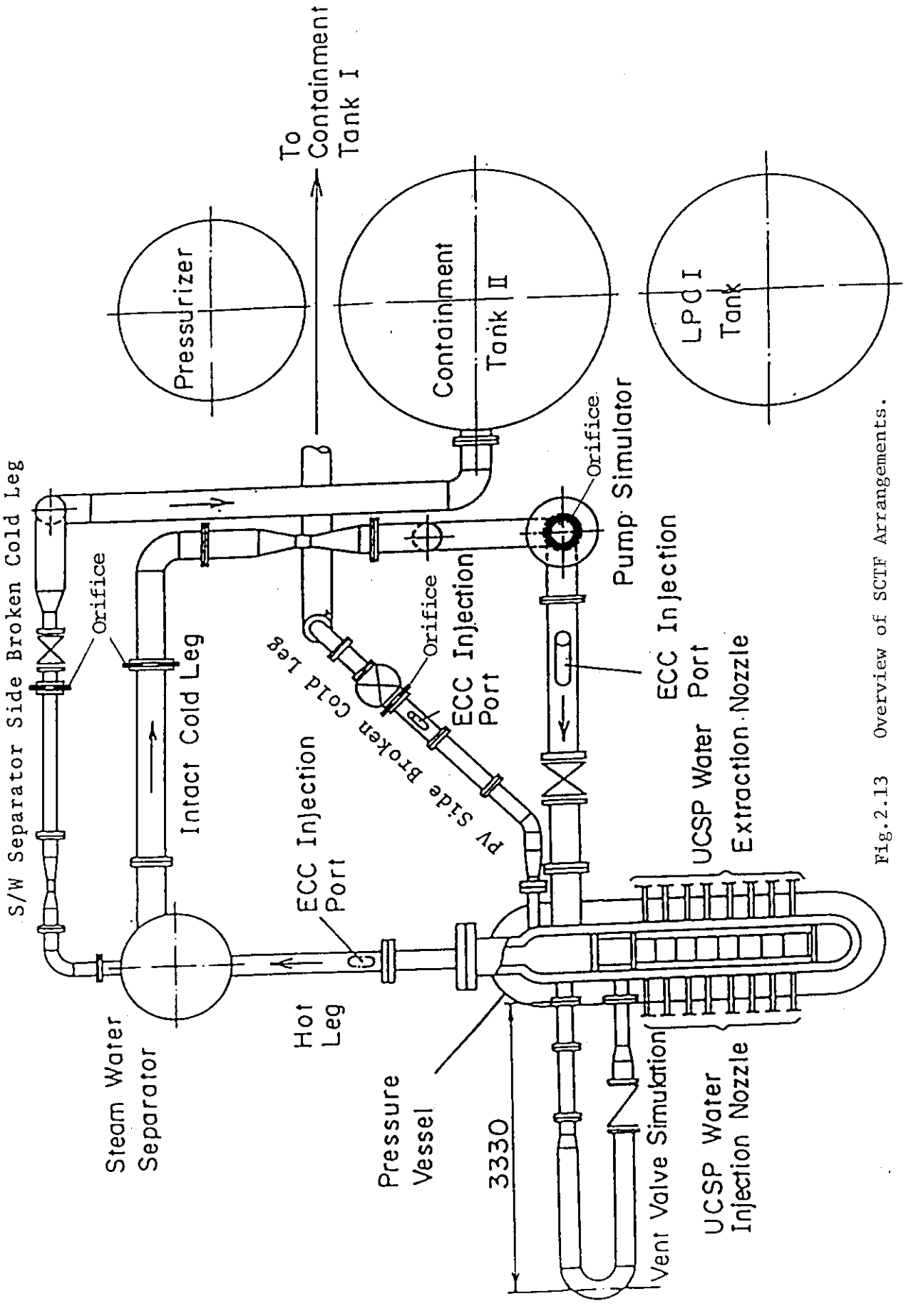

Fig.2.13 Overview of SCTF Arrangements.

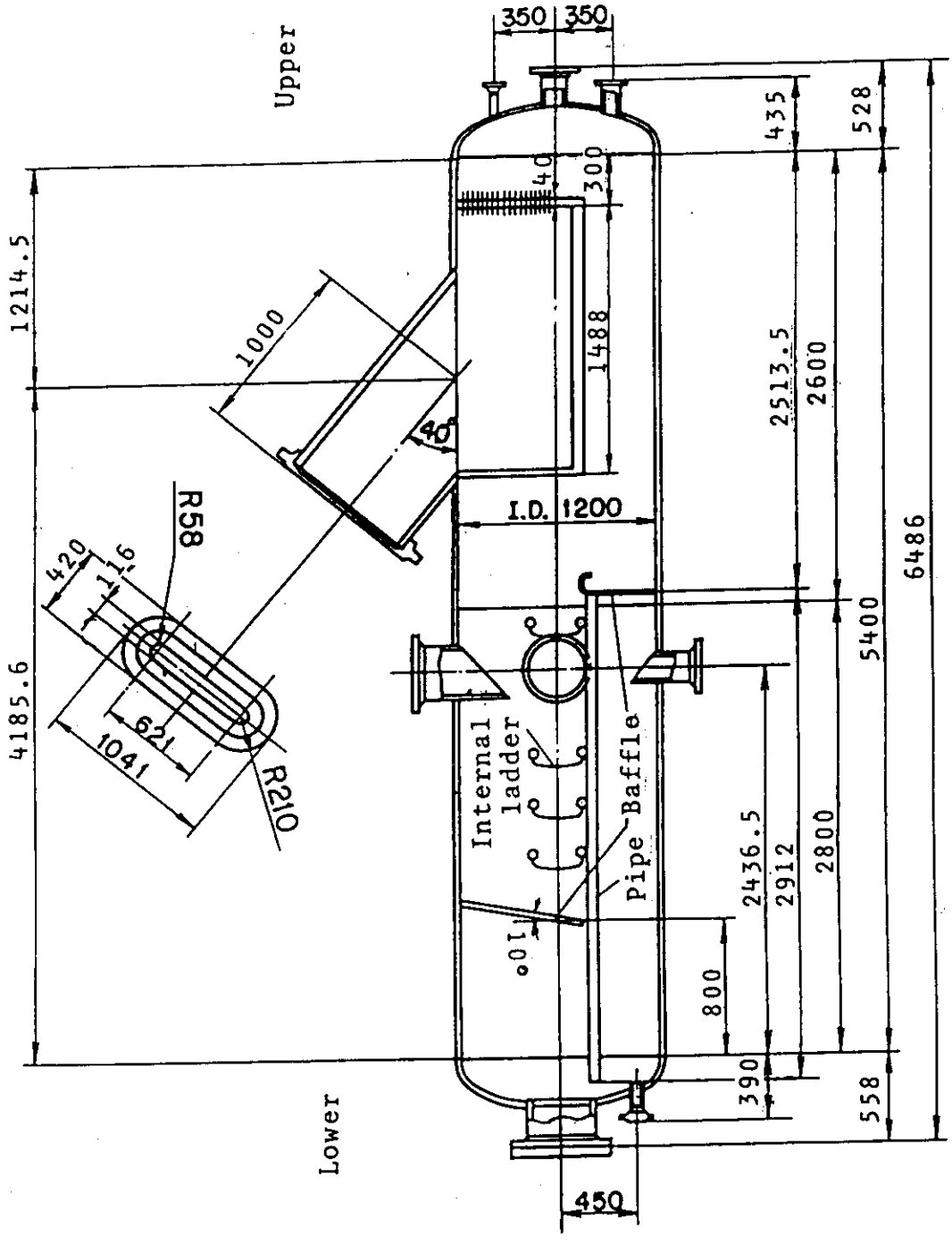

Fig.2.14 Steam Water Separator

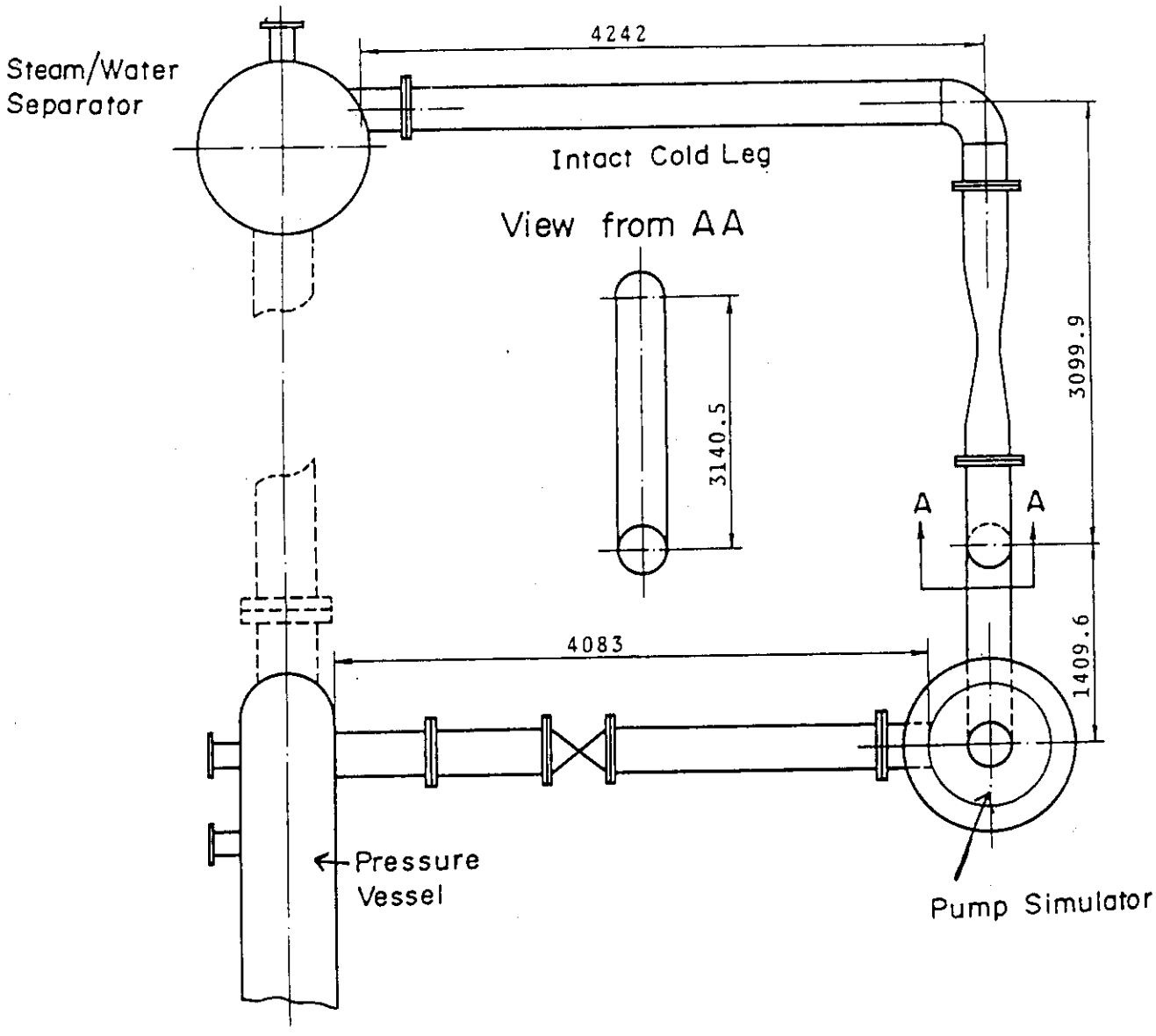

Fig.2.15 Arrangement of Intact Cold Leg

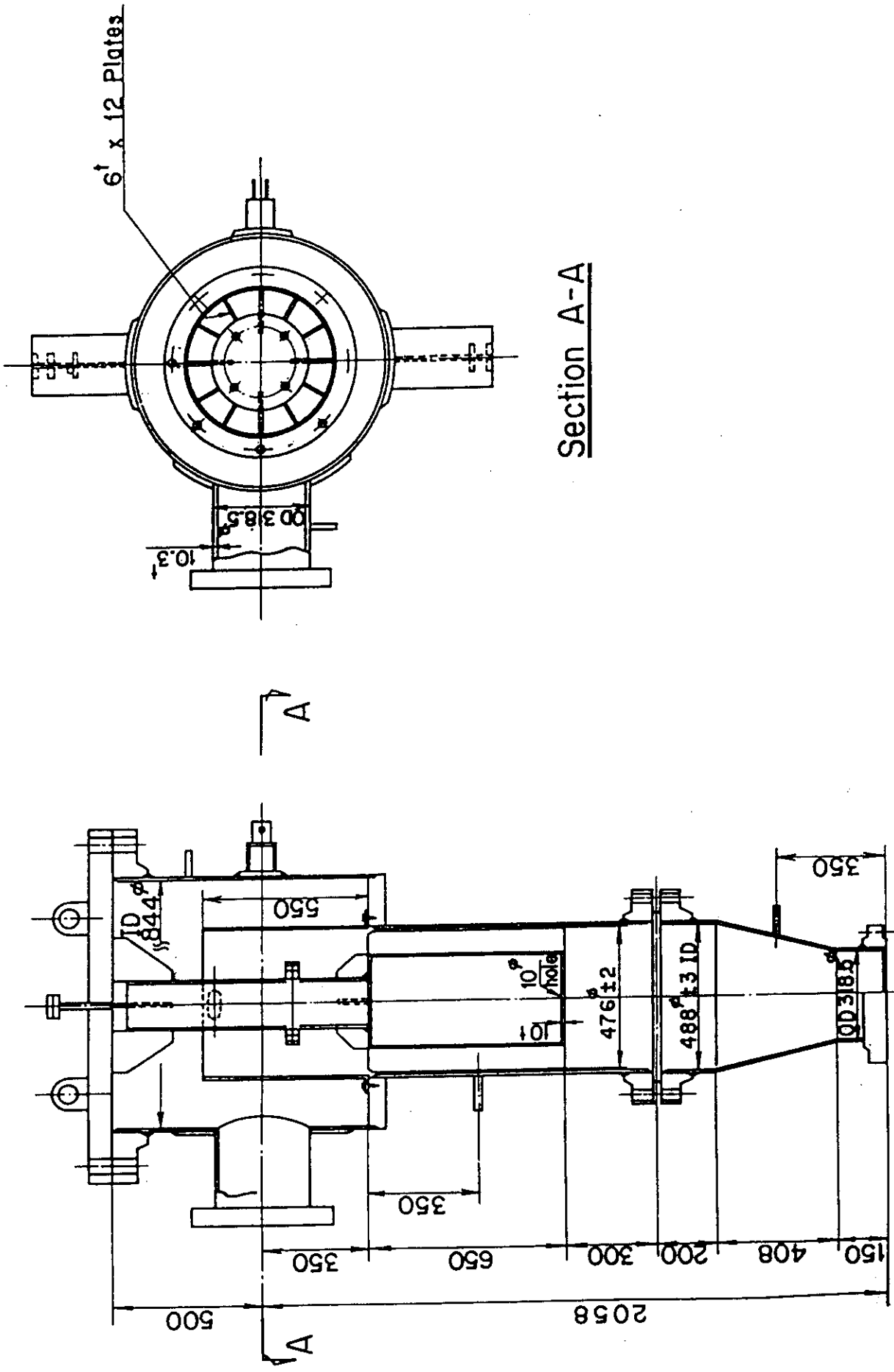

Fig.2.16 Configuration and Dimension of Pump Simulator

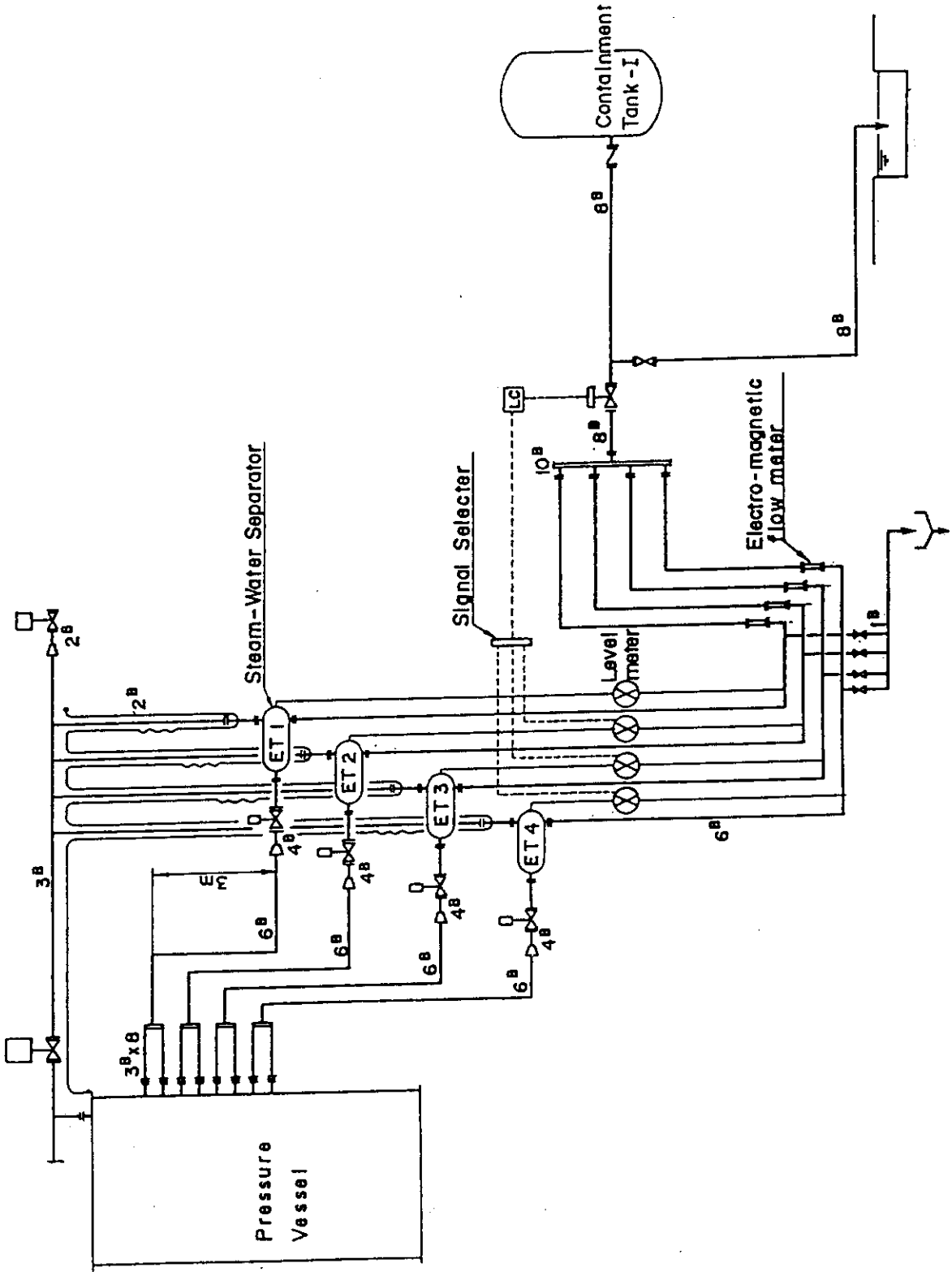

Fig.2.17 Schematic of UCSP Water Extraction System

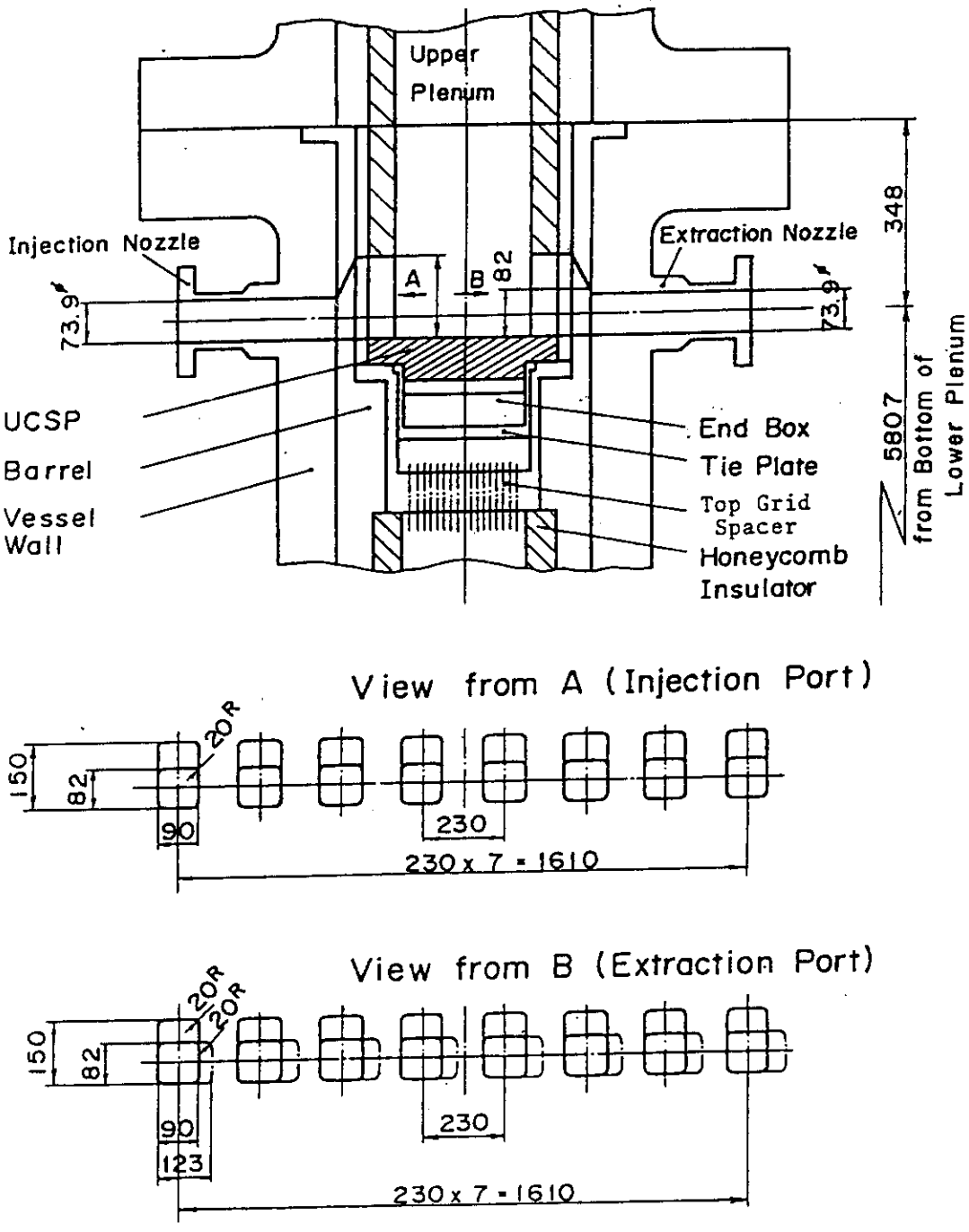

UCSP Injection & Extraction Nozzles

Fig.2.18 Arrangement and Dimension of the UCSP Water Injection and Extraction Nozzles

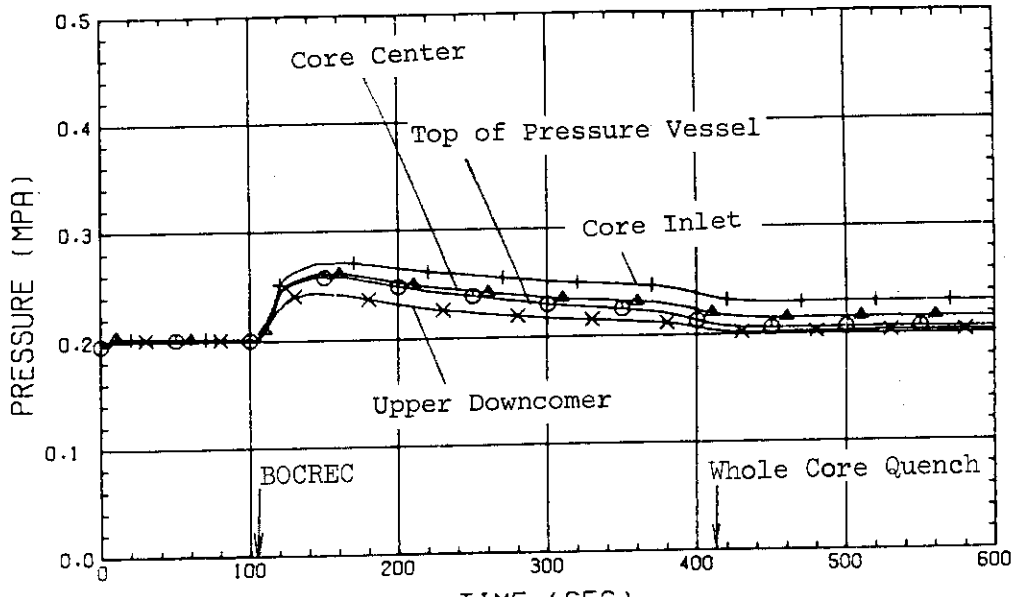

(a) Test S1-03

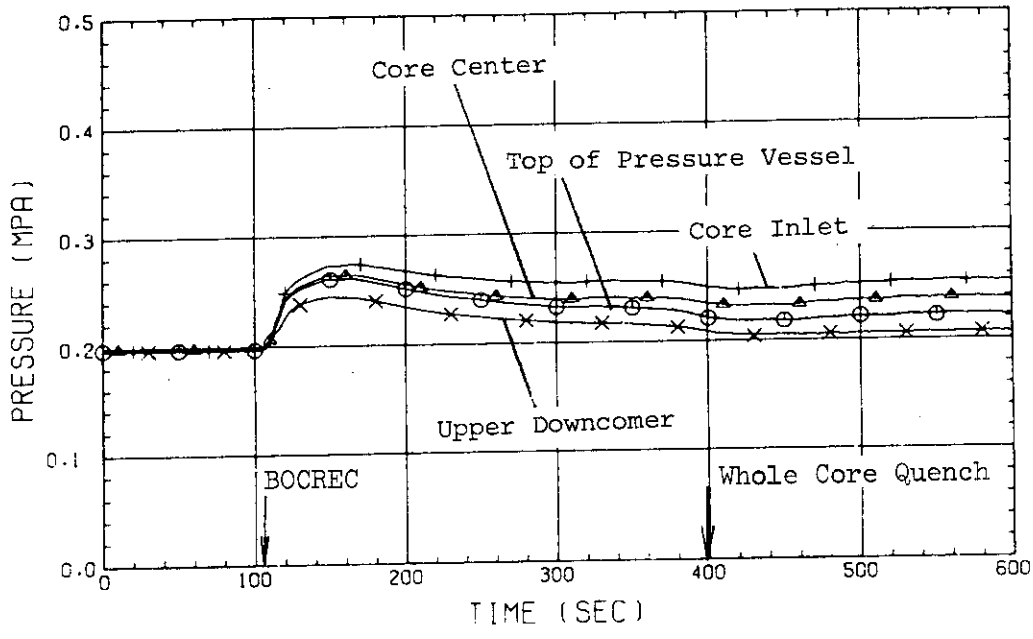

(b) Test S1-01

Fig.2.19 Comparison between Test S1-03 and Test S1-01 of Transients of Pressure at Top of Pressure Vessel, Center of Core, Core Inlet and Upper Plenum

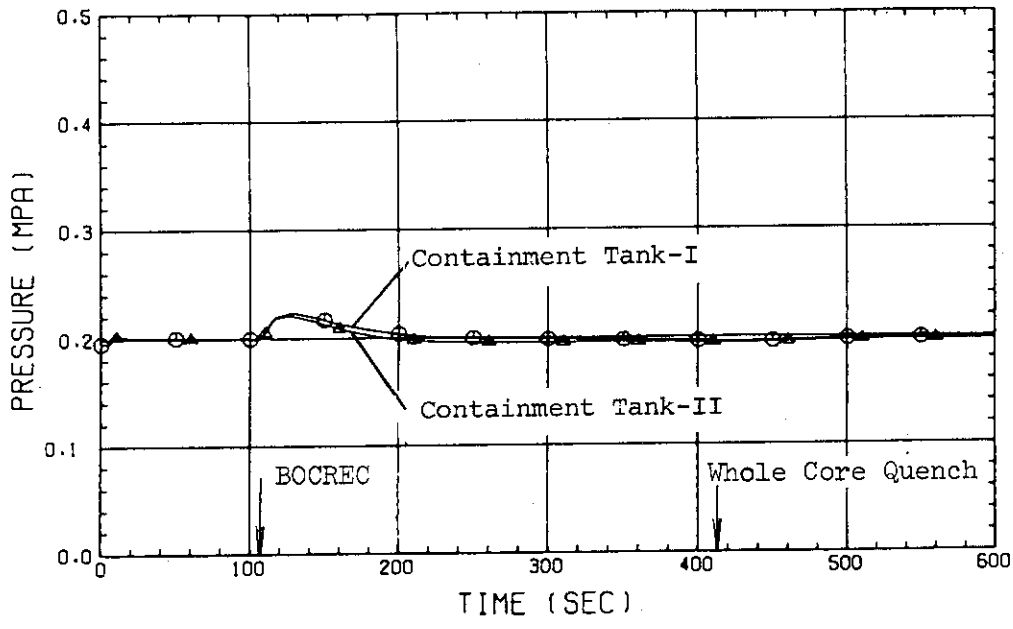

(a) Test S1-03

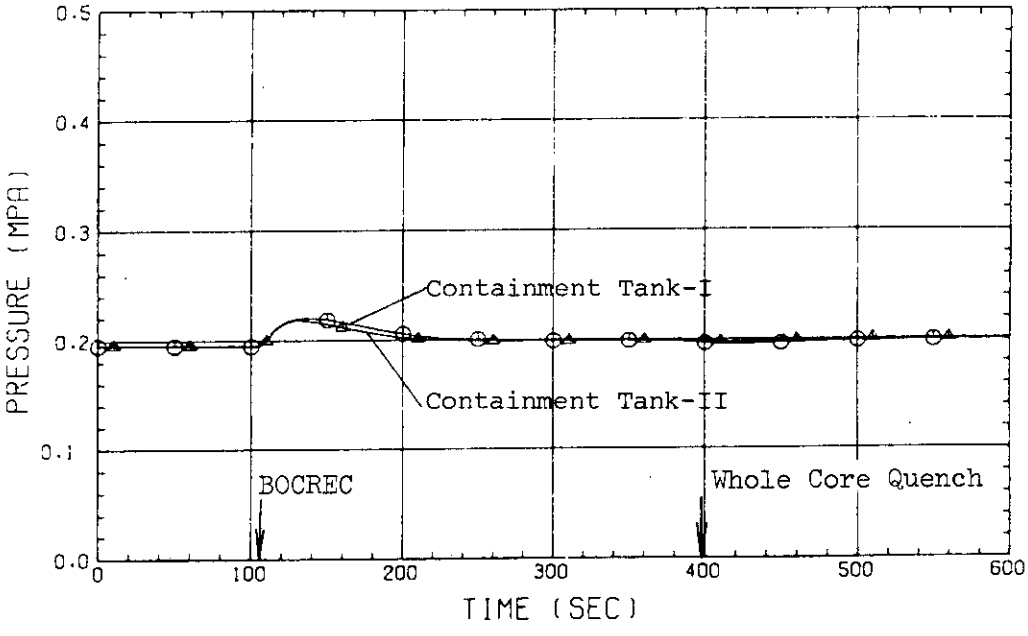

(b) Test S1-01

Fig.2.20 Comparison between Test s1-03 and Test S1-01 of Transients of Pressures at Top of Containment Tanks I and II

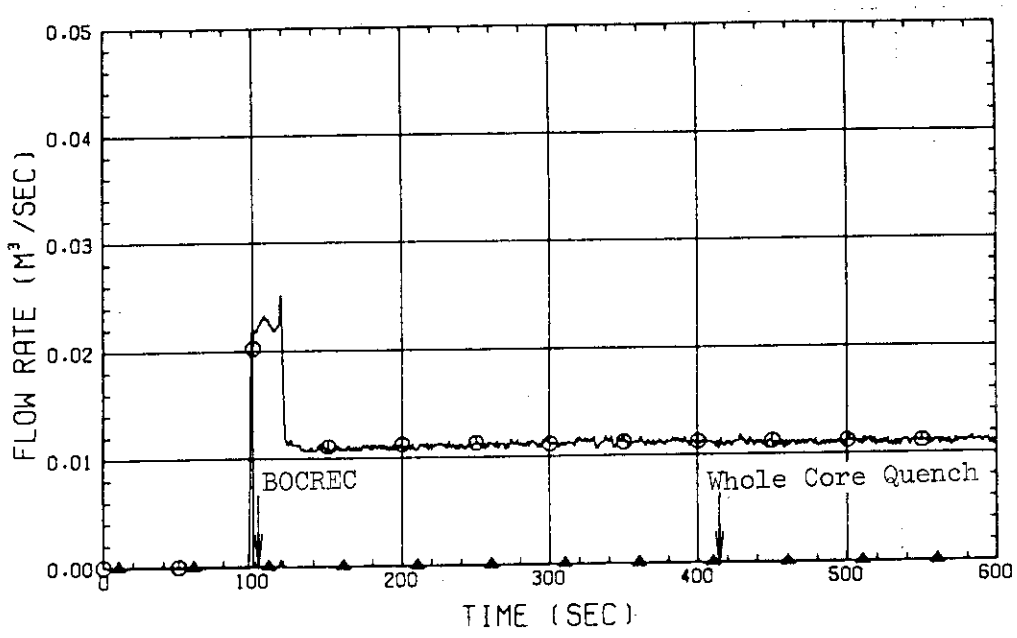

(a) Test S1-03

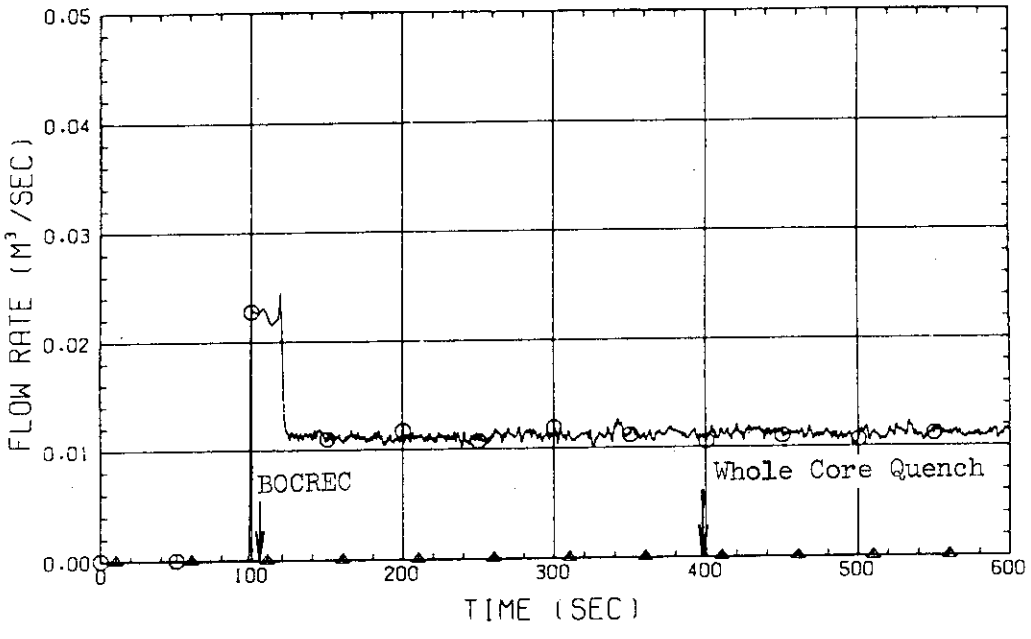

(b) Test S1-01

Fig.2.21 Comparison of Flow Rate of ECC Water between Test S1-03 and Test S1-01

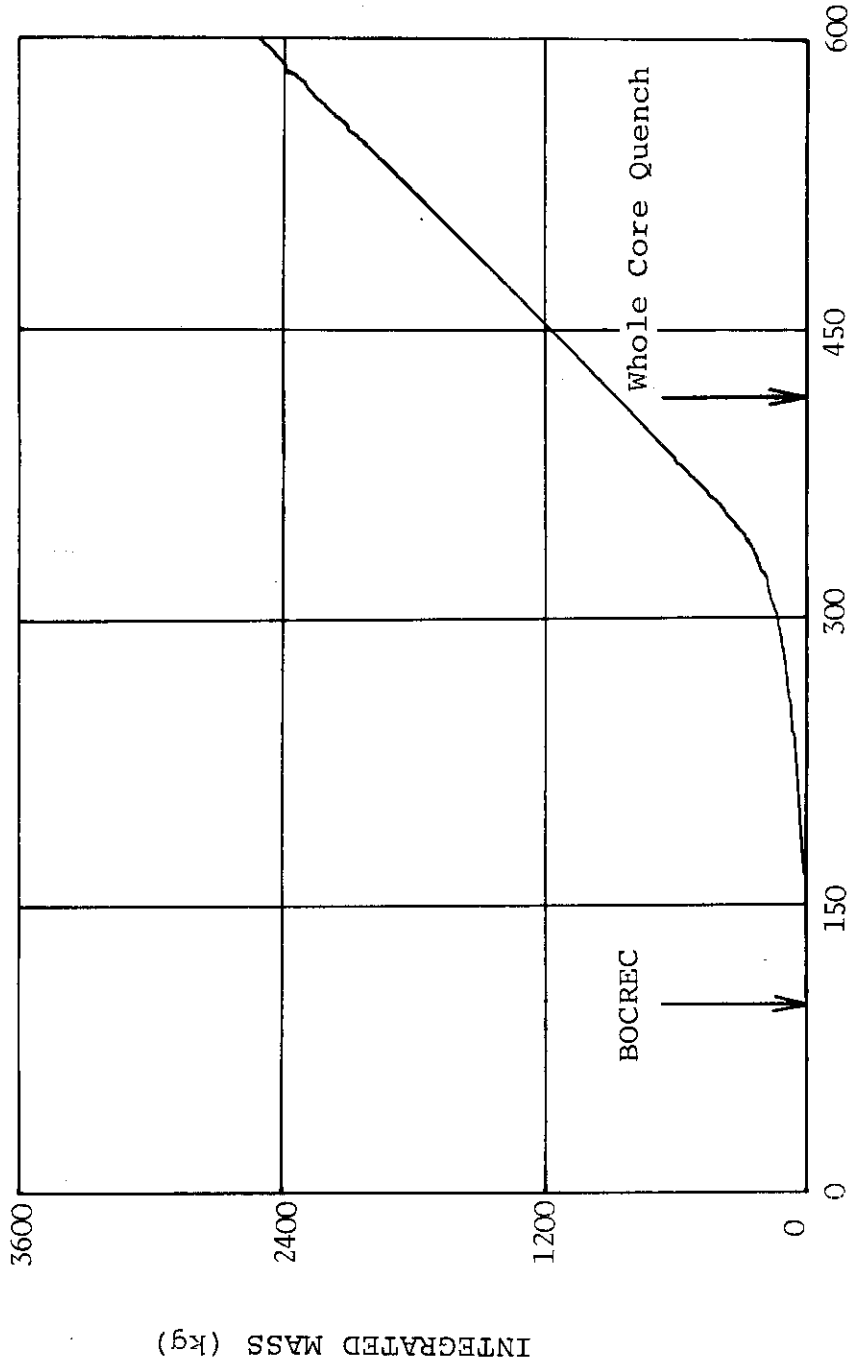

Fig.2.22 Transient of integrated water mass which was extracted from upper plenum in Test S1-03

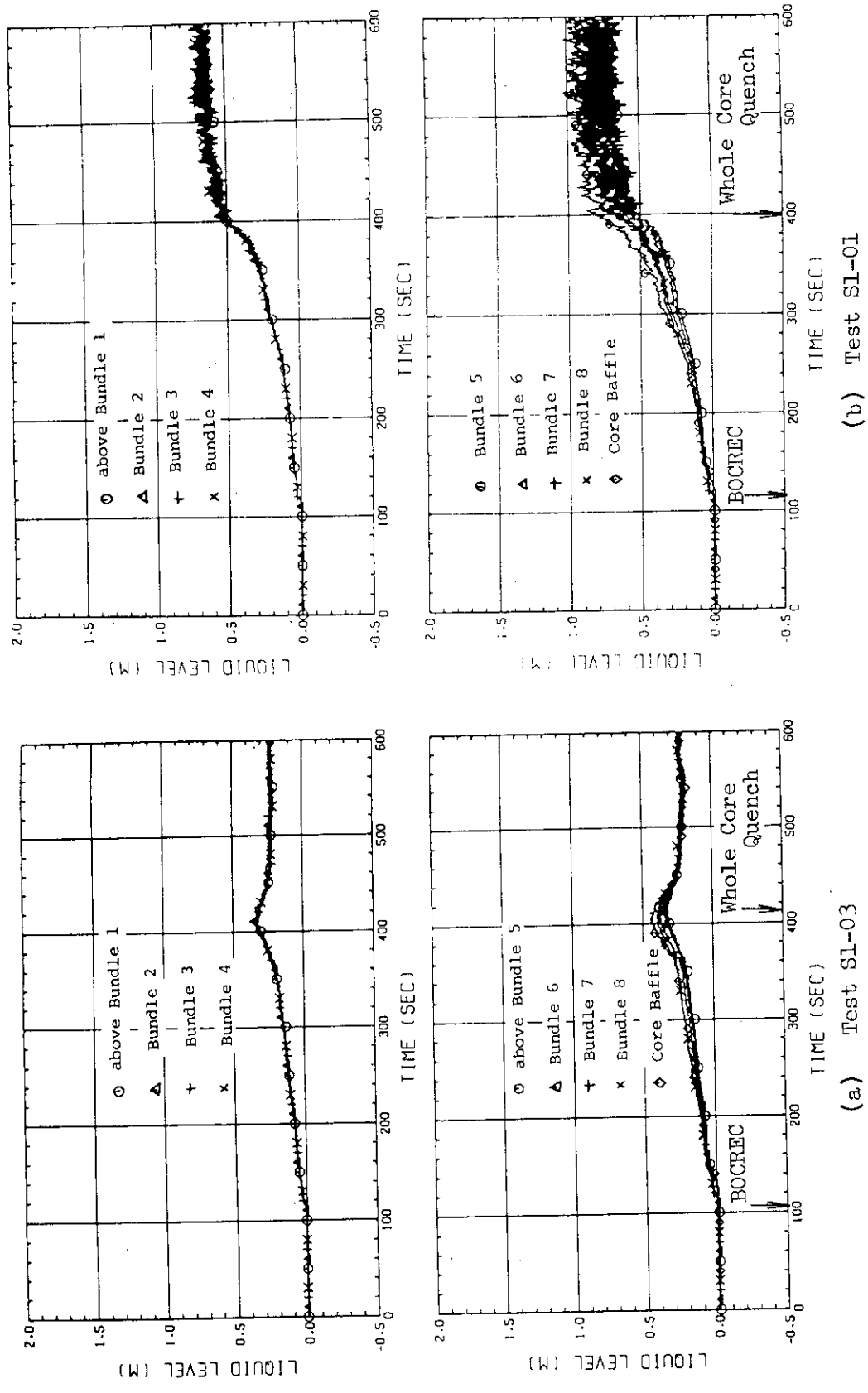

(a) Test S1-03 (b) Test S1-01

Fig.2.23 Comparison between Test S1-03 and Test S1-01 of Transients of Water Level in Upper Plenum

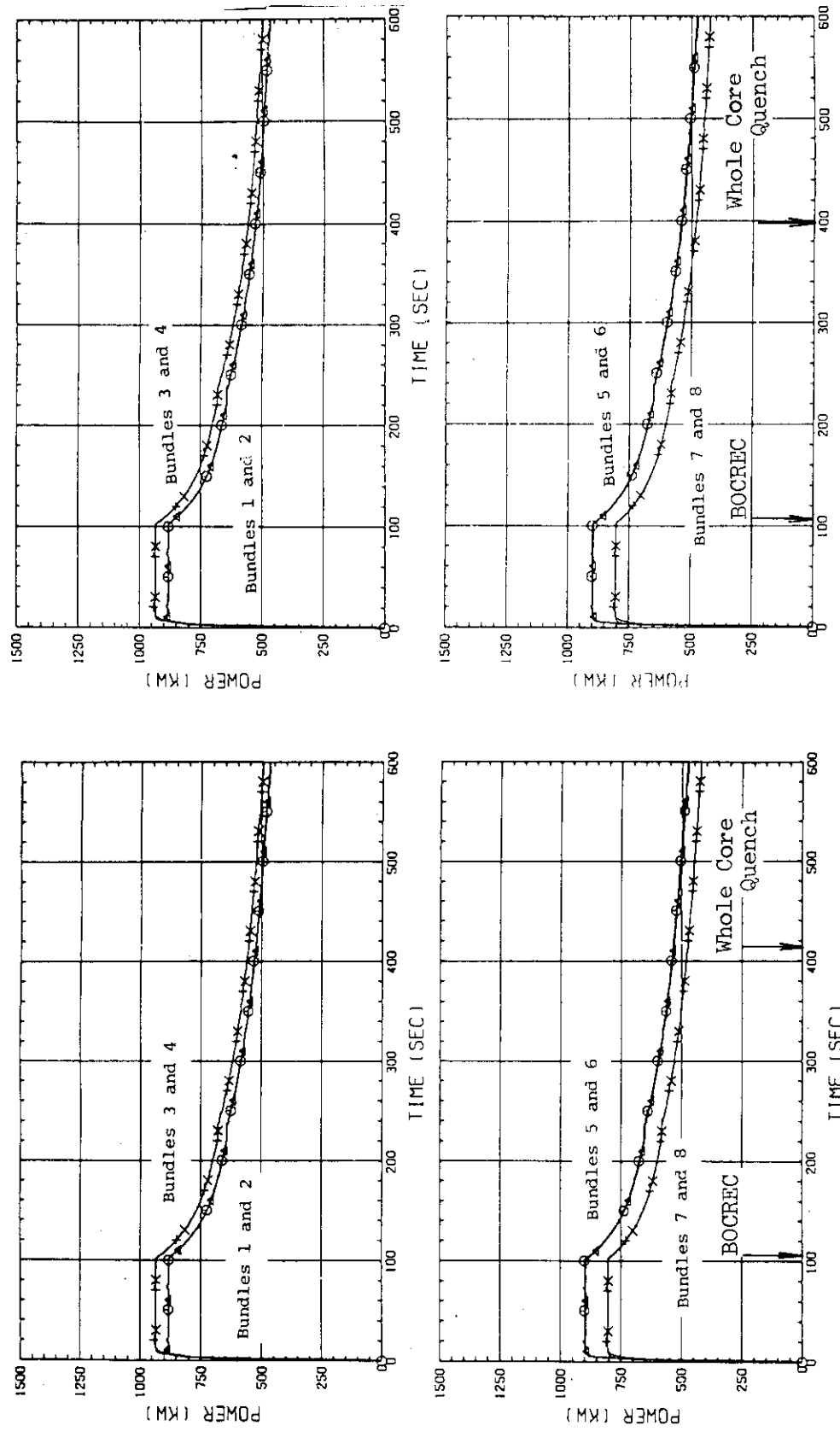

Fig.2.24 Comparison between Test S1-03 and Test S1-01 of Transients of Core Heating Power

3. Overall Hydrodynamic Behavior in the System

3.1 Introduction

In this chapter, the effects of upper plenum water accumulation on the overall hydrodynamic behavior in the system is discussed between the two tests with respect to fluid effluent from the pressure vessel and water accumulation in the pressure vessel. To this end, steam effluent from the pressure vessel, water effluent from the pressure vessel and water accumulation in the pressure vessel are, first, investigated for the two tests and then, the effect of upper plenum water extraction are investigated through the comparison between the two tests.

3.2 Fluid Effluent from Pressure Vessel and Water Accumulation in Pressure Vessel

The mass of steam effluent from the pressure vessel, the mass of water effluent from the pressure vessel, and the mass of water accumulated in the pressure vessel are calculated based on the test data, and the sum of effluent and accumulation is compared with the ECC water flow into the pressure vessel. The downcomer is excluded from the pressure vessel because these two tests are forced-feed flooding tests.

The calculation method for fluid effluent and water accumulation has been described in the previous report[5] which discussed the system pressure effects. In the calculation, the following items are investigated. Each item is shown in Fig. 3.1.

(1) Mass of steam effluent from the pressure vessel
   1. Integrated mass effluent from the steam/water separator to the containment tank-II ($M_{g,I}$)
   2. Integrated mass effluent from the containment tank-I to the containment tank-II ($M_{g,II}$)
   3. Mass of steam accumulated in the containment tank-I ($M_{g,III}$)

(2) Mass of water effluent from the pressure vessel
   1 Mass of water accumulated in the steam/water separator ($M_{\ell,S/W}$)
   2 Mass of water accumulated in the inlet plenum simulator ($M_{\ell,Inlet}$)
   3 Mass of water accumulated in the downcomer ($M_{\ell,III}$)
   4 Mass of water accumulated in the containment tank-I ($M_{\ell,I}$)
   5 Mass of water accumulated in the containment tank-II ($M_{\ell,II}$)
   6 Mass of water accumulated in the hot leg ($M_{\ell,\ Hot\ Leg}$)

(3) Mass of water accumulated in the pressure vessel

1 Mass of water accumulated in the core ($M_{\ell, \text{Core}}$)

2 Mass of water accumulated in the core baffle region ($M_{\ell, \text{baffle}}$)

3 Mass of water accumulated above the upper core support plate (UCSP) ($M_{\ell, \text{UCSP}}$)

(4) Mass of ECC water into the pressure vessel

1 The integrated mass of water injected by the Acc injection and the LPCI (Acc+LPCI)

The mass balance is confirmed by comparing the sum of (1), (2) and (3) with (4). The results are shown in Figs. 3.2 and 3.3 for Tests S1-01 and S1-03, respectively. The integrated mass of injected ECC water agrees well with the sum of mass effluent and accumulated mass except the early period of Test S1-03, as shown in Fig. 3.3.

The reason for rather larger error in the early period of the test might be considered as follows. The liquid level in the gap between the pressure vessel wall and the core barrel was considered to be the same as that in the core region in estimate for liquid mass in the pressure vessel ($M_{\ell, \text{core}}$) though it should be actually lower than that in the core in this period for Acc injection. Therefore, the liquid mass inside the pressure vessel was overestimated.

3.3 Effect of Water Extraction

The effect of water extraction on the mass of water accumulated in the core (including the core baffle region) and the upper plenum is shown in Fig. 3.4 along with the steam effluent from the pressure vessel.

It is noted from this figure that the mass of water accumulated in the core is smaller in Test S1-03 from about 200 seconds after the BOCREC. It is suggested that the fall back water from the upper plenum to the core is smaller in the water extraction test, S1-03 than in the Base Case Test, S1-01.

It is also found that the amount of steam effluent from the pressure vessel is almost the same between these two tests.

The effect of water extraction on the carryover water through the hot leg calculated from the amount of water in the steam/water separator and the containment tank-II is shown in Fig. 3.5. The mass of carryover water is smaller in Test S1-03 than in Test S1-01 from about 260 seconds after the BOCREC.

To investigate the reason for the difference in the characteristics of carryover water through the hot leg, the transients of steam velocity in the hot leg are shown in Fig. 3.6, and the amount of water accumulated in the hot leg is shown in Fig. 3.7. Fig. 3.7 shows that the amount of water accumulated in the hot leg is much smaller in Test S1-03 from about 260 seconds after the BOCREC, and Fig. 3.6 shows that the steam velocity is lower in Test S1-03 from about 280 seconds after the BOCREC. Therefore, it is easily understood that the difference of steam velocity in the hot leg is due to the difference in the flow area for steam flow which is caused by the difference in the elevation of water accumulated in the hot leg because the steam mass flow rate is almost the same between the two tests as shown in Fig. 3.4. Besides, it is pointed out that the reason why the difference in water accumulation in the hot leg is due to the difference in the water accumulation in the upper plenum as shown in Fig. 3.4. Thus, it is pointed out that the difference of carryover water through hot leg between these two tests is due to the difference in the steam velocity in the hot leg and the amount of water accumulated in the hot leg, which are caused by the differences in water level in the upper plenum.

3.4 Summary

(1) In these forced-feed flooding tests with or without water extraction from the upper plenum, the mass of injected ECC water agrees well with the sum of the mass of water accumulated in the SCTF system and the mass of steam effluent from the pressure vessel.

(2) The mass of water accumulated in the core is smaller and the mass of carryover through hot leg is smaller in Test S1-03 than in Test S1-01.

(3) The amount of steam effluent from the pressure vessel is almost the same between Test S1-03 and Test S1-01.

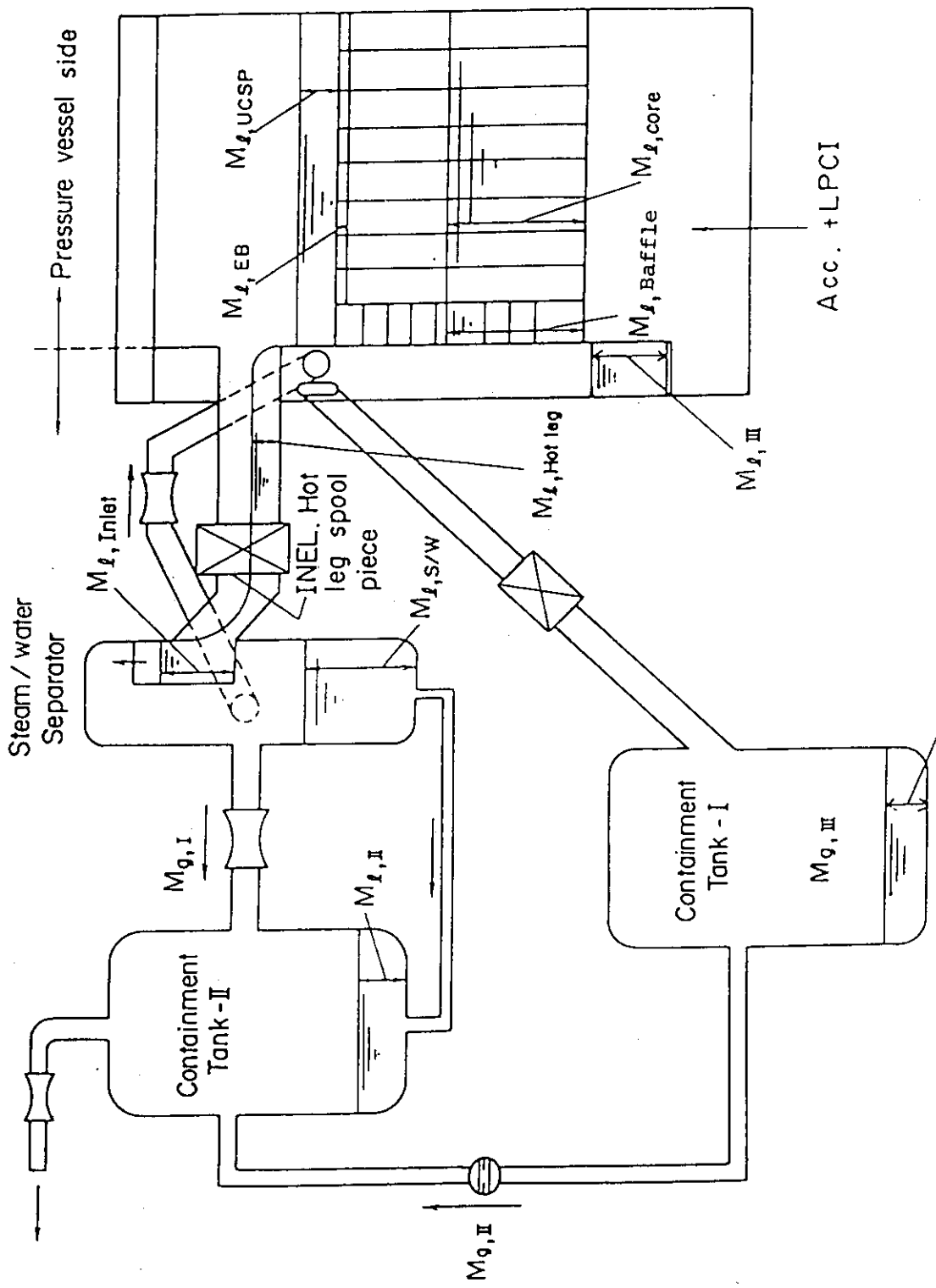

Fig.3.1 Model and Definition of Variables for Mass Balance

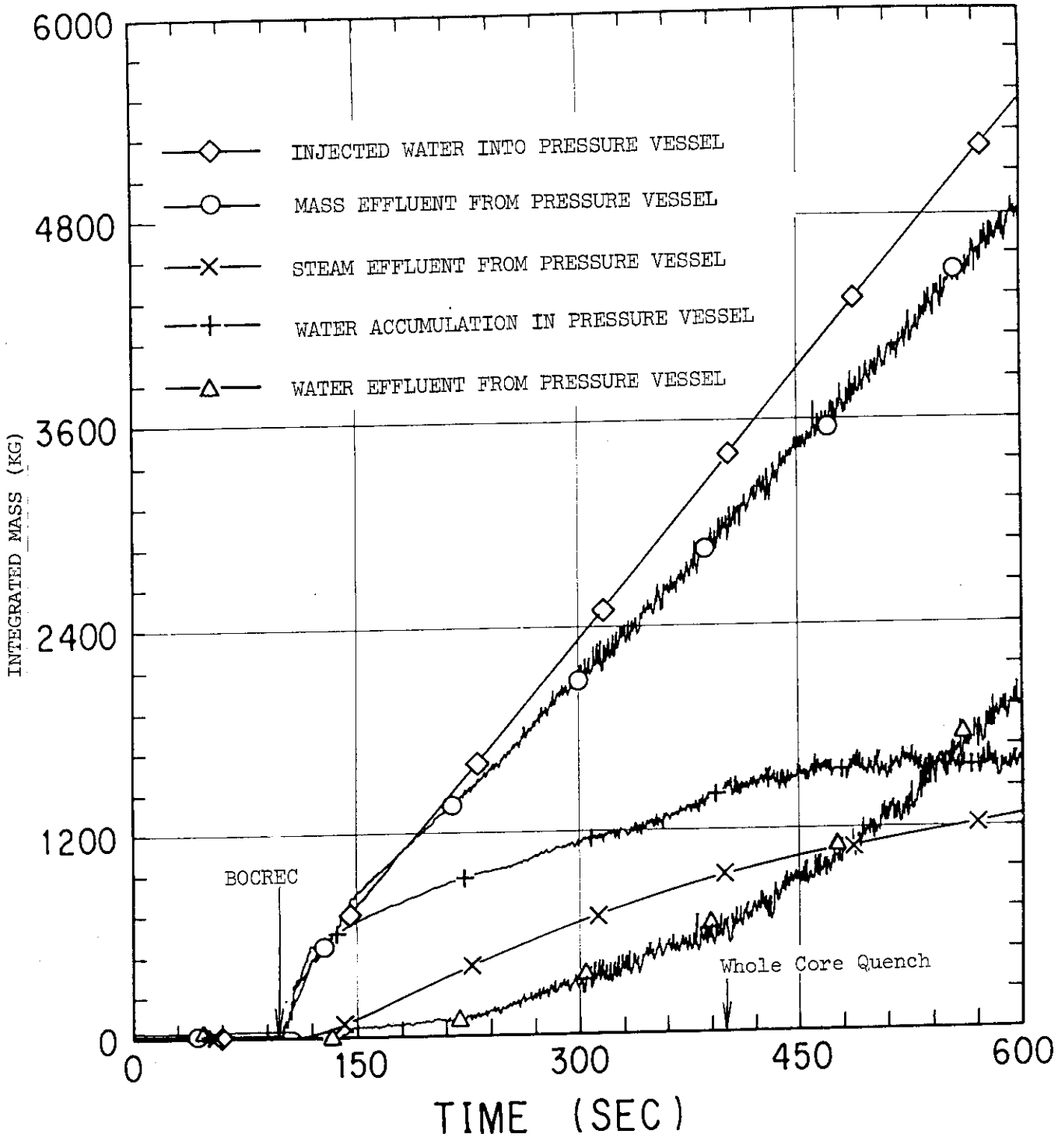

Fig.3.2 Mass Balance in Test S1-01

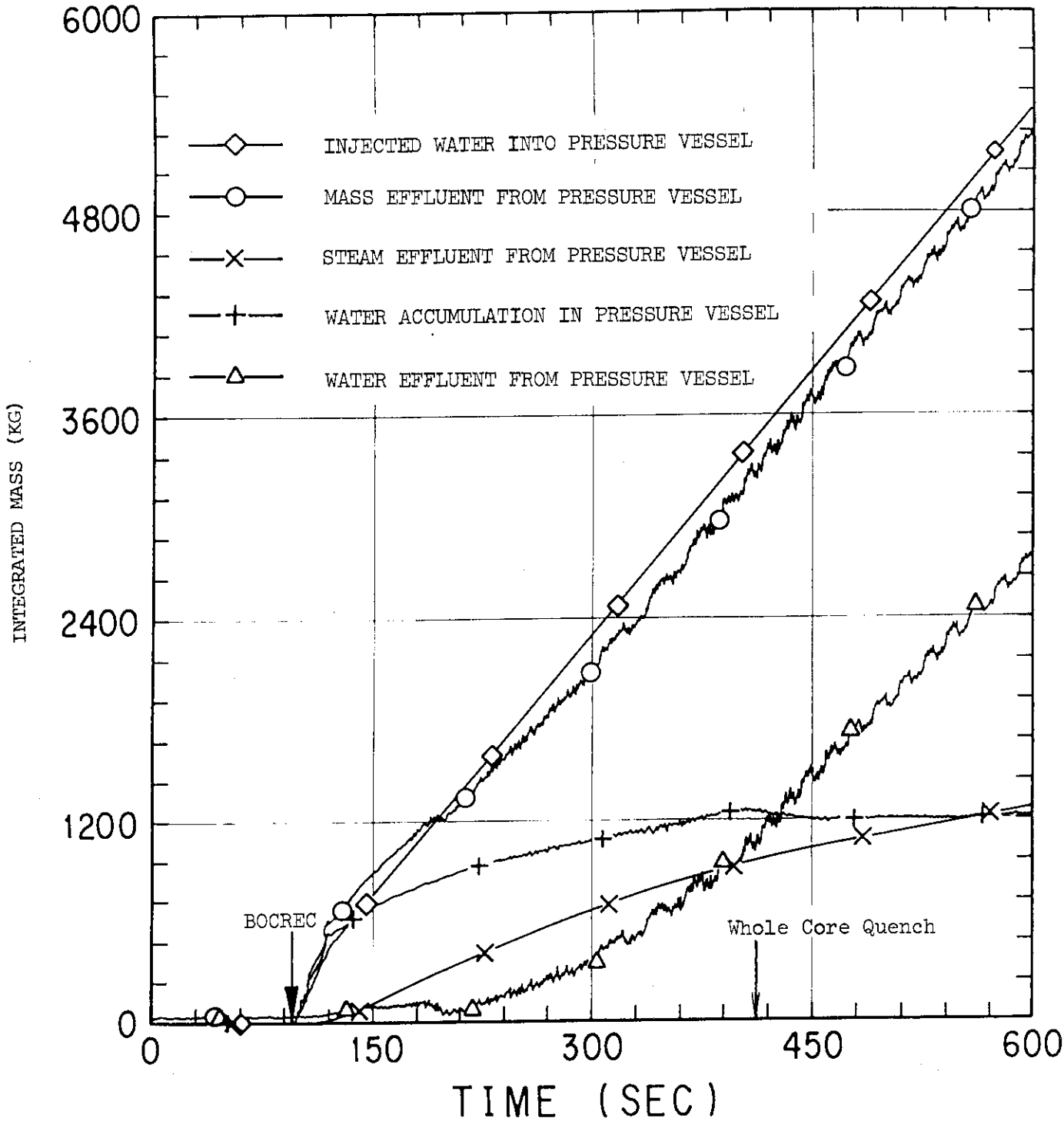

Fig.3.3 Mass Balance in Test S1-03

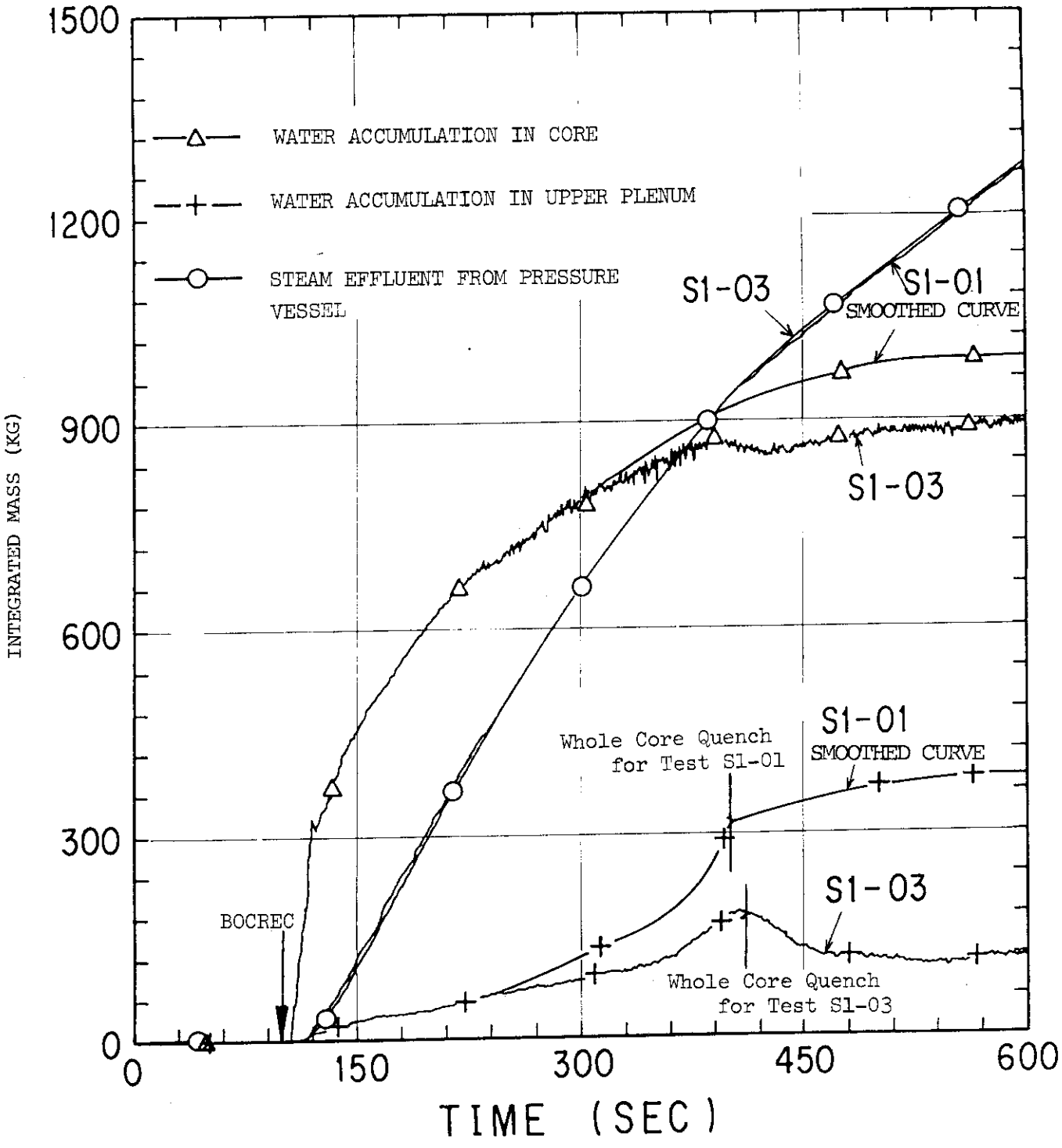

Fig.3.4 Water Accumulation in Pressure Vessel and Steam Outflow from Pressure Vessel

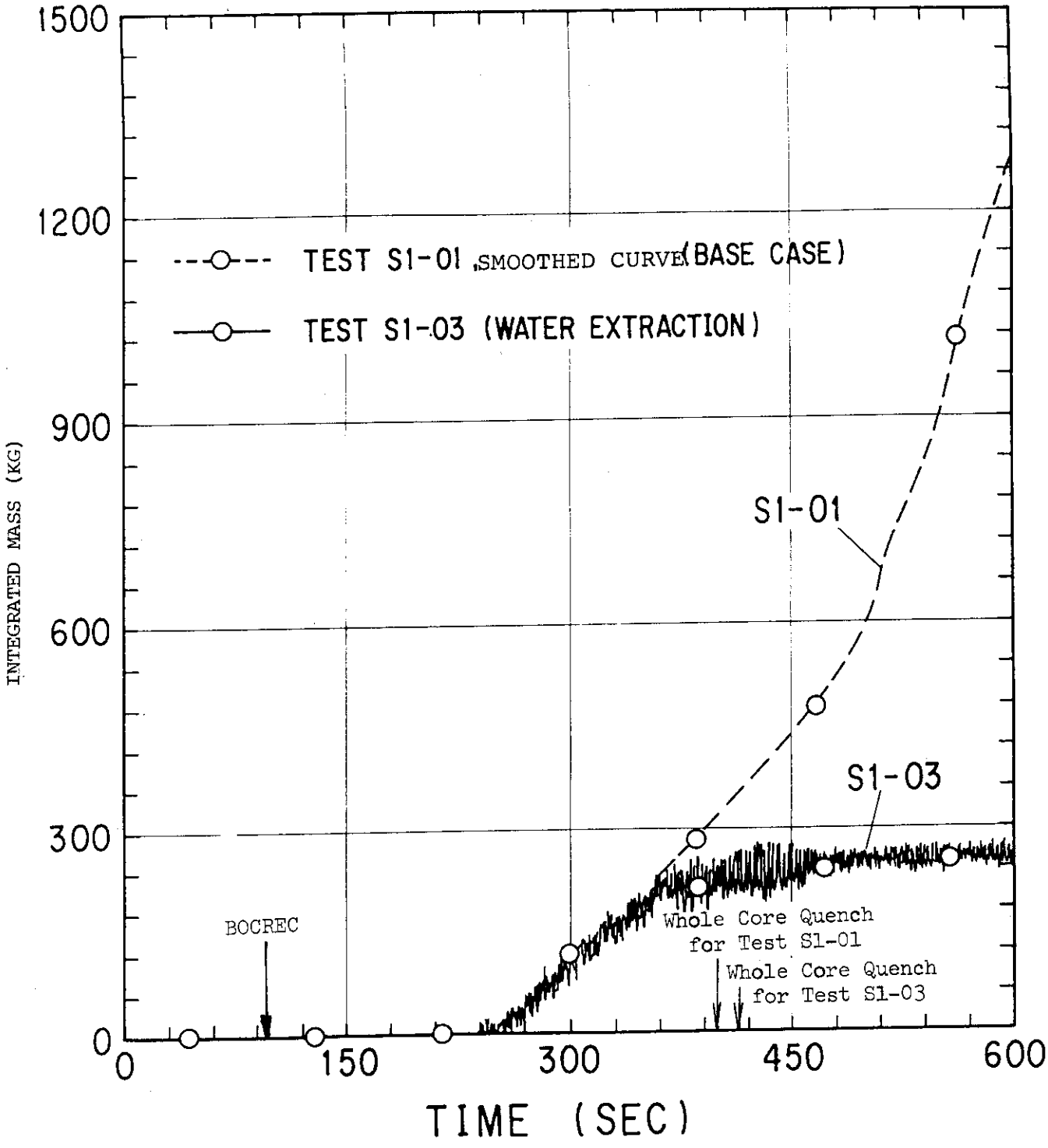

Fig.3.5 Integration of Carryover Water through Hot Leg

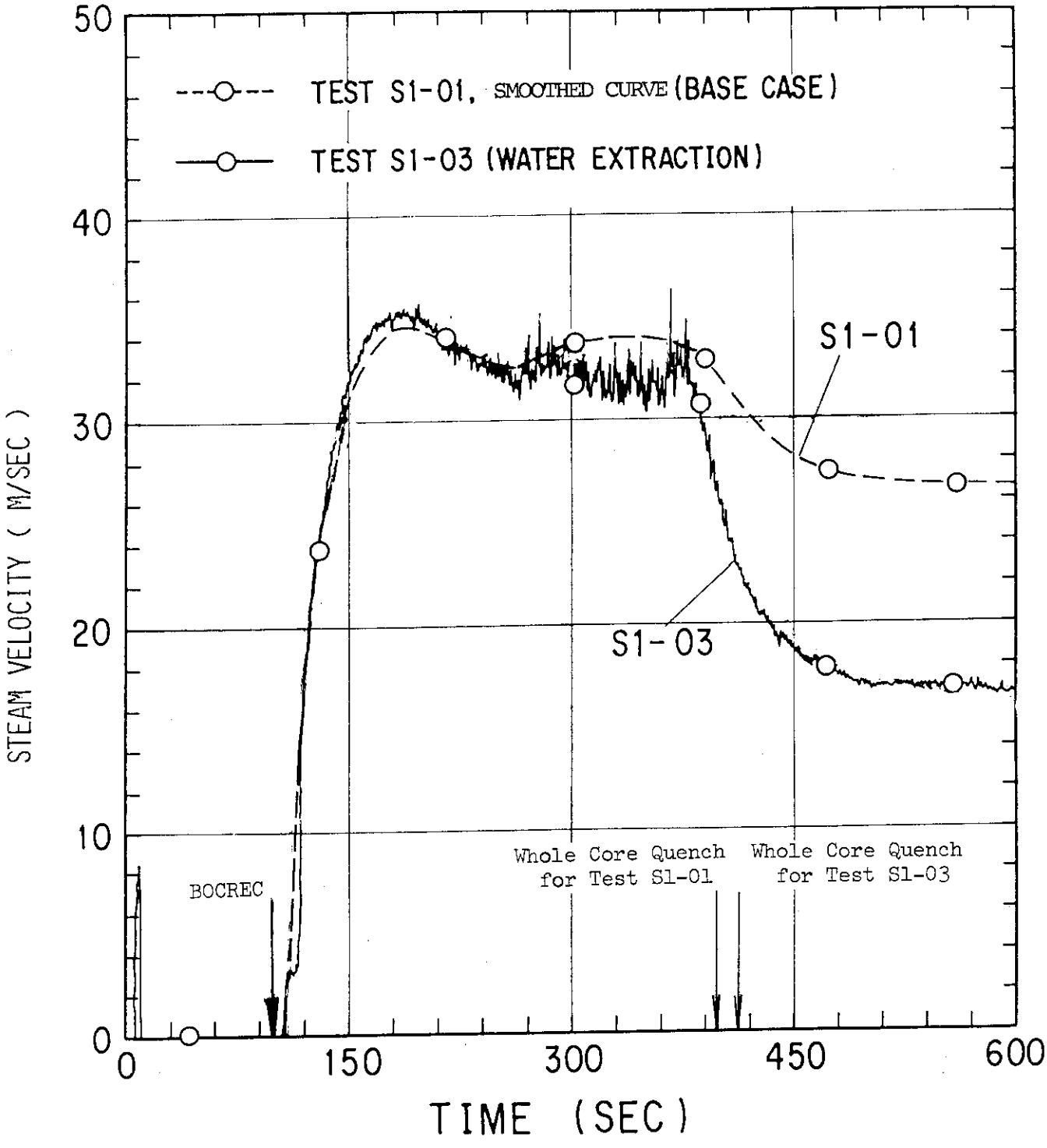

Fig.3.6 Steam Velocity in Hot Leg

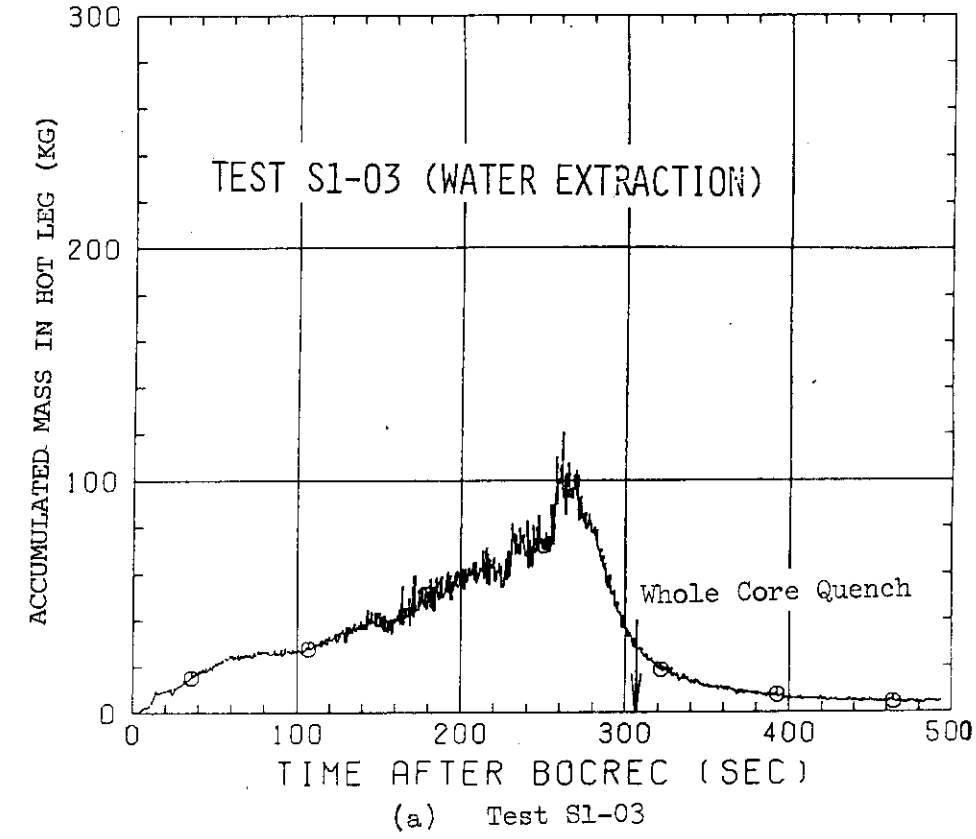

(a) Test S1-03

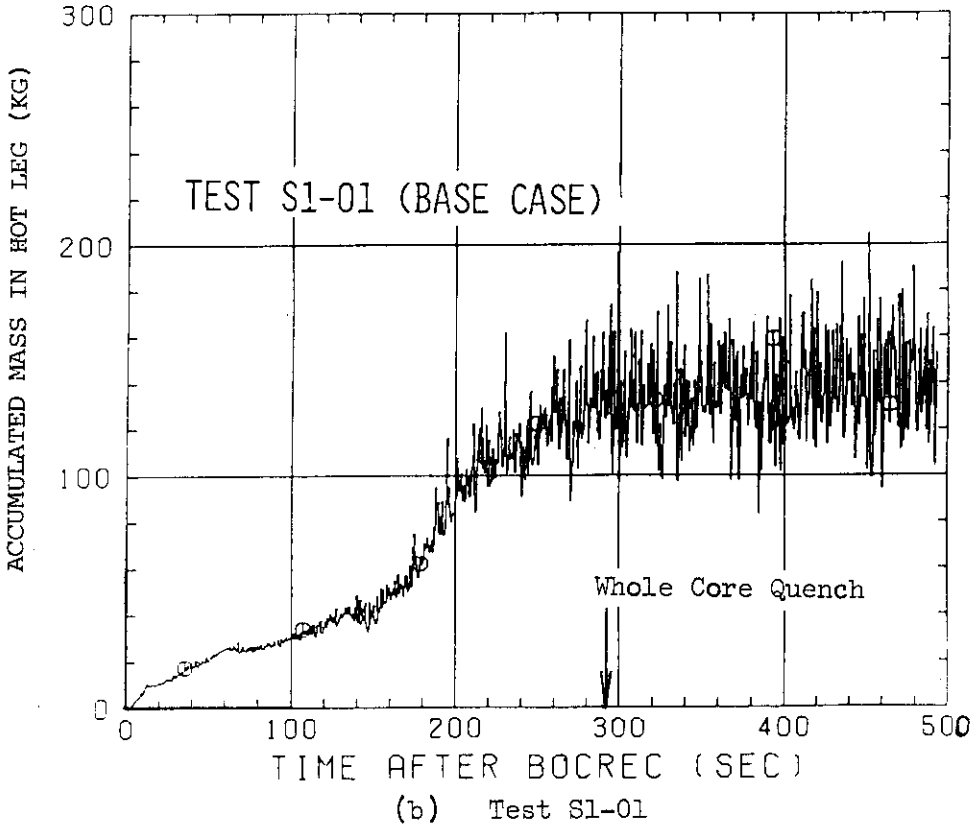

(b) Test S1-01

Fig.3.7 Mass of Water Accumulated in the Hot Leg

4. Core Thermal Behavior

4.1 Introduction

In this chapter, the effects of the water accumulation in the upper plenum on the core thermal behavior under forced-feed flooding condition are investigated.

The locations of thermocouples on the surface of the heater rods are shown in Fig. 4.1. The arrangement of the heater rods and non-heated rods is shown in Fig. 4.2.

Fig. 4.3 represents typical cladding temperature histories observed in Tests S1-03 and S1-01 and shows temperatures of heater rods located in the center of the blocked bundle (bundle 4). The thermocouple elevations are 1735, 1905, 2760 and 3190 mm above the bottom of the heated length. The first two thermocouples are located immediately upstream and downstream of the blockage sleeve, respectively, as shown in Fig. 4.3. It is noted from Fig. 4.3 that the cladding temperature behaviors are very similar in these two tests except a small difference at the upper part of the core.

In general, after reaching a mzximum value, the cladding temperature decreases slowly. Then, the temperature suddenly drops as marked with arrow in Fig. 4.3 and this phenomenon is called quench. The time from the BOCREC to the quench is defined as quench time and the temperature just before the quench is defined as quench temperature. The maximum temperature is called turnaround temperature. The time from the BOCREC to the maximum temperature is called turnaround time.

4.2 Quench Behavior

Typical quench envelope profiles for the blocked bundle (bundle 4) and the unblocked bundle (bundle 5) (See Fig. 2.4) are shown in Fig. 4.4. The effects of the blockage sleeves on the quench behavior are not significantly recognized in this figure.

During the tests, the quench front progressed upward from the bottom to the top (bottom quench) or downward from the top to the bottom (top quench). Below the elevation of 2330 mm (T/C elevations No. 1 through 7), the bottom quench was always observed. At the elevations of 2760 and 3190 mm (No. 8 and 9), the top quench occurred at the specific heater rods (1D, 1B, and 2B regions in Fig. 4.1) though the bottom quench is still dominant. At the elevation of 3620 mm (T/C No. 10), the top quench always occurred in all bundles.

It is seen from Fig. 4.4 that the bottom quench velocity is almost the same for the both tests, however, top quench in Test S1-03 is delayed in comparison with Test S1-01. The top quench occurs due to a precursory cooling by water droplets coming from the lower part of the core and by fall back water from the upper plenum. As described in Chapter 2, the amount of water accumulation in the upper plenum was clearly smaller in Test S1-03 especially after about 160 seconds from the BOCREC because of the water extraction from the upper plenum. It is, therefore, suggested from the comparison of the top quench behavior between these two tests that the amount of fall back water from the upper plenum through the UCSP into the the core depends on the water level in the upper plenum.

Top quench tends to occur randomly and sometimes does not show a rapid drop but a slow one in temperature, so that the quench time and temperature of top quench are not clearly defined while the bottom quench propagates almost monotonously for the eight bundles and the quench time and temperature to bottom quench can be clearly defined. In order to distinguish the thermal characteristics for bottom quench from those for top quench, comparison between Tests S1-03 and S1-01 are made for two groups with respect to heater elevations, one for the thermocouple elevations No. 1 to 7 and the other for the thermocouple elevations No. 8 to 10 in the following discussions.

Fig. 4.5 shows the comparison of the quench times which were obtained for the same thermocouples in Tests S1-03 and S1-01. For the thermocouple elevations No. 1 to 7 (left figure in Fig. 4.5), there is no significant difference in the quench times between the two tests. On the other hand, the quench times for the thermocouple elevations No. 8 to 10 (right figure in Fig. 4.5) tend to be longer in Test S1-03 than in Test S1-01. Fig. 4.6 shows the comparison of radial distribution of quench time in the upper part of the core. This figure also shows the above-mentioned trend clearly in the radial distribution of quench time in the upper part of the core. This trend is considered to be due to less fall back of water from the upper part of the core in case of less water accumulation in Test S1-03. Some heater rods adjacent to non-heated rods (1D and 2B locations in Fig. 4.1, which are marked with symbol □ in Fig. 4.6) exhibited earlier quench at 3160 mm above the bottom of heated length of rod than the others at the same elevation. The effect of non-heated rod on the early quench phenomenon has been already discussed in reference (5). Fig. 4.6 also shows that the top quench times in bundle 1 and 8 are significantly shorter than those in the other bundles especially for Test S1-03, suggesting the wall effect for

heat transfer.

The quench temperatures of Test S1-03 are compared with those of Test S1-01 in Fig. 4.7. No significant difference in the quench temperature can be recognized between the two tests though scattering for TC elevations 8 to 10 is observed which should be due to the random top quench at the upper part of the core.

Fig. 4.8 shows the comparison of quench velocities (which is defined with moving velocity of quench front) at the thermocouple elevations 2 to 6. The quench velocity was obtained as the average quench velocities between the thermocouples just below and above the thermocouple elevation where the quench velocity was investigated. From Fig. 4.8, no significant effect of the amount of water accumulated in the upper plenum can be recognized on the quench velocity for the bottom quench.

4.3 Turnaround Time, Turnaround Temperature, Temperature Rise from BOCREC and Temperature at BOCREC

Fig. 4.9 and 4.10 show the comparison of turnaround temperature and turnaround time. No significant difference in the turnaround time and temperature can be recognized between the two tests though scattering is observed for TC elevations 8 to 10 at the upper part of the core.

Since the BOCREC is the beginning of the reflooding, the temperature rise from the GOCREC to the turnaround is an important value in the analysis of the test results. The comparison plots of the temperature rise from the BOCREC to the turnaround and the cladding temperature at the time of BOCREC are presented in Figs. 4.11 and 4.12, respectively.

These figures show that the temperature in Test S1-03 is slightly higher and that the turnaround temperature becomes almost the same for the two tests because the temperature at the BOCREC (initial temperature for reflood) in Test S1-03 is slightly lower in the same magnitude as the temperature rise.

4.4 Summary

(1) The amount of water accumulated in the upper plenum has no significant effect on the core thermal behavior below the elevation of 2330 mm where the quench progressed only upward from the bottom of the core.

(2) The top quench was clearly observed in Test S1-03 (water extracted) above the elevation 2760 mm in spite of smaller amount of water accumulated in the upper plenum. The quench time at the upper part

of the core, however, became longer in Test S1-03 due to smaller amount of water accumulated in the upper plenum.

(3) In Test S1-03, the temperature rise from the BOCREC to turnaround was slightly higher, but no significant effect of water accumulated in the upper plenum was recognized on the turnaround temperature because the turnaround temperature became almost the same for the two tests with slightly lower temperature at the BOCREC in Test S1-03 than in Test S1-01.

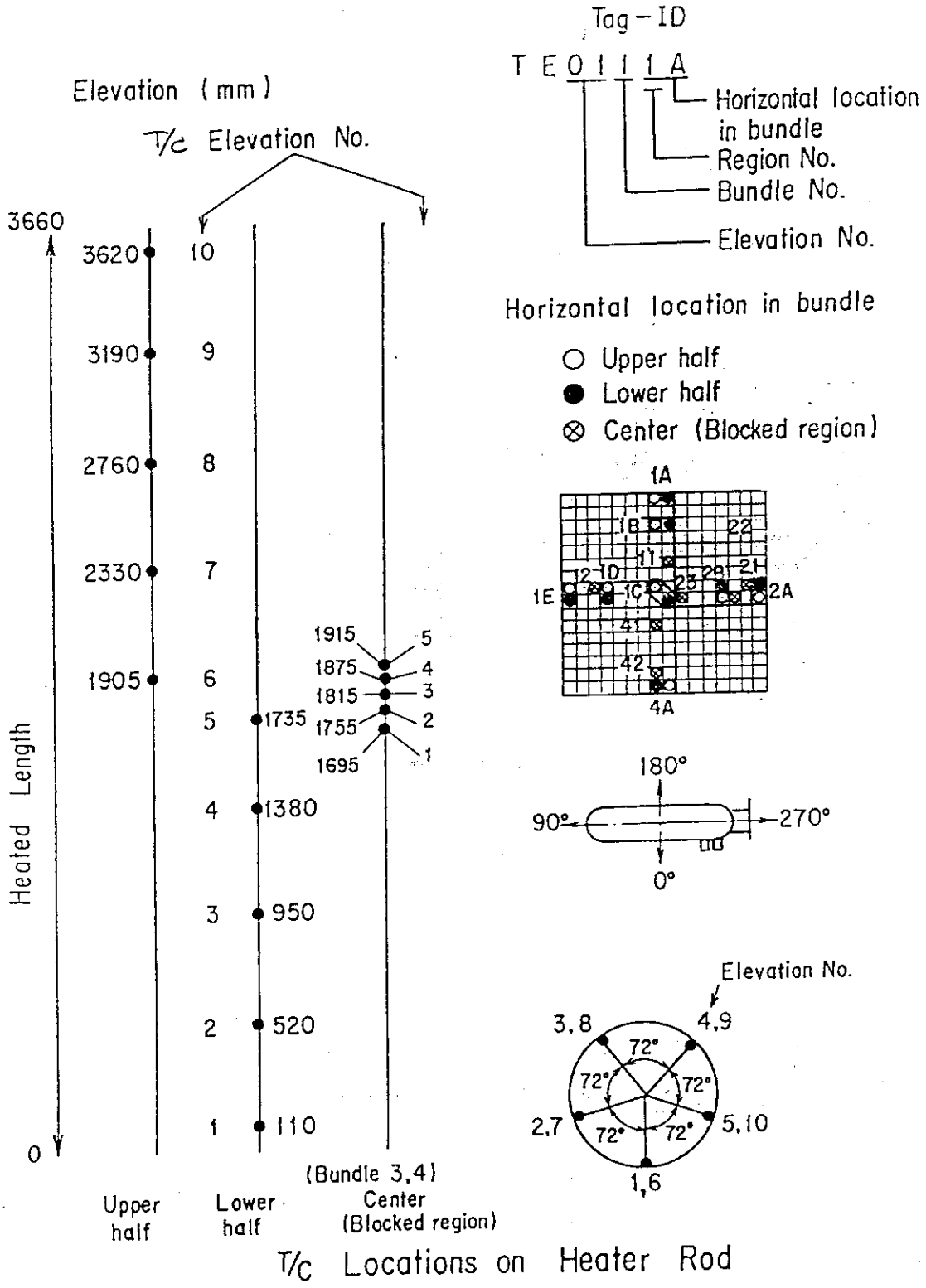

Fig.4.1 Measurement Locations of Heater Rod Surface Temperature.

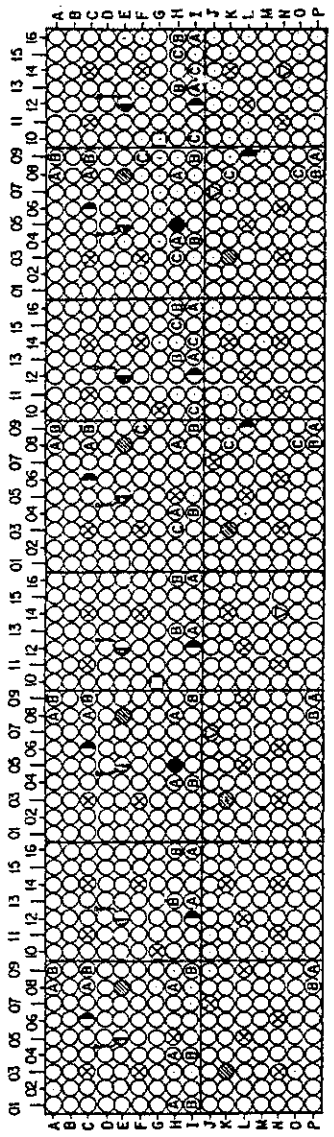

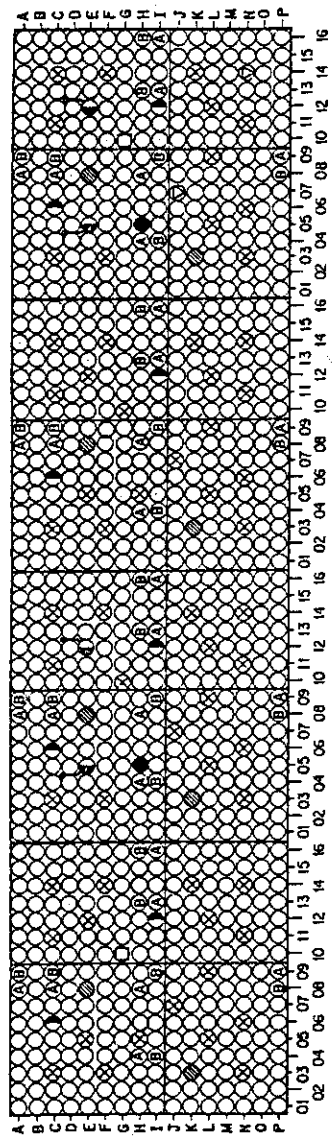

Bundle No.		1	2	3	4	5	6	7	8	Total	Symbol
Heater Rod Surface Temp.		16	14	21	21	14	14	14	14	128	Ⓐ Ⓑ Ⓒ
Heater Rod with No Instrument		218	220	213	213	220	220	220	220	1744	○
Non Heated Rod With Instrument	Surface Temp.	2	2	3	3	2	2	2	2	18	◐
	Fluid Temp.	2	2	2	2	2	2	2	2	16	⊘
	Steam Temp.	2	2	2	2	—	2	—	2	12	◑
	Film Probe	—	2	—	2	—	—	—	2	6	⊘
	Flag Probe	—	1	—	1	1	—	—	1	4	○
	L L D	—	1	—	1	—	1	—	1	4	●
Tie Rod		16	12	15	11	17	15	18	12	116	⊗
Total		256	256	256	256	256	256	256	256	2048	

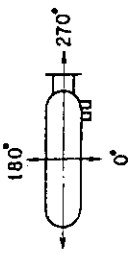

Fig.4.2 Horizontal Arrangement of Instrumented Rods.

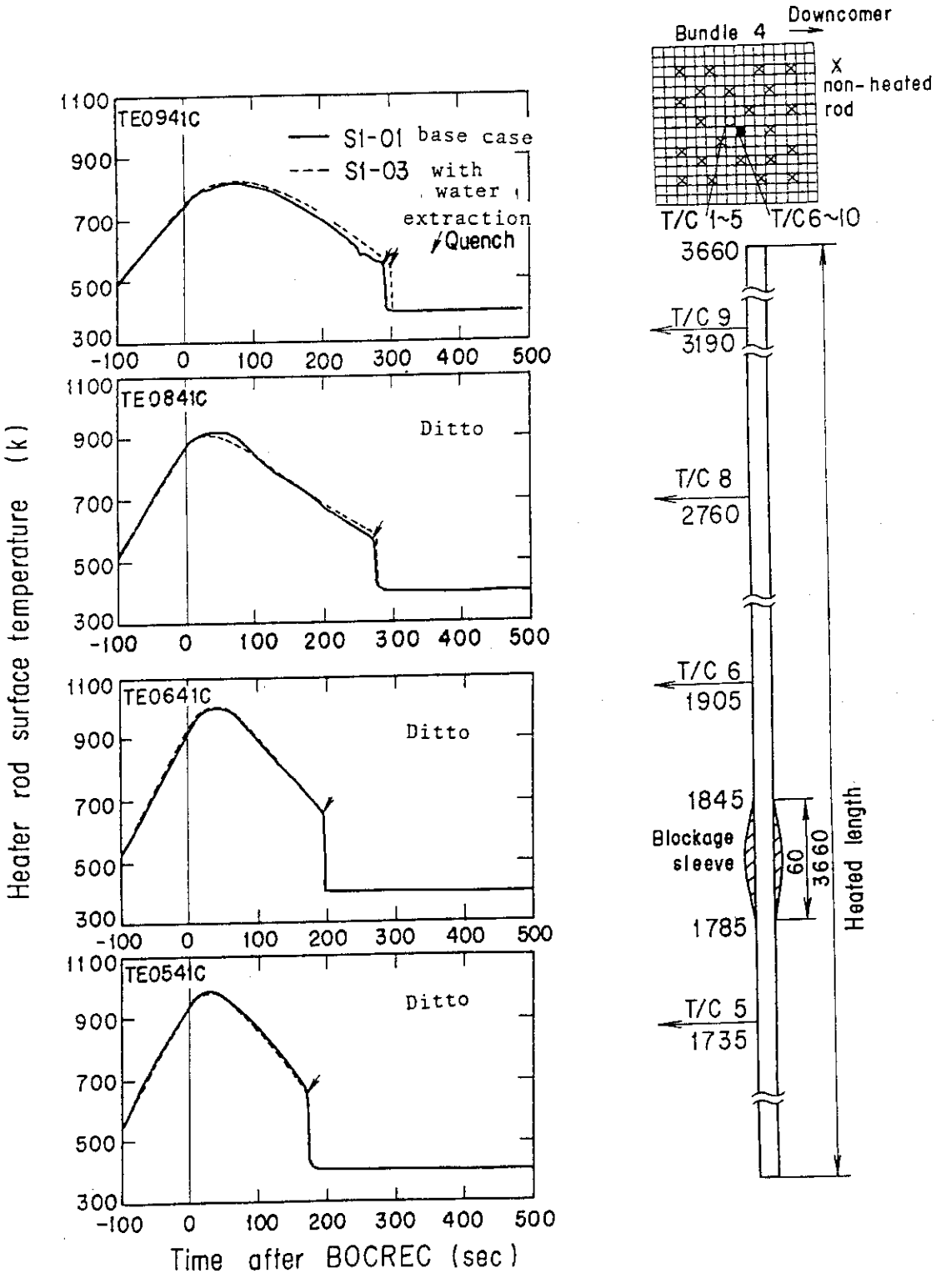

Fig.4.3 Typical Cladding Temperature Histories in Tests S1-03 and S1-01.

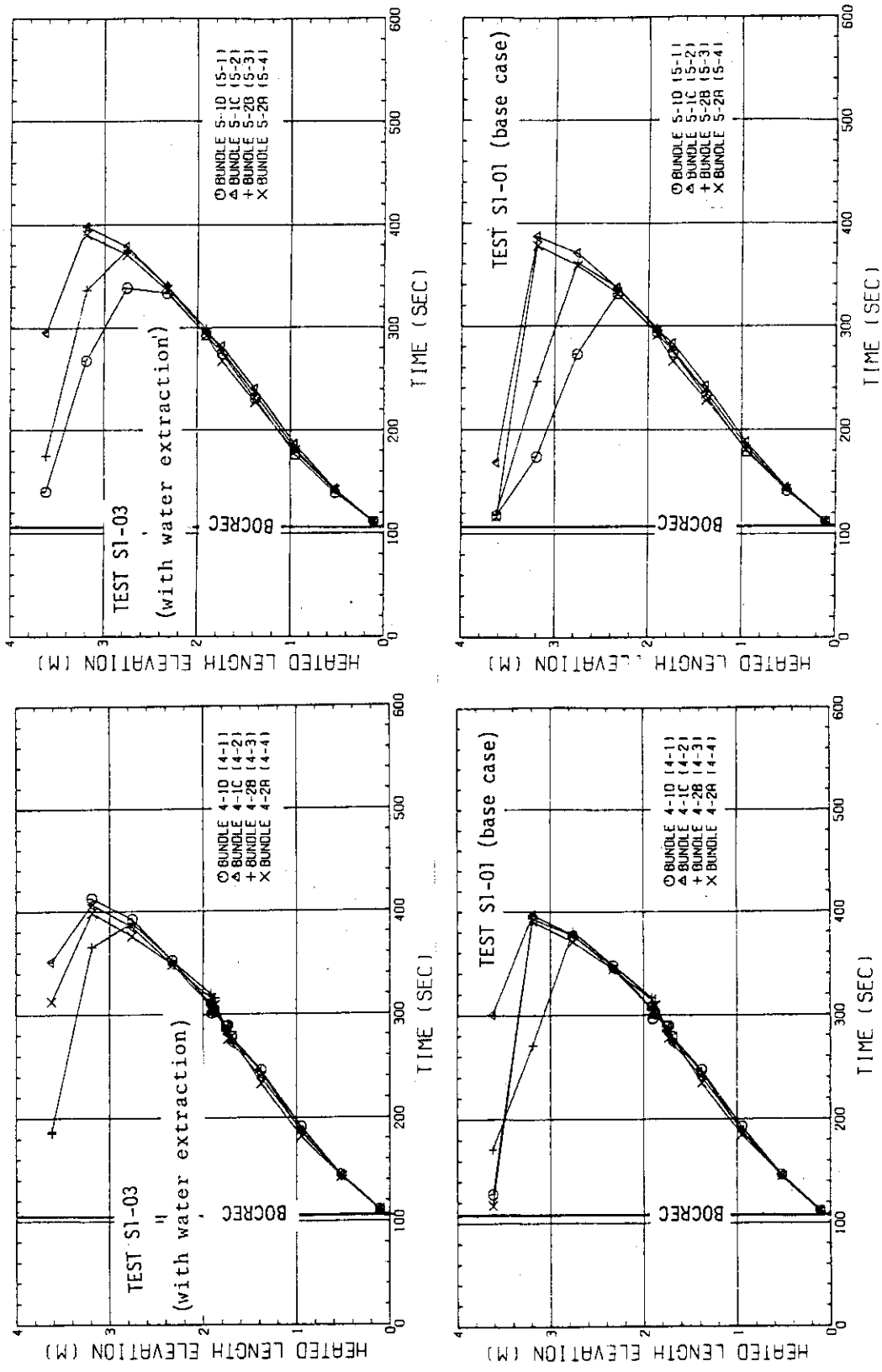

(a) blocked bundle (b) unblocked bundle

Fig.4.4 Comparison of Typical Quench Envelope with Base Case.

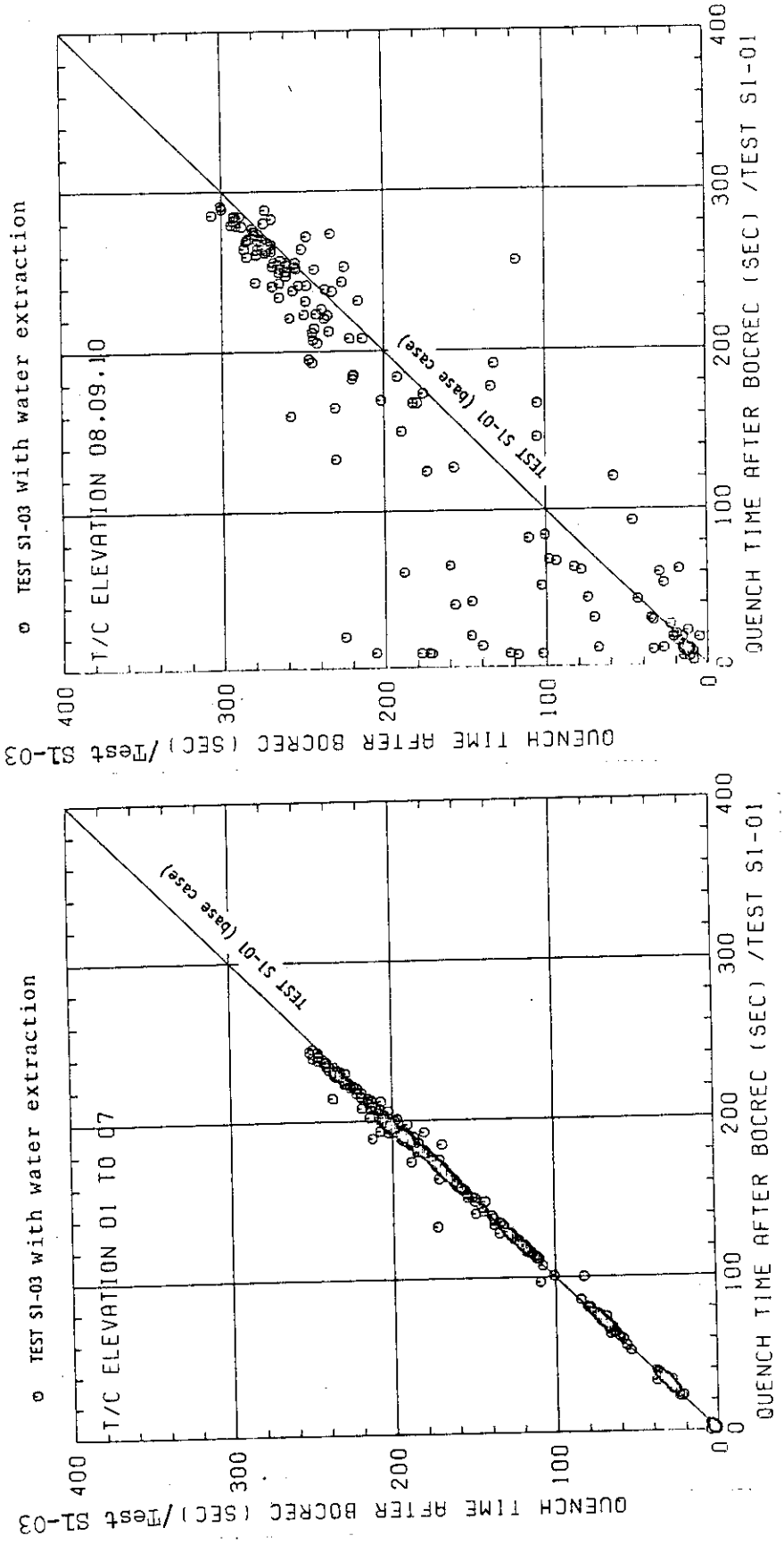

Fig.4.5 Effect of Water Accumulation above UCSP on Quench Time.

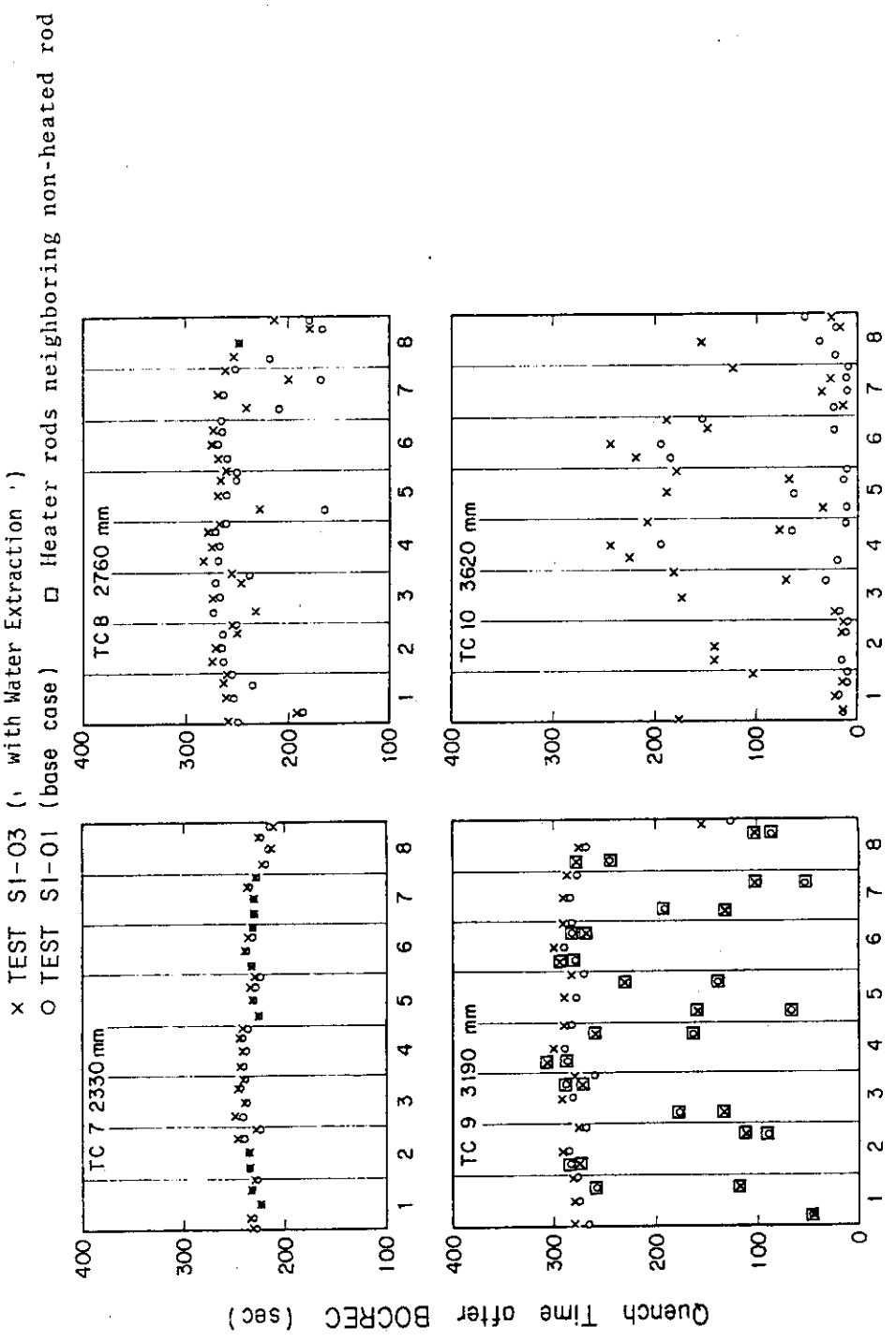

Fig.4.6 Comparison of Radial Distribution of Quench Time in the Upper Part of Core.

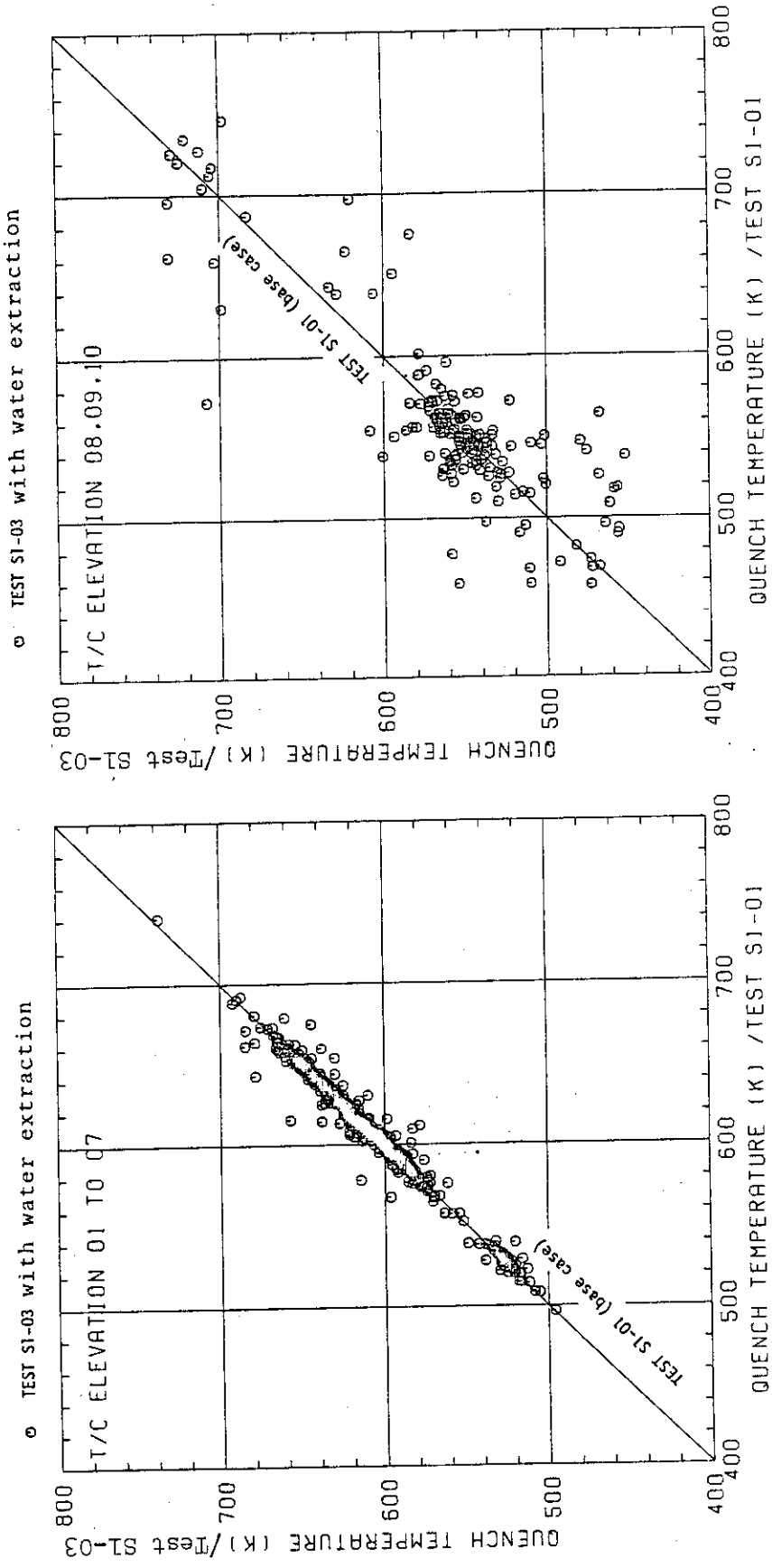

Fig.4.7 Effect of Water Accumulation above UCSP on Quench Temperature.

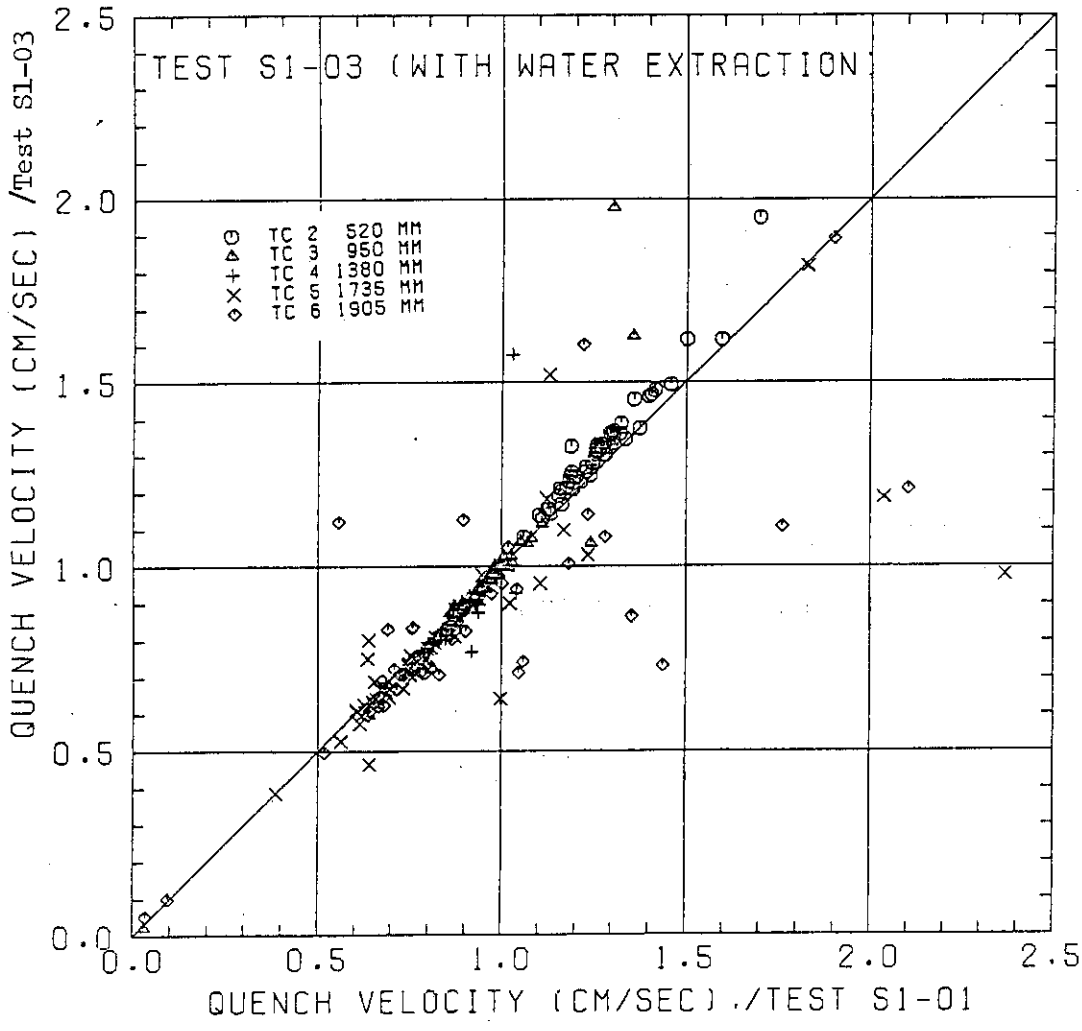

Fig.4.8 Effect of Water Accumulation above UCSP on Bottom Quench Velocity.

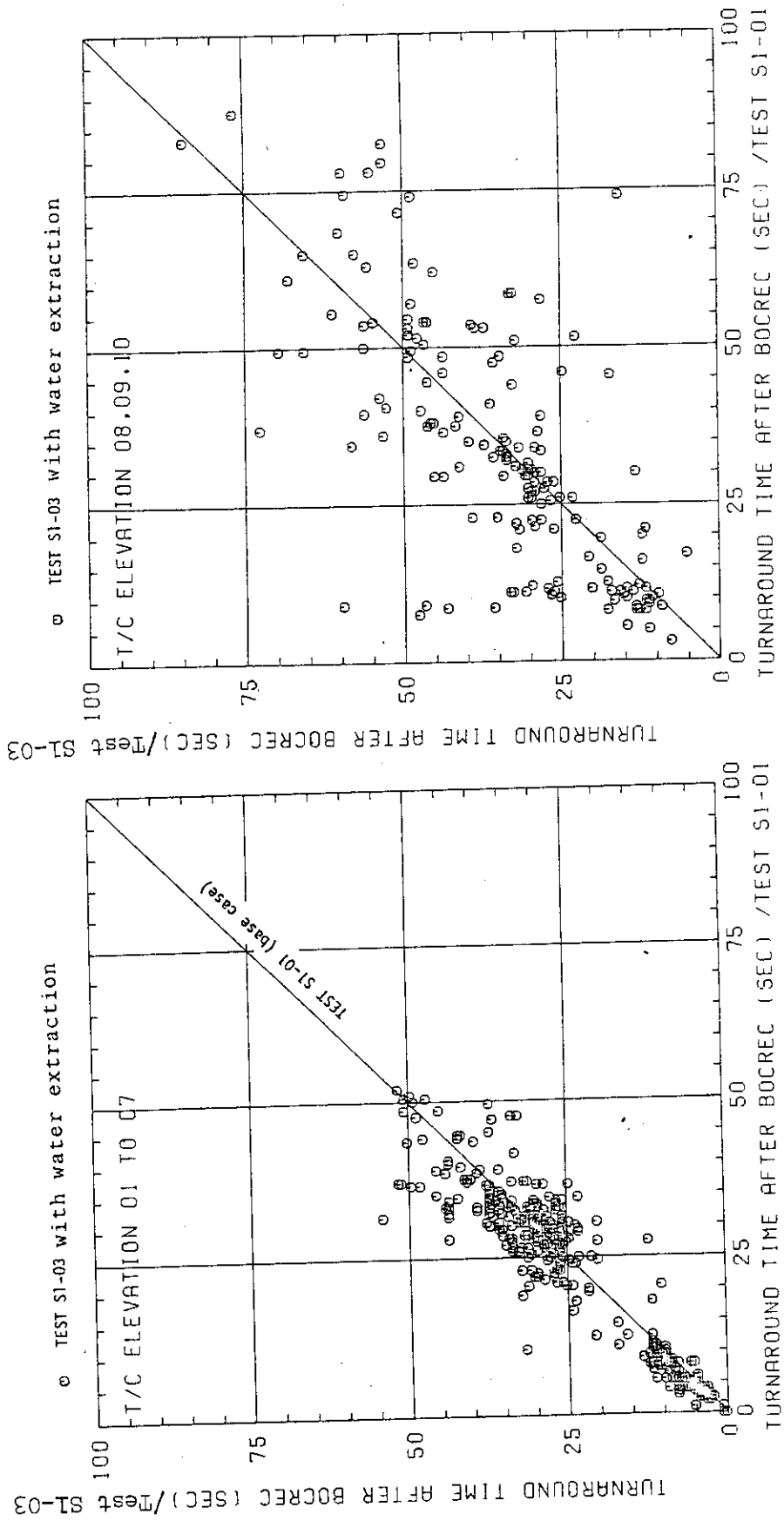

Fig.4.9 Effect of Water Accumulation above UCSP on Turnaround Time.

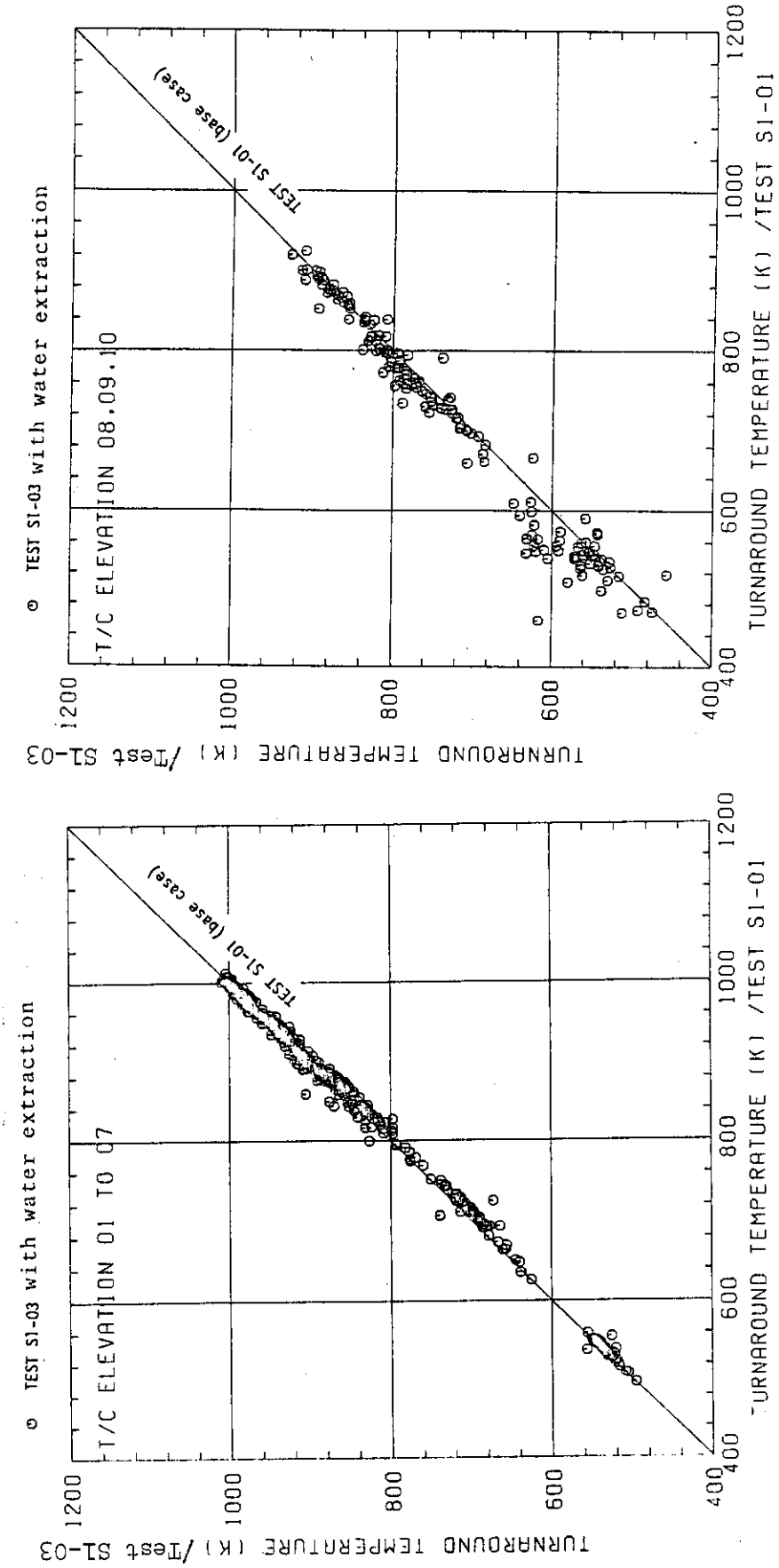

Fig.4.10 Effect of Water Accumulation above UCSP on Turnaround Temperature.

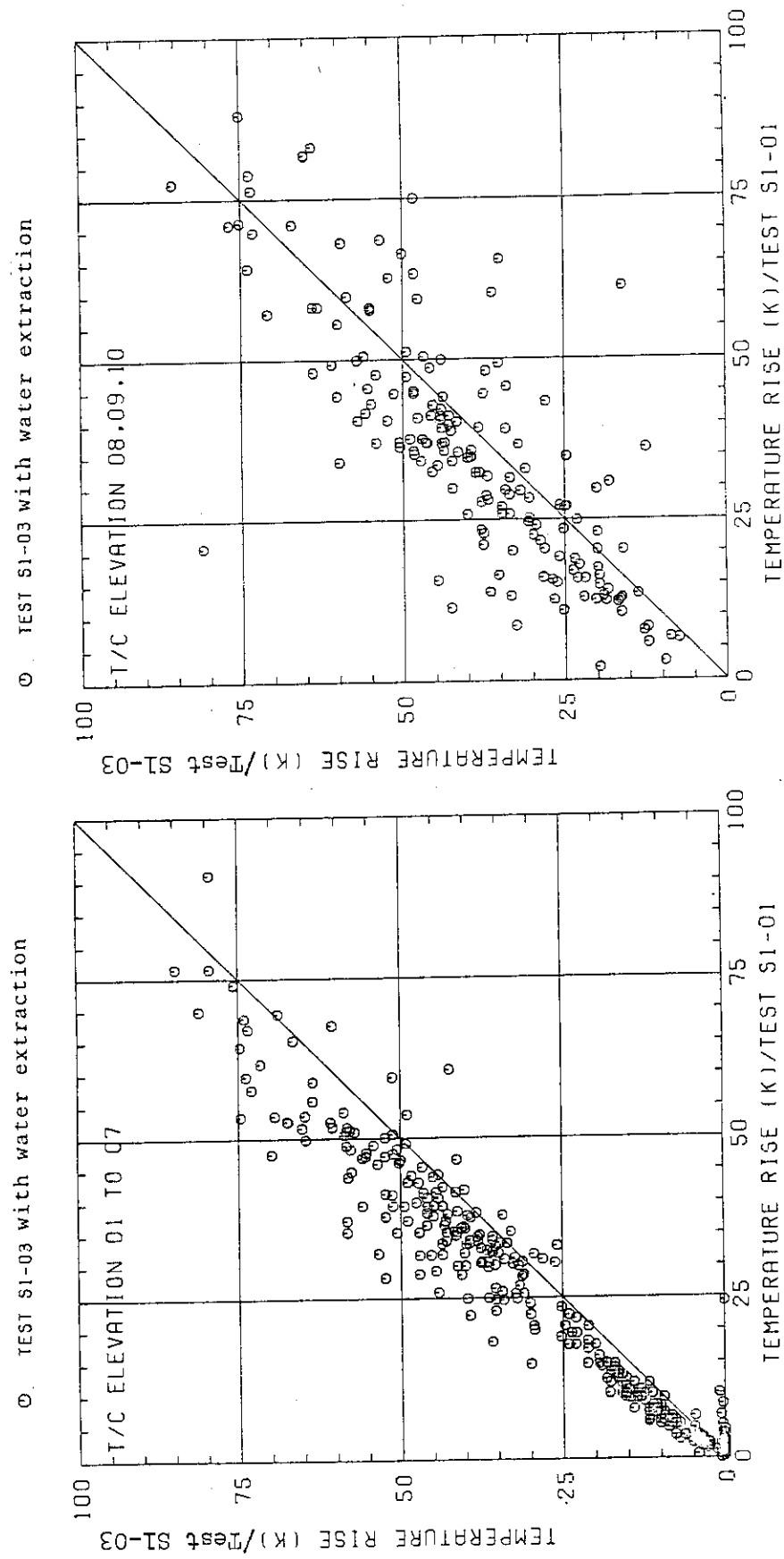

Fig.4.11 Effect of Water Accumulation above UCSP on Temperature Rise from BOCREC to Turnaround.

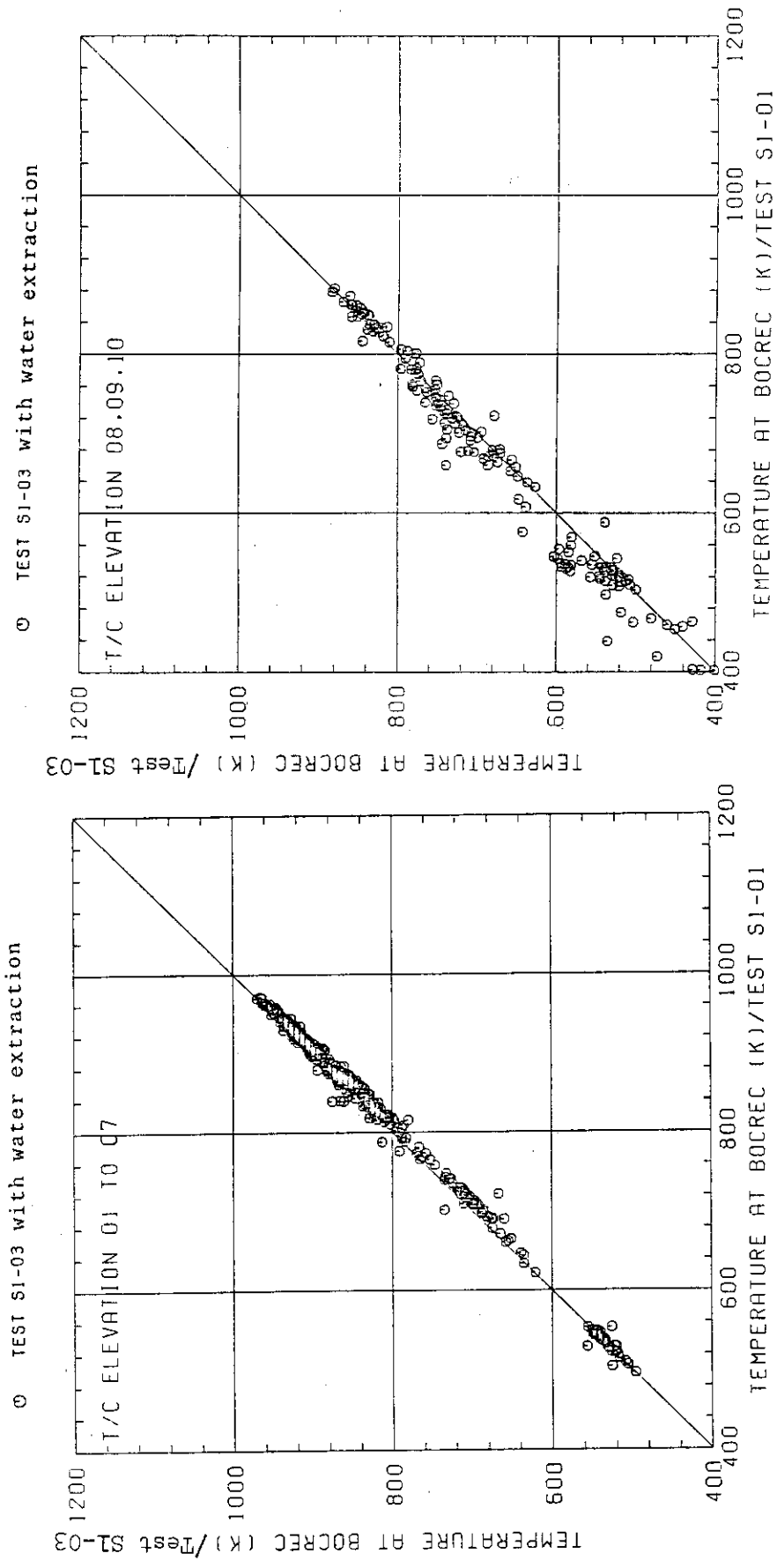

Fig.4.12 Comparison of Cladding Temperatures at BOCREC.

5. Core Heat Transfer

5.1 Introduction

Heat transfer above the quench front during the reflood phase is important because it determines the peak cladding temperature. Heat transfer calculation code HEATQ was developed for the analysis of the SCTF test. The temperature dependence of the physical properties and the axial heat conduction along the heater rod were considered in this code.

The typical transients of heat transfer coefficients at the elevations 950, 1735 and 2760 mm above the bottom of heated length are discussed in this chapter.

5.2 Effect of Upper Plenum Water Extraction

Shown in Figs. 5.1, 5.2 and 5.3 are the comparison of calculated heat transfer coefficients at three different elevations 950, 1735 and 2760 mm above the bottom of heated length for bundle 2. The bottom quench was observed at elevations 950 and 1735 mm. On the other hand, the top quench was observed at elevation 2760 mm. The results of Test S1-03 are presented in these figures along with those of Test S1-01. The transient of the heat transfer coefficient in Test S1-03 at each of the three elevations is nearly the same as Test S1-01. The heat transfer coefficient at bundle 4 is also the same as Test S1-01 as shown in Fig. 5.4. It is, however, considered that the difference in magnitude of upper plenum water accumulation should cause the difference in magnitude of water fall back from the upper plenum into the core. The difference in magnitude of water fall back would then cause the difference in water fraction $(1-\alpha)$ (α: void fraction) especially at the upper part of the core. Therefore, the water fraction between elevations 2695 and 3235 mm was investigated. Figure 5-5 shows the comparison of water fraction $(1-\alpha)$ between Tests S1-03 and S1-01. Water fraction measured between elevations 2695 and 3235 mm is smaller in Test S1-03 than in Test S1-01 as expected by the smaller amount of falling water from the upper plenum into the core.

Bromley[8] developed the theory for the film boiling heat transfer on the vertical heated surface,

$$h = h_{sat} + 3/4\ h_R \quad , \tag{5-1}$$

where $h_{sat} = C[\lambda_g^3 \rho_g (\rho_\ell - \rho_g) H_{fg}' g/(L_Q \mu_g \Delta T_{sat})]^{1/4}$

$H_{fg}' = H_{fg}[1+0.4C_p \Delta T_{sat}/H_{fg}]^2$

h : Heat transfer coefficient (W/m^2)
λ : Thermal conductivity ($W/(m \cdot k)$)
ρ : Density (kg/m^3)
g : Acceleration due to gravity (m/s^2)
μ : Dynamic viscosity ($Pa \cdot s$)
ΔT_{sat} : Superheat (k)
L_Q : Distance from the quench front (m)
H_{fg} : Latent heat of evaporation (J/kg)
h_R : radiation heat transfer coefficient given by

$$h_R = \sigma \{(\frac{T_w}{100})^4 - (\frac{T_{sat}}{100})^4\} / (T_w - T_{sat}),$$

where T_w : Cladding temperature (k)
T_{sat} : Saturation temperature (k)
σ : Stefan - Boeltsman Constant ($w/(cm^2 \cdot k^4)$)

The constant C lies between 0.5 and 0.707 by the laminar theory of the vapor film. Equation (5-1) can be written as follows.

$$C = (h - 3/4\ h_R)/[\lambda_g^3 \rho_g (\rho_\ell - \rho_g) H_{fg}' g/(L_Q \mu_g \Delta T_{sat})]^{1/4} \qquad (5\text{-}2)$$

The measured heat transfer coefficient h was substituted into Eq. (5-2) to obtain C. The constant C obtained thus at elevation 2760 mm for bundle 4 is shown in Fig. 5.6. The constant C near the quench front is between 0.6 and 0.9. There is no significant difference in C between Tests S1-03 and S1-01 except for the first 70 s after the BOCREC. The effects of void fraction on the constant C in Eq. (5-2) were investigated as shown in Fig. 5.7. This figure also show no significant difference in dependence of C on void fraction between Test S1-03 and Test S1-01. Therefore, it is concluded that the effects of difference in void fraction is rather small so that the heat transfer coefficients are nearly the same at the elevation 2760 mm in Test S1-03 as in Test S1-01.

It should be mentioned here what effect the scattered top quench times

observed in Fig. 4.5 give to the histories of heat transfer coefficient between the two tests. Fig. 5.8 shows the histories of heat transfer coefficients for the top quenches at the elevation 3190 mm at bundle 4 for the two tests. The heat transfer coefficient in Test S1-03 is a little lower than in Test S1-01 before the quench occurs in Test S1-01. The reason why the heat transfer is higher in Test S1-01 than in Test S1-03 is considered that the more water falls back from the upper plenum into the core in Test S1-01 than in Test S1-03 for this case. However, some thermocouples show earlier quench in Test S1-03 than in Table S1-01. It is considered that top quench would occur strongly depending on the local fluid condition and then it occurs at random.

5.3 Summary

(1) The transients of the heat transfer coefficients are narly the same in Test S1-03 as the base case test.

(2) Water fraction ($1-\alpha$) at the elevation 2760 mm is a little smaller in Test S1-03 compared with the base case test. But this does not affect the heat transfer coefficient.

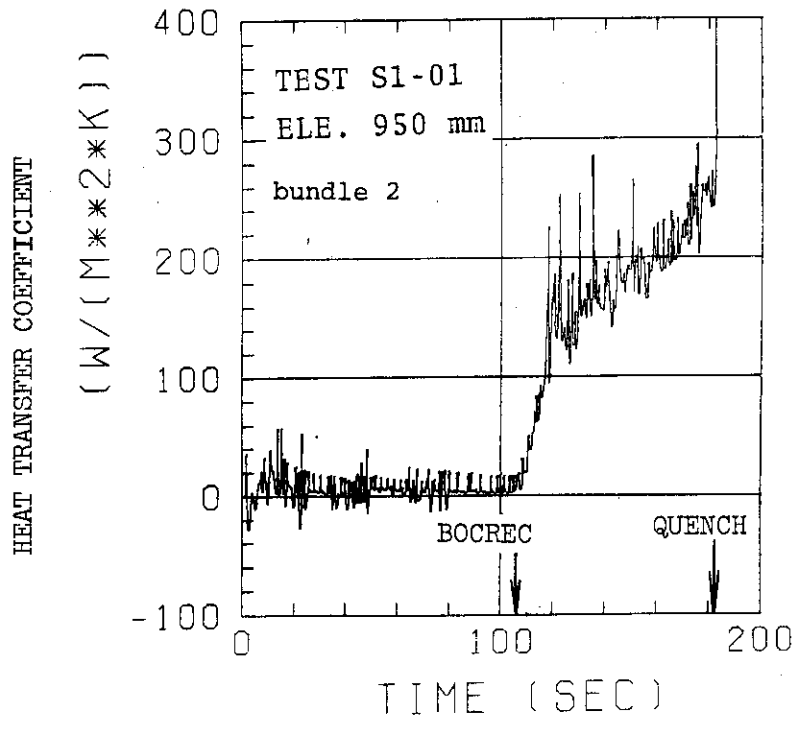

(a) Test S1-01

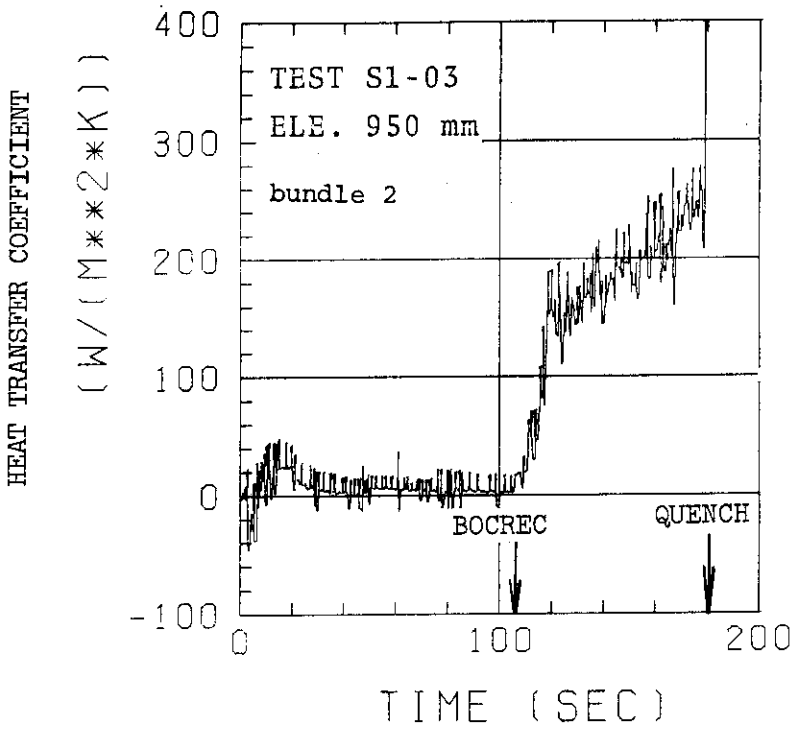

(b) Test S1-03

Fig.5.1 Heat transfer coefficient at elevation 950 mm

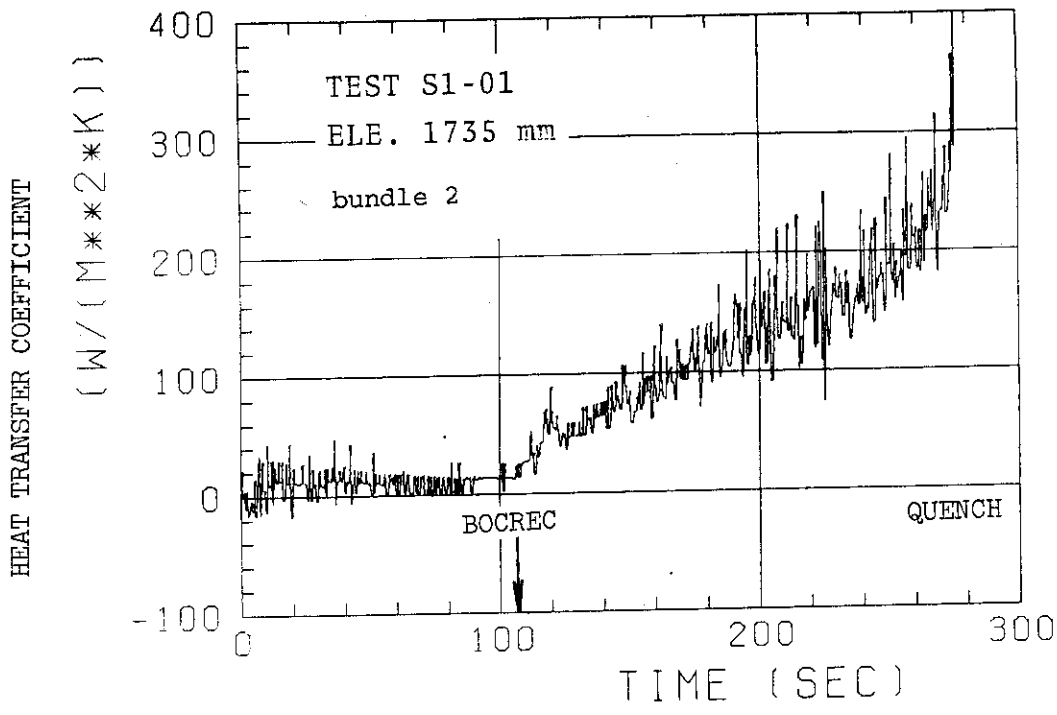

(a) Test S1-01

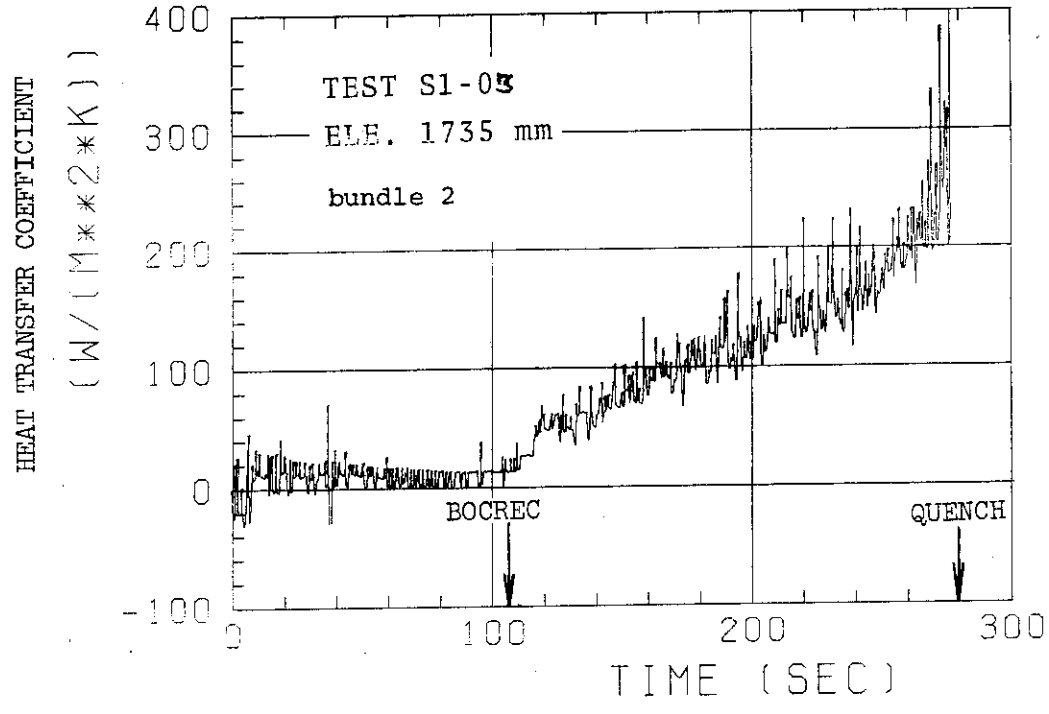

(b) Test S1-03

Fig.5.2 Heat transfer coefficient at elevation 1735 mm

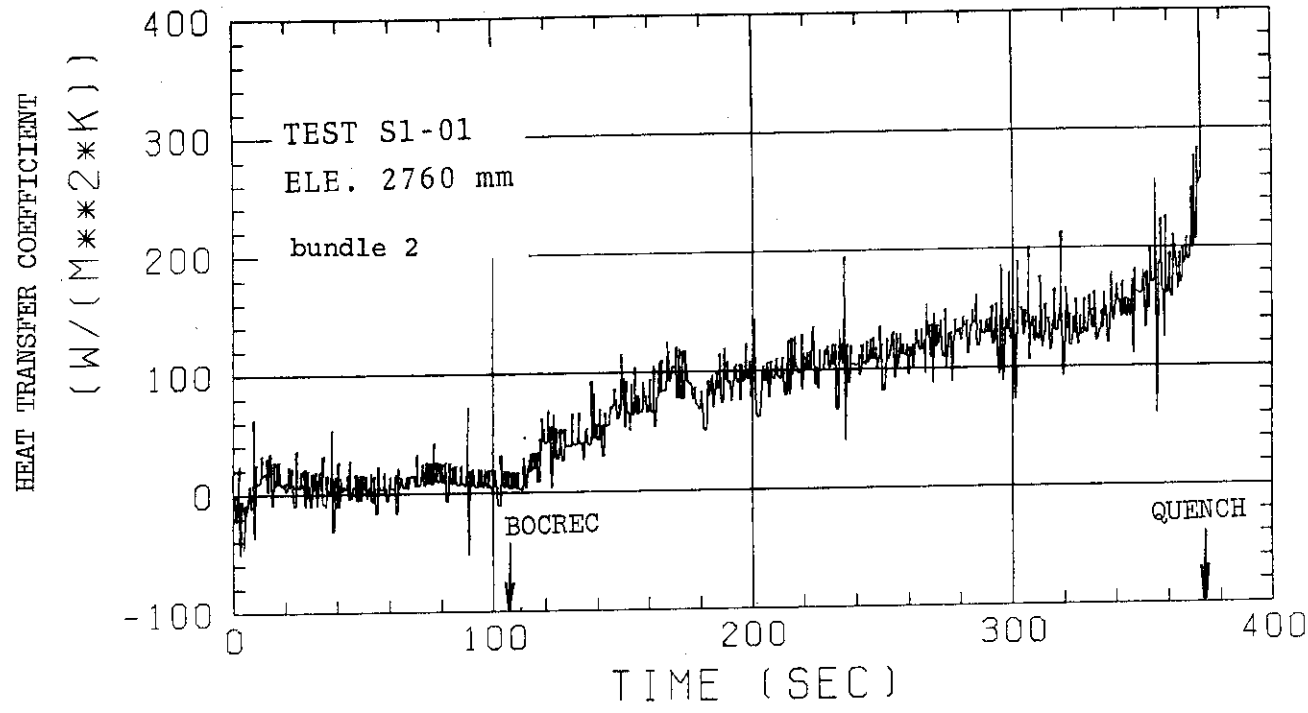

(a) Test S1-01

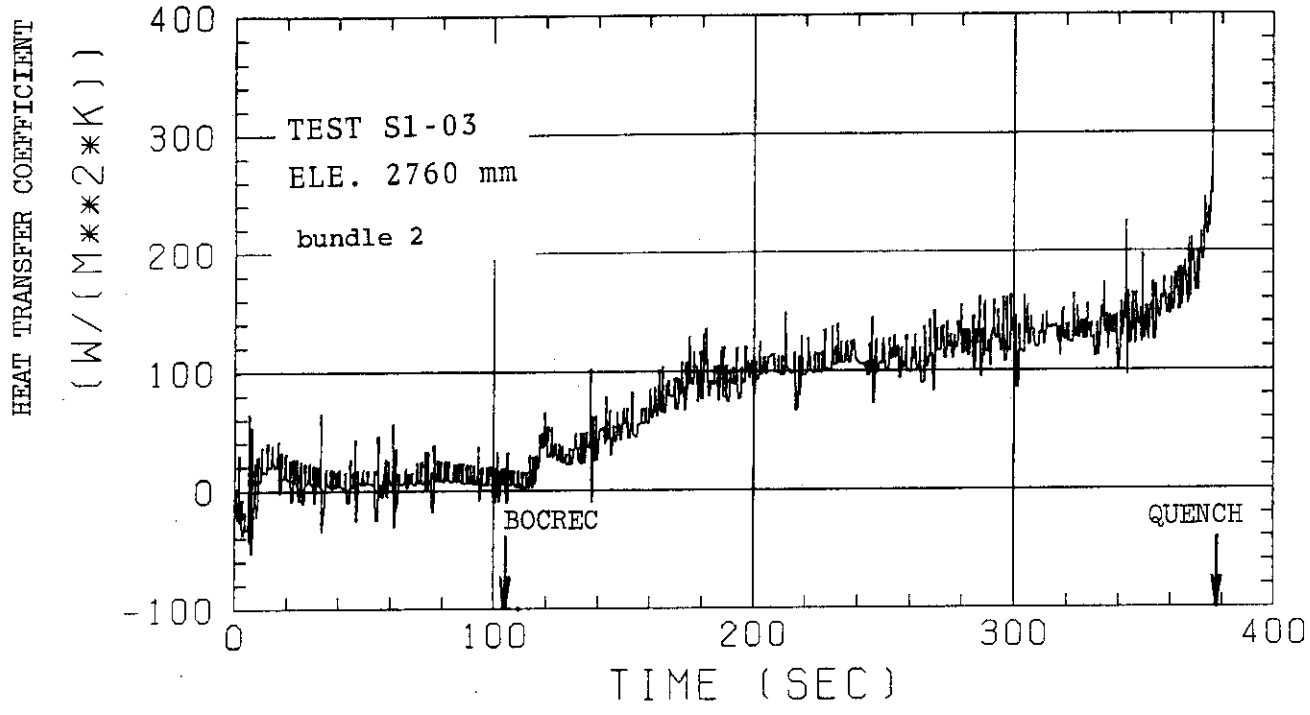

(b) Test S1-03

Fig.5.3 Heat transfer coefficient at elevation 2760 mm (Bundle 2)

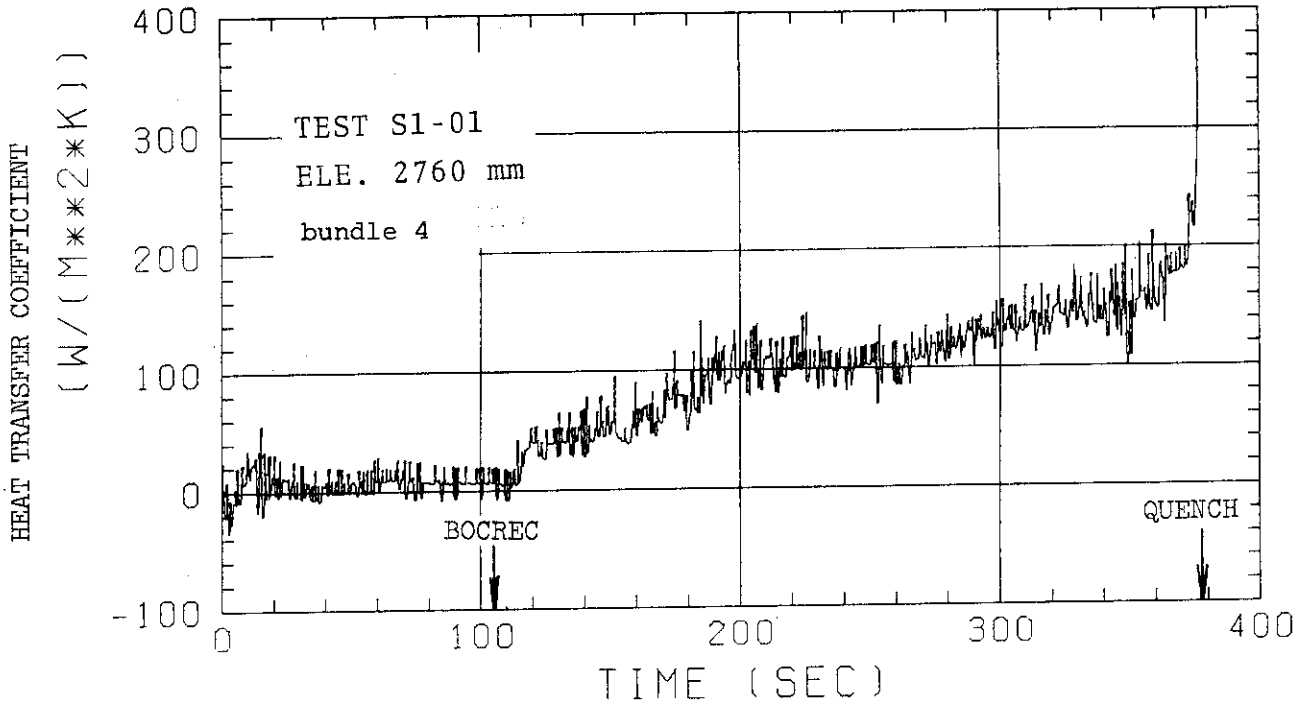

(a) Test S1-01

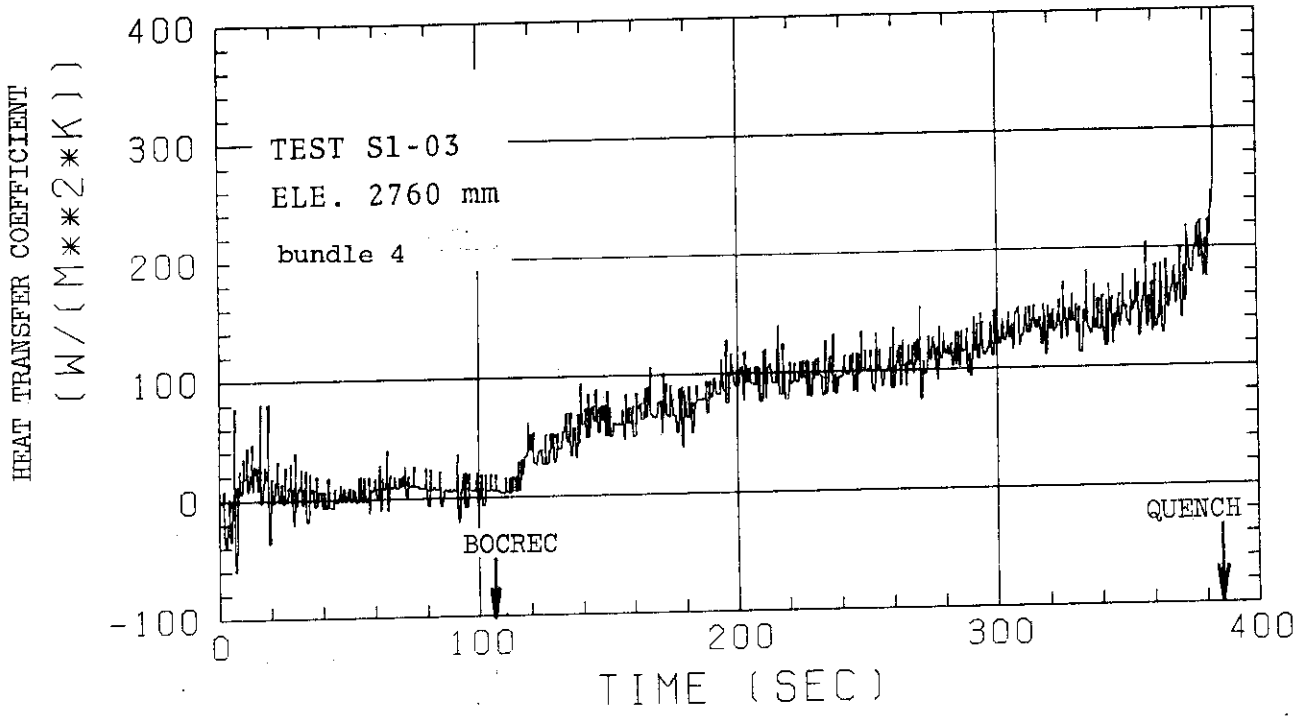

(b) Test S1-03

Fig.5.4 Heat transfer coefficient at elevation 2760 mm (Bundle 4)

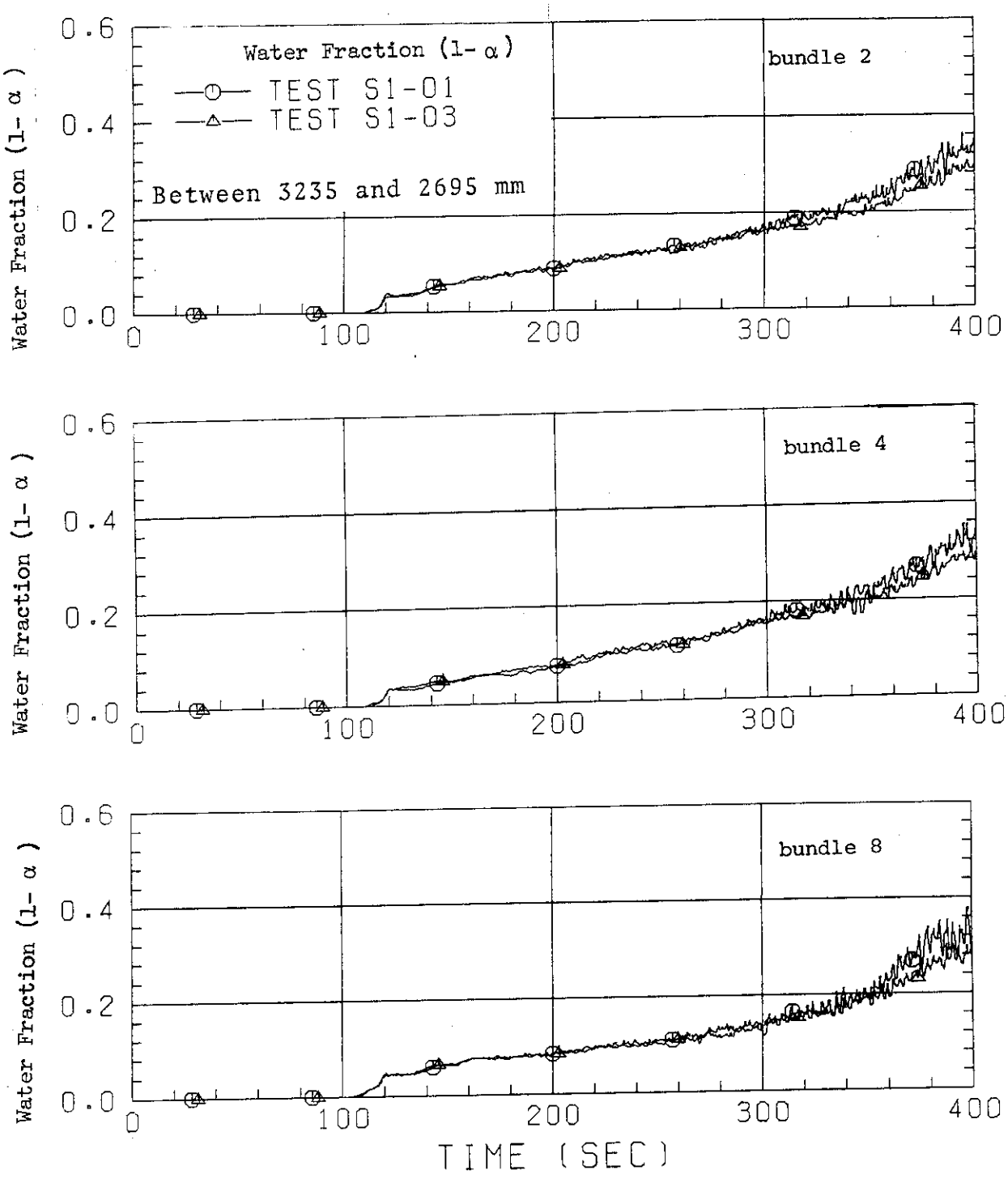

Fig.5.5 Water fraction history at bundle 2, 4, and 8 between 3235 and 2695 mm

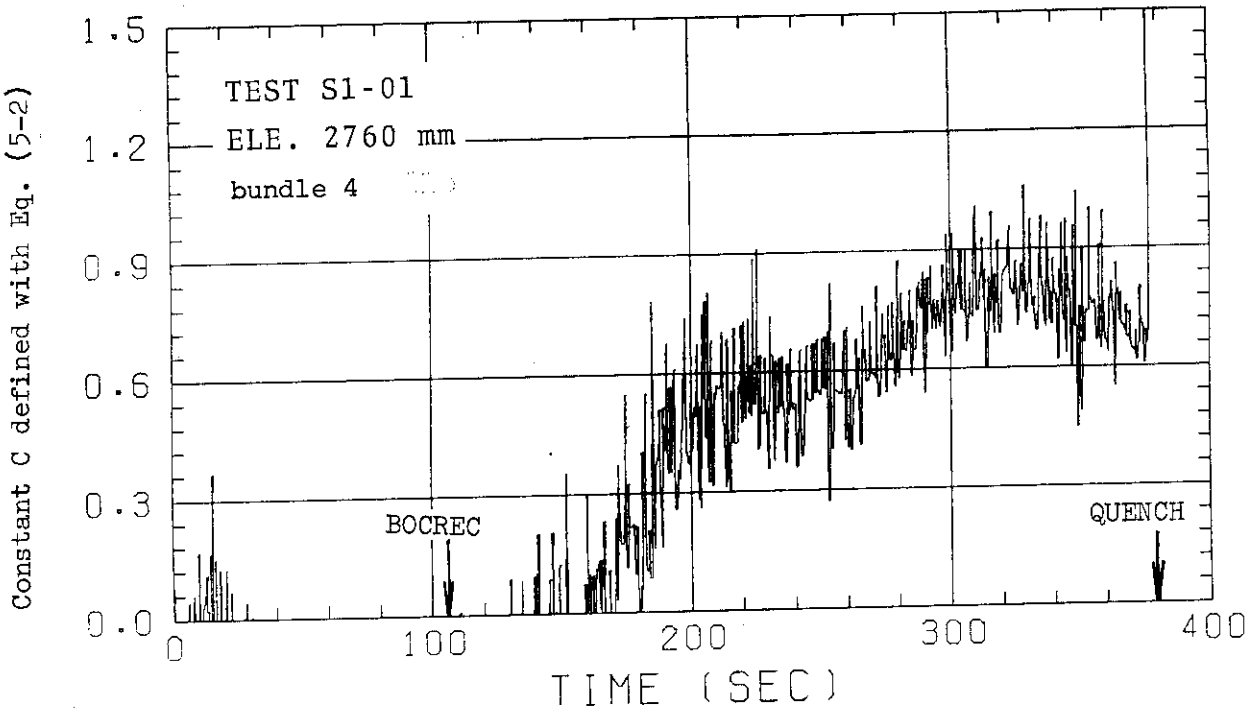

(a) Test S1-01

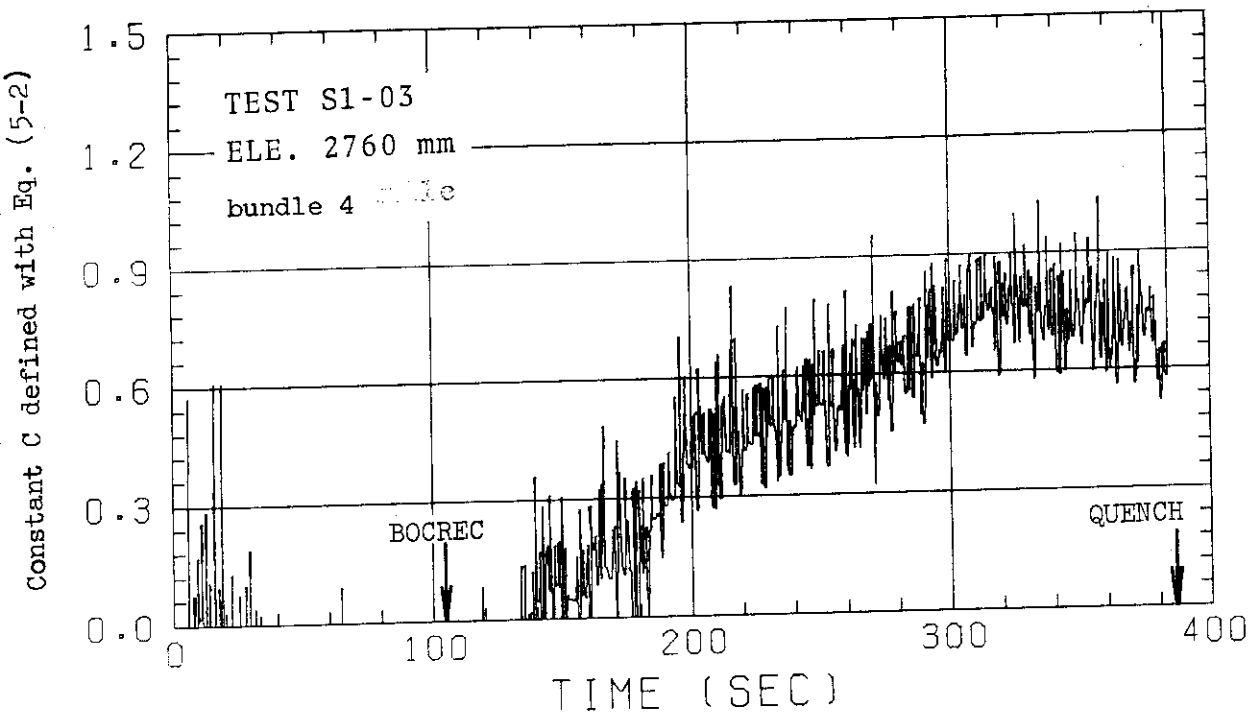

(b) Test S1-03

Fig.5.6 History of constant C defined with Eq. (5-2) at elevation 2760 mm

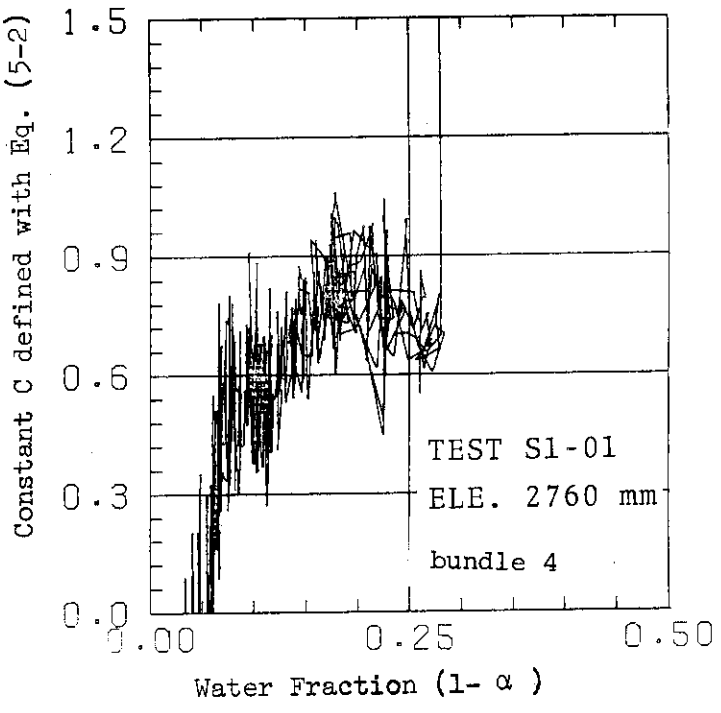

(a) Test S1-01

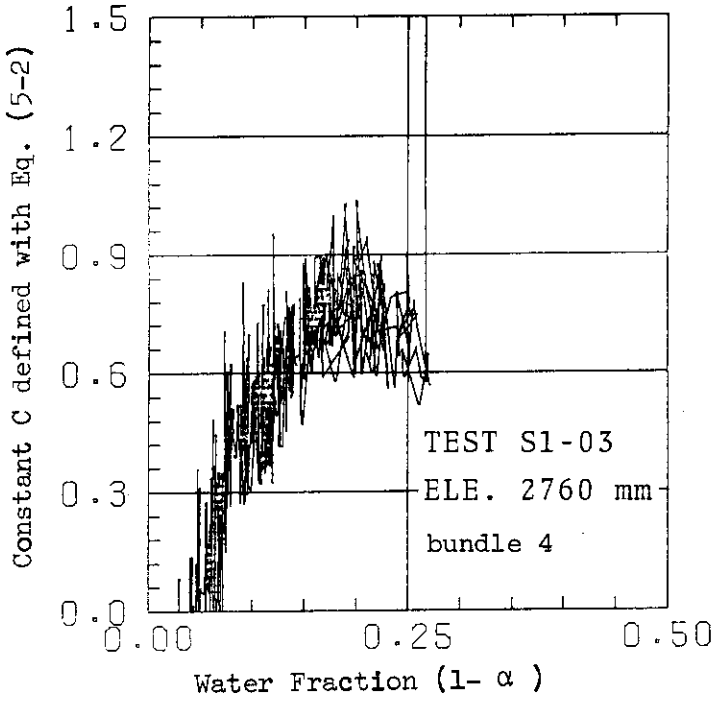

(b) Test S1-03

Fig.5.7 Relation of constant C defined with Eq. (5-2) vs water fraction

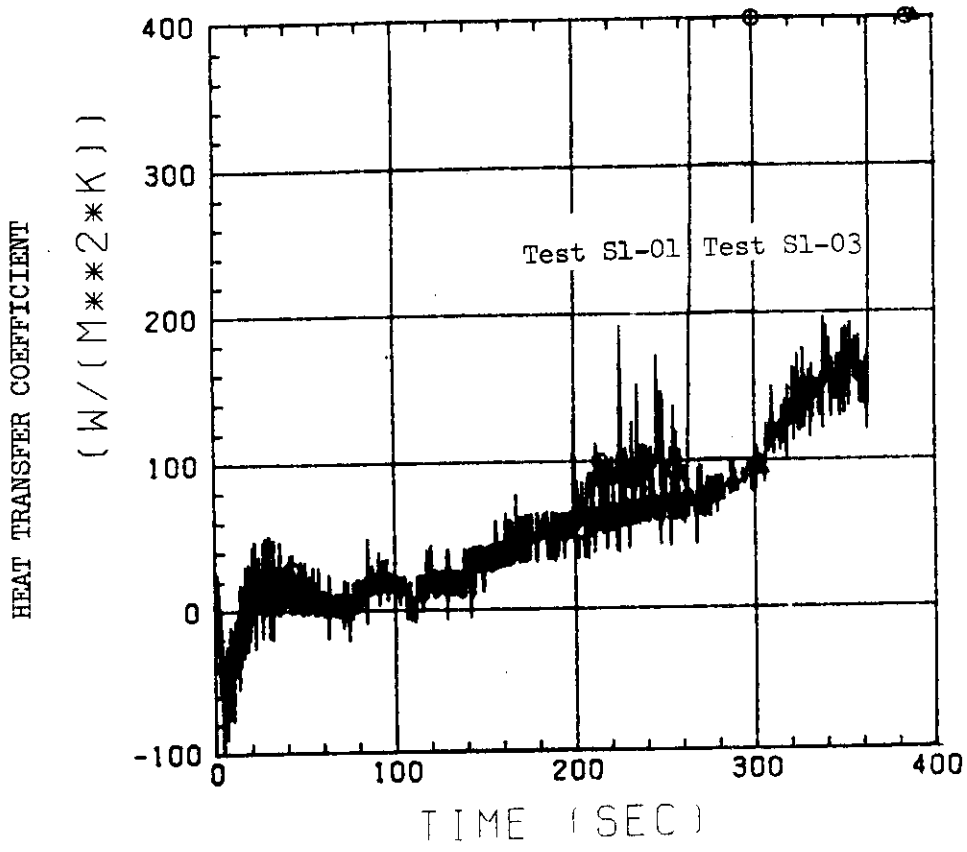

Fig.5.8 Heat Transfer Coefficient at Elevation 3190 mm at Bundle 4.

6. Two-Dimensional Hydrodynamic Behavior in Pressure Vessel

6.1 Introduction

In this chapter, fluid behavior in the pressure vessel is investigated especially as for how the two-dimensionality of hydrodynamic behavior occurs in the wide core, and is affected by the amount of water accumulated in the upper plenum.

The two-dimensionality is expected due to the wide core itself as well as the difference in the electric power supplied to each bundle of the core and the effect of the blocked bundles. Besides, the effect of water extraction from the upper plenum should be significant on the fluid behavior in the core because as already pointed out in Chapter 4, water fall bcack from the upper plenum into the core should be one of predominant factors which governs fluid behavior in the core. Here, the effect of water extraction from the upper plenum on the fluid behavior is discussed and compared to the base case test in which no water is extracted from the upper plenum.

The investigated items are the characteristics of (i) differential pressure across the core full height, (ii) accumulated water level on the UCSP, (iii) fluid behavior around the end box tie plate and (iv) fluid behavior in the core including fluid density and horizontal differential pressure.

6.2 Differential Pressure across Core Full Height

Comparison of core full height differential pressure transients is shown in Fig. 6.1 for Tests S1-03 and S1-01. Comparisons are given for Bundle 2, 4, 6 and 8, respectively. From this comparison, it is clear that the transients of differential pressure for both tests are the same for about 100 seconds after the BOCREC but that after that, Test S1-03 with water extraction gives lower differential pressure across the core full height than the base case test for all bundles. The reason why the difference exists in the two tests is that the magnetude of water fall back from the upper plenum into the core is different. In Fig. 6.2, comparison of core full height differential pressure profile over the 8 bundles is shown for Tests S1-03 and S1-01 at 100, 200, 300 and 400 seconds after the BOCREC, respectively. As already pointed out in Reference (5), the horizontal distribution of the core full height differential pressure is uniform over the eight bundles for Test S1-01, and is almost uniform

also for Test S1-03 at any time after the BOCREC. As already shown in Fig. 6.1, there exists the difference of differential pressure at the same bundle number between the two tests, although the difference is not so significant. The maximum differences at each time at bundle 4 are as follows; 0.01 m of water head at 100 s, 0.09 m at 200 s, 0.18 m at 300 s, 0.25 m at 400 s, and 0.25 m at 500 s.

Therefore, it is concluded from the Figs. 6.1 and 6.2 that (i) water extraction from the upper plenum gives the core full height differential pressure lower than the case of no water extraction and that (ii) the characteristics of almost uniform core full height differential pressure profile over the eight bundles is preserved also for the test with water extraction.

Fig. 6.3 shows where the difference of core full height differential pressure exists, comparing the differential pressures for each measured section between these two tests. From this figure we can see that (i) at the measured section 1 (the lowest part of the core) there is no difference in the two tests, (ii) at the measured section 2 there is a difference as much as 0.07 m of water head at 500 seconds after the BOCREC and (iii) at the measured sections 3 to 6 there are differences of about 0.03 water head at 500 seconds after the BOCREC. Therefore, it is known that the differences are scattering in each section except for the measured section 1.

Next, it is discussed in the following where this difference comes from, based on the correlation for void fraction proposed by Cunningham & Yeh[9]. Figure 6.4 shows the transients of steam mass flow generated in the core for Tests S1-03 and S1-01 along with mass flux calculated from the assumption that steam is generated only from the electric power supplied to the core. Although the difference of steam mass flow rate should be one of the main reason of difference in core full height differential pressure, it is understood easily that steam mass flow rate does not make the difference of the core full height differential pressure for both tests because of the same mass flow rate in both tests as shown in Fig. 6.4. From Fig. 6.4 it is clear that before whole core quench, the steam mass flow rate is determined by the release of heat energy stored in the core into fluid and after that, the steam mass flow rate is determined by the electric power supplied to the core. Figs. 6.5 and 6.6 show the transients of water temperature at the core inlet for each bundle in Tests S1-03 and S1-01, respectively, along with the saturation temperature

at the lower plenum and at the center of the core. For a reference, water temperature at the elevation 950 mm from the bottom of the heated length of heater is also shown in the figure. The difference between the saturation temperature at the center of the core and the water temperature at the core inlet gives approximate value of core inlet water subcooling. From the comparison of Figs. 6.5 and 6.6 it is known that the transient of ECC water temperature at the core inlet is almost the same between the two tests but that the saturation temperature at the inlet of the core is a little lower in Test S1-03 than in Test S1-01 because the system pressure history is a little different from each other (See Fig. 2.19). This shows core inlet water subcooling is a little lower in Test S1-03 than in Test S1-01 especially in the later part of the tests as shown in Tables 6.1 and 6.2.

Therefore, there is a possibility that the difference of core inlet water subcooling causes the difference of the core full height differential pressure especially in the later part of the tests.

In order to investigate quantitatively the possibility described above, the core full height differential pressure was calculated by using a correlation for void fraction derived by Cunningham & Yeh with the core inlet water subcooling, power profile along the heater rod, pressure at the center of the core and the steam flow rate. The calculation were carried out under the assumption that there was no fluid communication between bundles. Therefore, the horizontal core differential pressure profile over the eight bundles can be obtained at each given time, with no fluid communication between bundles and we can see how much core full height differential pressure is equalized by fluid communication between bundles, comparing with the experimental results of the horizontal differential pressure profile.

Cunningham & Yeh's correlation for void fraction is as follows:

$$\alpha = 0.925 \left(\frac{\gamma_g}{\gamma_\ell}\right)^{0.239} \cdot \left(\frac{A_{gS}}{V_{BCR}}\right)^{A} \left(\frac{V_{gS}}{V_{gS}+V_{\ell S}}\right)^{0.6} , \qquad (6\text{-}1)$$

$$A = 0.47 \text{ for } \frac{V_{gS}}{V_{BCR}} > 1.0 ,$$

$$A = 0.67 \text{ for } \frac{V_{gS}}{V_{BCR}} \leq 1.0 ,$$

$$V_{BCR} = \frac{2}{3}\sqrt{g\, R_{BCR}} ,$$

$$R_{BCR} = \left(\frac{4.59}{2}\right)^2 \frac{\sigma}{\sqrt{\gamma_\ell}} \quad ,$$

where α: void fraction (-),

γ_g, γ_ℓ : specific weights of steam and water (kg/m^3),

V_{gs}, $V_{\ell s}$: superficial velocities of steam and water (m/s),

g : acceleration of gravity (m/s^2), and

σ : surface tension (kg/m).

To evaluate the core full height differential pressure, the head losses such as the frictional loss except for static water head are neglected here. The static water head is determined with the void fraction. That is, core full height differential pressure ΔP_{core} is written as

$$\Delta P_{core} = \int^{L} \{\gamma_\ell(1-\alpha)+\gamma_g\alpha\}dZ \quad , \tag{6-2}$$

where L : full height of the core (m) and

dZ : increment of length (m).

In order to evaluate the void fraction at any elevation in the core, V_{gS} is calculated first and then, ΔP_{core} is obtained from Eqns. (6-1) and (6-2) for each bundle.

P_{core} is calculated from the two steps, (i) determination of the elevation ℓ_C where steam starts to be generated in the bundle and below where void fraction is zero, and (ii) calculation of void fraction with V_{gS} above ℓ_C.

Step 1: Determination of ℓ_C

The water temperature rise dT for an increment dZ is calculated with bundle power $Q(\frac{kcal}{ms})$, water mass flow rate W_ℓ(kg/S), specific heat of water $C_{p\ell}(\frac{kcal}{kg\,K})$ as

$$dT = \left(\frac{Q}{C_{p\ell}\, W_\ell}\right)\cdot dZ \quad . \tag{6-3}$$

At the specified time after the BOCREC, ℓ_C is determined as the elevation where temperature rise from the bottom of the core (the sum of dT) equals to the core inlet water subcooling ΔT_{in}. It should be noted that ΔT_{in} is a little different in each bundle as shown in Fig. 6.6, and this effect is taken into account. The temperature rise dT is calculated with the assumption of no fluid communication between bundles.

Step 2: Void fraction calculation with V_{gs} above ℓ_C

As shown in Fig. 6.4, the flow rate of steam generated in the core is much different from that calculated from the electric power supplied to the core before the quench of the whole core. Therefore, evaluation of V_{gS} should be based on the local heat release from the surface of rods into fluid. However, as a conventional estimation of V_{gs} it is assumed in the present analysis that the local steam generation dW_g/dZ is proportional to the electric power Q_i supplied to each bundle and to the power ratio P_i along the length of rod against the total steam flow rate W_g above. Therefore, superficial steam velocity V_{gs} at elevation is evaluated as

$$V_{gS} = \frac{\sum_{\ell_C}^{\ell} \left(\frac{dW_g}{dZ}\right) dZ}{\gamma_g A_C} = \frac{1}{\gamma_g A_C} \sum_{\ell_C}^{\ell} \left(W_g \frac{Q_i}{\sum_{i=1}^{8} Q_i} P_i \, dZ\right) ,$$

where A_C is the flow area in a bundle. The local void fraction is calculated with V_{gS} from Eq. (6-1) and the ΔP_{core} from Eq. (6-2).

Fig. 6.7 and 6.8 show the analytical results for the test conditions of S1-03 and S1-01, respectively at 100, 200, 300, 400 and 500 s after the BOCREC for each bundle. First of all, we can see from these figures that (i) the horizontal profile of core full height differential pressure is not uniform among bundles with the 0.15 m of water head difference at 100 s after the BOCREC and with 0.12 0.14 m of water head difference even at 500 s after the BOCREC, in both test conditions and that (ii) from 400 s after the BOCREC, the core full height differential pressure becomes almost constant.

As for the first item, the horizontal difference of core full height differential pressure over the eight bundle comes from the difference of electric power supplied to the core. The bundle with the higher power gives the lower differential pressure due to the more steam generation in the bundle. On the other hand, the experimental results that the horizontal profile of the core full height differential pressure is almost uniform (flat) over the eight bundles at any time show that fluid (water and/or steam) flows from the bundle with the lower electric power into the bundle with the higher power to equalize the fluid behavior in the bundles. This is a so-called chimney effect which is expected in a wide core. This phenomena is clearly observed in both tests.

Fig. 6.9 shows the comparison of the core full height differential

pressure transients between Tests S1-03 and S1-01 and the analytical results for each bundle. From this comparison, it is observed clearly that the difference in core full height differential pressure between the analytical results for S1-03 and S1-01 starts to occur from 100 s after the BOCREC and the difference becomes 0.1 m of water head at 500 s after the BOCREC while the experimental results show the same tendency as for the start of difference but the difference at 500 s after the BOCREC is much larger with about 0.2 m of water head in the experiment than in the analysis.

The difference in the core full height differential pressure between Tests S1-03 and S1-01 is larger than the difference between the analytical results for Tests S1-03 and S1-01. Another factor, except for the inlet water subcooling cinsidered above, which should be taken into account is the difference in magnitude of water fall back from the upper plenum into the core. Although the water fall back can not be evaluation nor measured directly for the test, the result implies that more water accumulation in the upper plenum makes more water fall back. This implication is different from the result of previous studies[10] that counter current flow limitation is not affected by the water level in the upper plenum. However, in such a wide core as the SCTF the situation is different from the one bundle test or single pipe test because fluid is communicative both in the upper plenum and between bundles in the core.

6.3 Fluid Behavior around the End Box Tie Plate

The transients of the water level accumulated on the UCSP are compared between the Test S1-03 and S1-01 in Fig. 6.10. Test S1-03 was carried out, as already described, under extraction of water accumulated on the UCSP from the upper plenum. All water accumulated should have been extracted in the Test S1-03 and no water should be accumulated on the UCSP. However, as shown in Fig. 6.10, some amount of water was recognized to be accumulated. In the following, this effect of the water extraction is discussed more in detail.

Fig. 6.11 shows the comparison of liquid level distribution above end box tie plate over the eight bundles between Tests S1-03 and S1-01. From this figure, it is clear that the liquid level distribution above the end box tie plate are rather uniform during Test S1-03, while from about 250 seconds after the BOCREC the liquid level distribution for Test S1-01 has a peak at bundle 7 and 8 which are low power bundles corresponding

to the periphery of an actual PWR core and the magnitude of water level is much larger than for Test S1-03. Fig. 6.12 shows the comparison of liquid level transients above the end box tie plate for Tests S1-03 and S1-01 at bundles 2, 4, 6 and 8, respectively. Also from this figure, it is clear that for Test S1-03 the liquid level is very slowly increasing with time at each bundle but that for Test S1-01 the liquid level at Bundle 8 increases rapidly at 300 s after the BOCREC. It should be that the transients of liquid level is the same at the same bundles both for Tests S1-03 and S1-01 except for bundles 7 and 8 from 300 seconds after the BOCREC. The reason why the water level rapidly increases at about 250 s after the BOCREC above bundles 7 and 8 for Test S1-01 is that water flow reversal in the hot leg to the upper plenum begins to be significant, making water fall back significant from the upper plenum into the core at bundles 7 and 8.

Fig. 13 shows the comparison of horizontal distribution of differential pressure across the end box tie plate over the eight bundles. From this comparison, it is clear that for Test S1-03 the fluid behavior across the tie plate is uniform over the eight bundles and that the flow is a co-current upflow all through the test, which is judged from that the differential pressure is positive. However, in Test S1-01 the flow should be counter-current at bundles 7 and 8 with water downward from the end box into the core from 300 s after the BOCREC because the differential pressure is negative. This result also suggests water fall back from the upper plenum into the core at bundles 7 and 8 in Test S1-01. Fig. 6.14 shows the comparison of the differential pressure transients across the end box tie plate for Tests S1-03 and S1-01 above bundles 2, 4, 6 and 8 respectively. From this figure it can also be understood that the fluid behavior across the end box tie plate is rather uniform over the eight bundles and flow is a co-current upflow for Test S1-03, while at bundles 8 a counter-current flow occurs with water downward for Test S1-01.

6.4 Fluid Behavior in Core (Fluid Density, Horizontal Differential Pressure)

Fig. 6.15 shows the comparison of fluid density transients below the end box (at elevation 4952 mm above the bottom of heated length of heater) between Bundles 1 and 2, and between bundles 7 and 8 for Tests S1-03 and S1-01. This comparison clearly shows that fluid density is much higher between bundles 7 and 8 at about 250 s after the BOCREC for Test S1-01 than

for Test S1-03, while for Test S1-03 the fluid density transient is almost the same between Bundles 1 and 2, and between bundles 7 and 8. This also shows that water extraction gives more uniform fluid behavior also at the top of the core over the eight bundles, and that no water extraction gives the non-uniform fluid density distribution at the top of the core.

Figs. 6.16 and 6.17 show the horizontal differential pressure between Bundles 5 and 8 and between bundles 1 and 8, respectively, at the elevations 1905 (below spacer 4), 3235 (below spacer 6) and 3821 mm (below and box) for Tests S1-03 and S1-01. This comparison also shows the effect of water extraction that a uniform horizontal pressure distribution is established in the core for Test S1-03, while no water extraction gives higher pressure at the low power bundles at the periphery of the core than at any other bundles.

6.5 Summary

(1) Water extraction from the upper plenum gives lower core full height differential pressure and more uniform distribution over the eight bundles than without water extraction.

(2) The difference of core full height differential pressure between the two tests seems to come from the difference in the water fall back.

(3) Water extraction from the upper plenum gives much more uniform fluid behavior across the eight bundles. These phenomena are observed in the liquid level distribution above the end box tie plate, horizontal distribution of differential pressure across the tie plate over the eight bundles, fluid density distribution at the top of the core and horizontal differential pressure between bundles 5 and 8, and between bundles 1 and 8 at different elevations.

(4) Water accumulation in the upper plenum gives an intensive water fall back from the upper plenum into the core at the lower power bundles located at the periphery of the core.

Table 6.1 Core Inlet ECC Water Subcooling for Test S1-01

Core Inlet ECC Water Subcooling (K) for Test S1-01

Bundle No. 2	4	6	8	Average	Time after BOCREC(s)
16.5	16.8	16.0	16.0 /	16.3	100
12.5	12.6	13.0	12.0 /	12.5	200
7.8	6.3	8.3	7.0 /	7.3	300
6.2	5.5	5.5	6.0 /	5.8	400
5.8	5.9	5.9	6.1 /	5.9	500

Table 6.2 Core Inlet ECC Water Subcooling for Test S1-03

Core Inlet ECC Water Subcooling (K) for Test S1-03

Bundle No. 2	4	6	8	Average	Time after BOCREC(s)
15.8	16.2	15.8	15.4 /	15.8	100
11.9	11.5	11.0	9.5 /	11.0	200
6.9	7.3	6.9	6.1 /	6.8	300
3.8	3.8	4.2	3.4 /	3.8	400
2.7	2.7	3.5	3.9 /	3.2	500

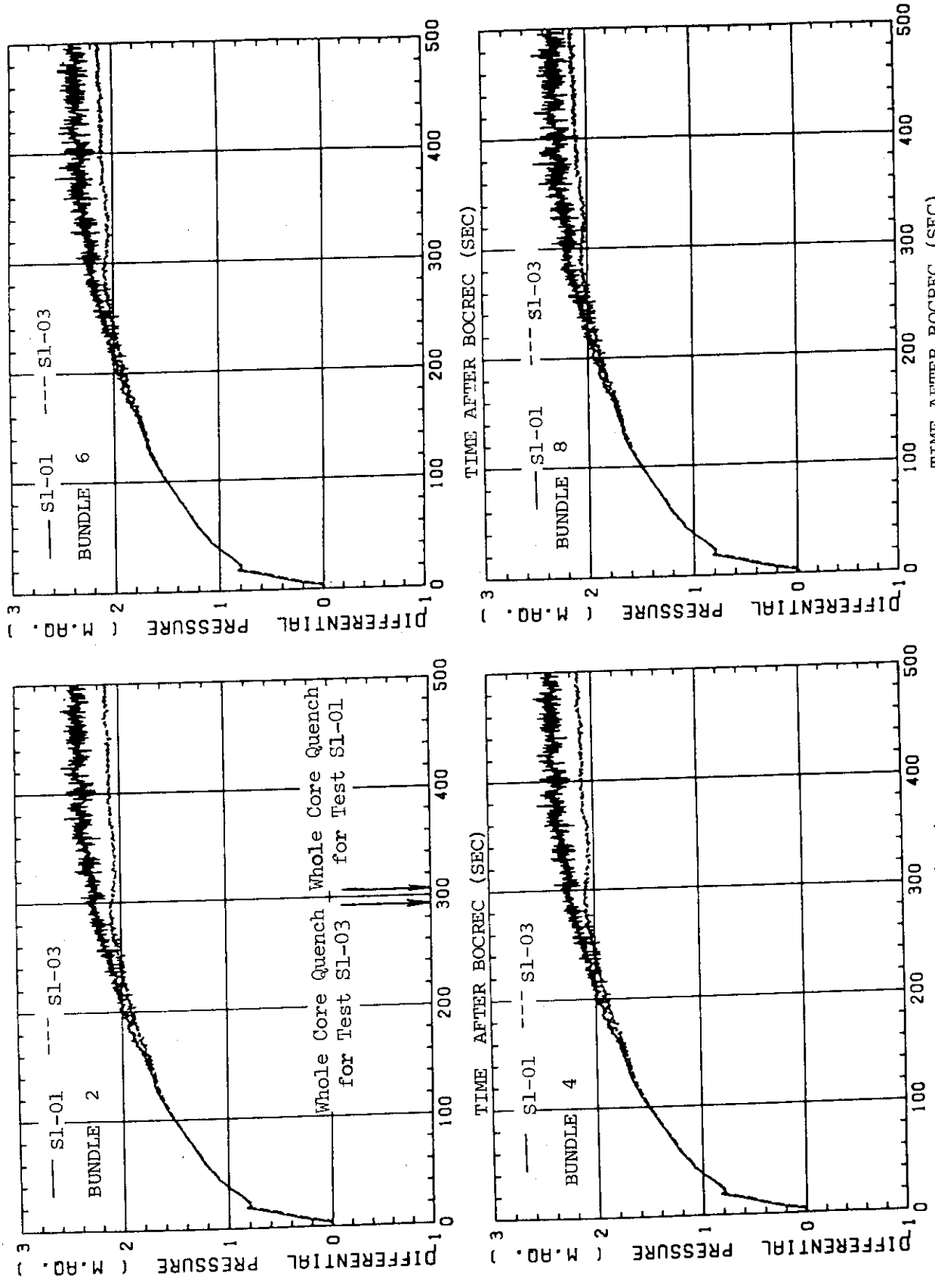

Fig.6.1 Comparison of Core Full Height Differential Pressure Transients for Tests S1-01 and S1-03 (Bundles 2, 4, 6 and 8)

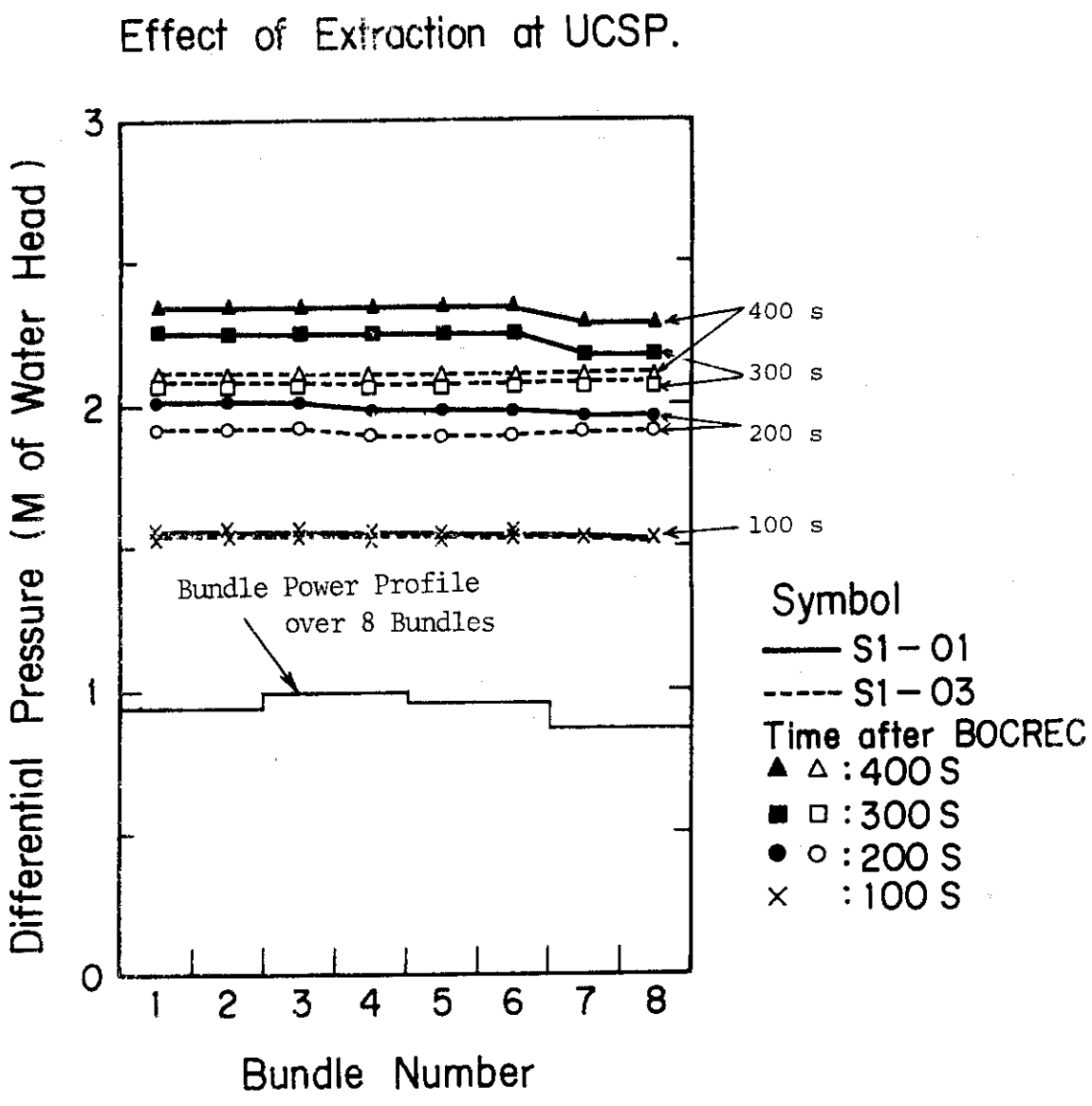

Fig.6.2 Comparison of Core Full Height Differential Pressure Profile over 8 Bundles for Tests S1-01 and S1-03 (100, 200, 300 and 400 sec after BOCREC)

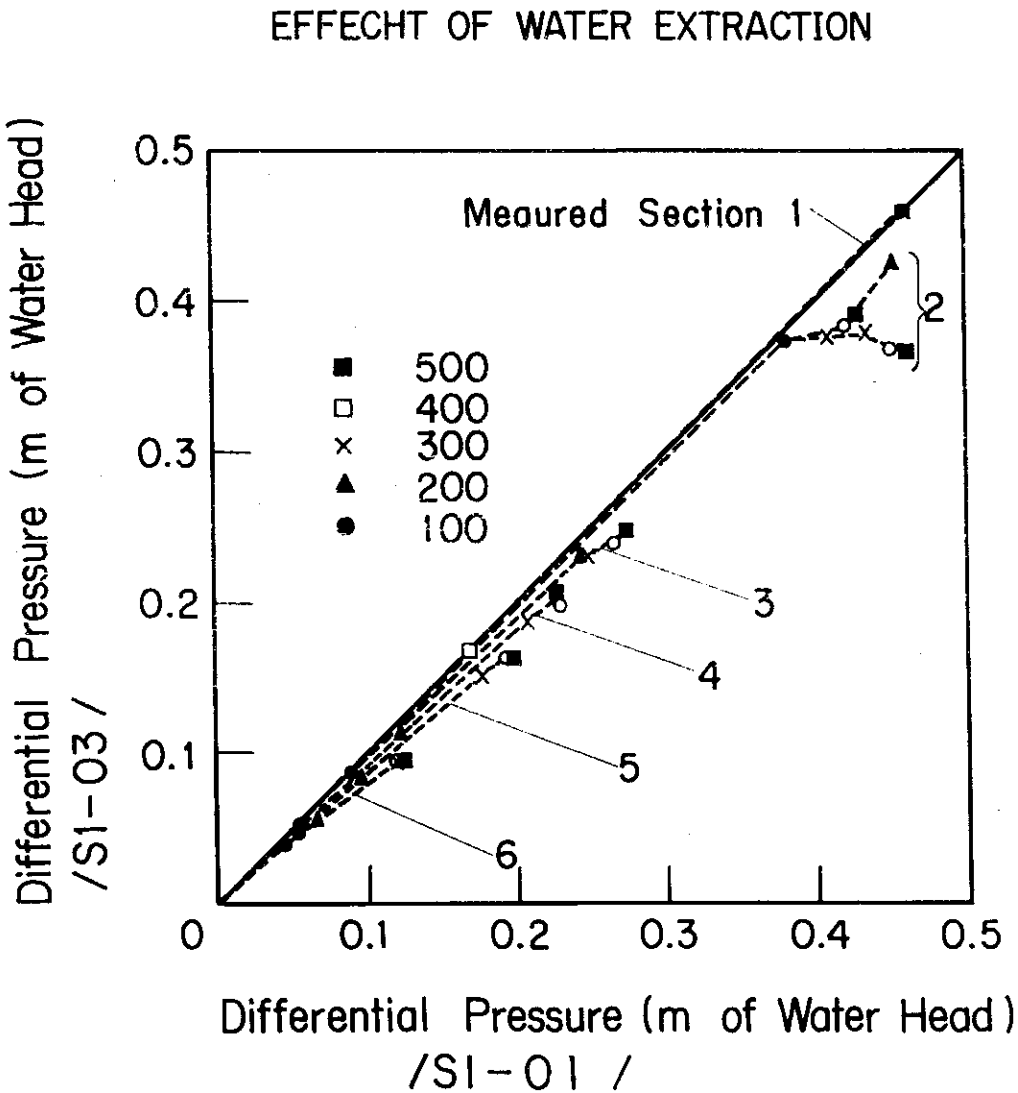

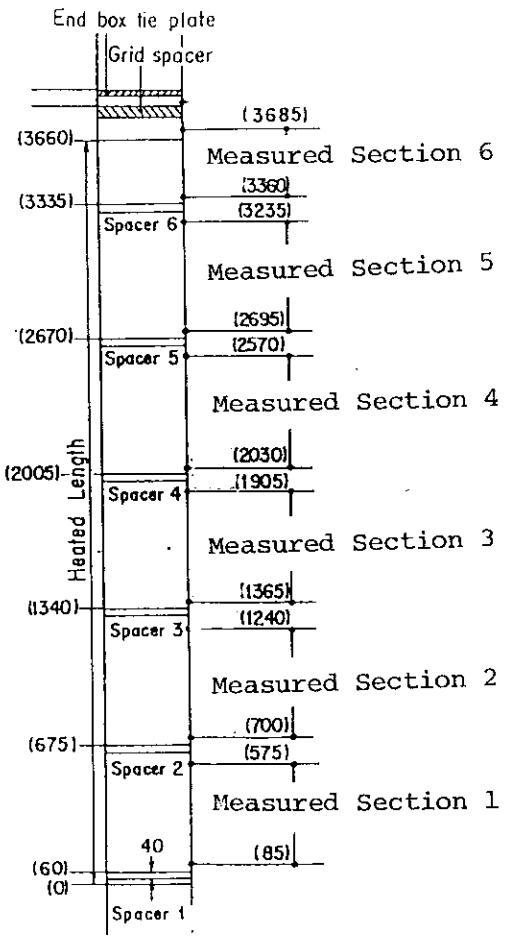

Illustration of Measured Section

Fig.6.3 Illustration of Difference of Core Differential Pressure at Each Section between Tests S1-01 and S1-03.

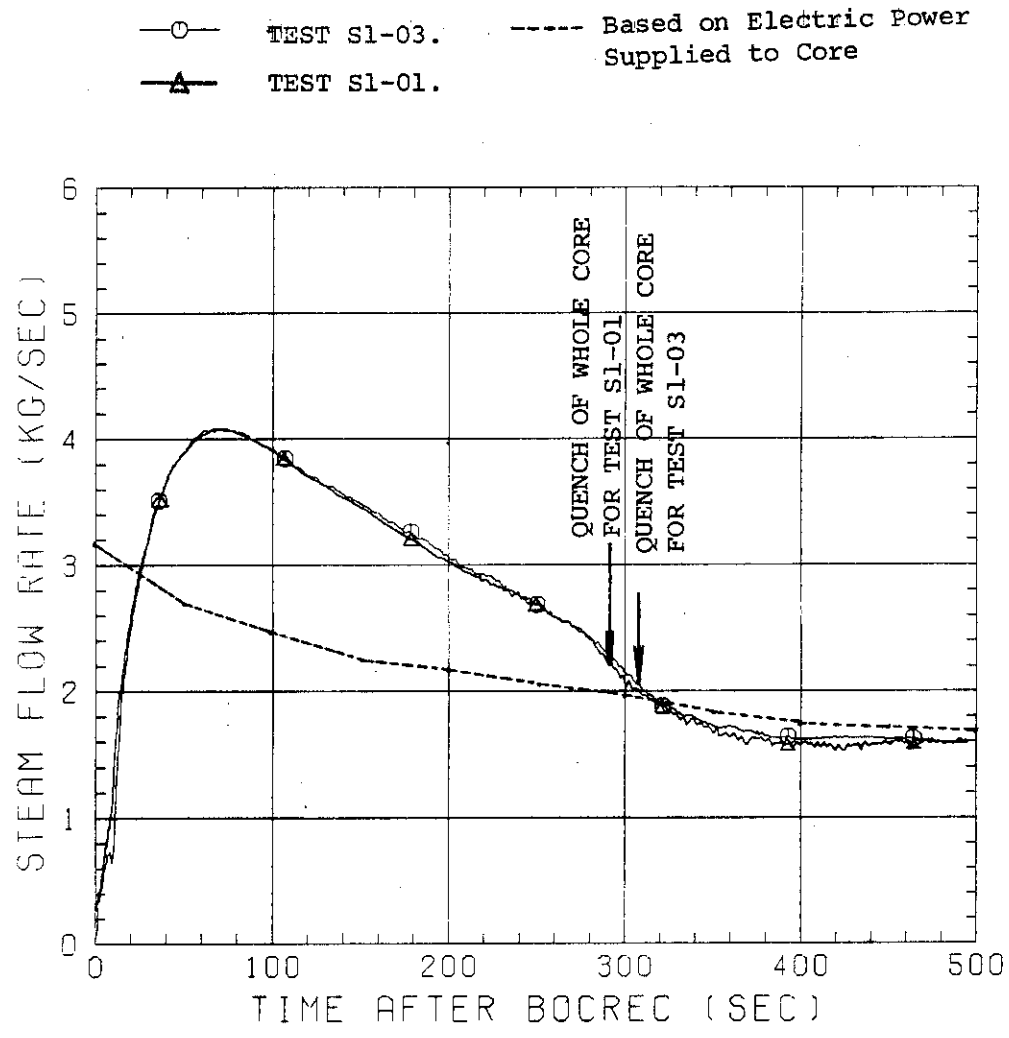

Fig.6.4 Comparison of Steam Mass Flux Generated in Core for Tests S1-01 and S1-03 and Steam mass Flux based on the Electric Power Supplied to Core.

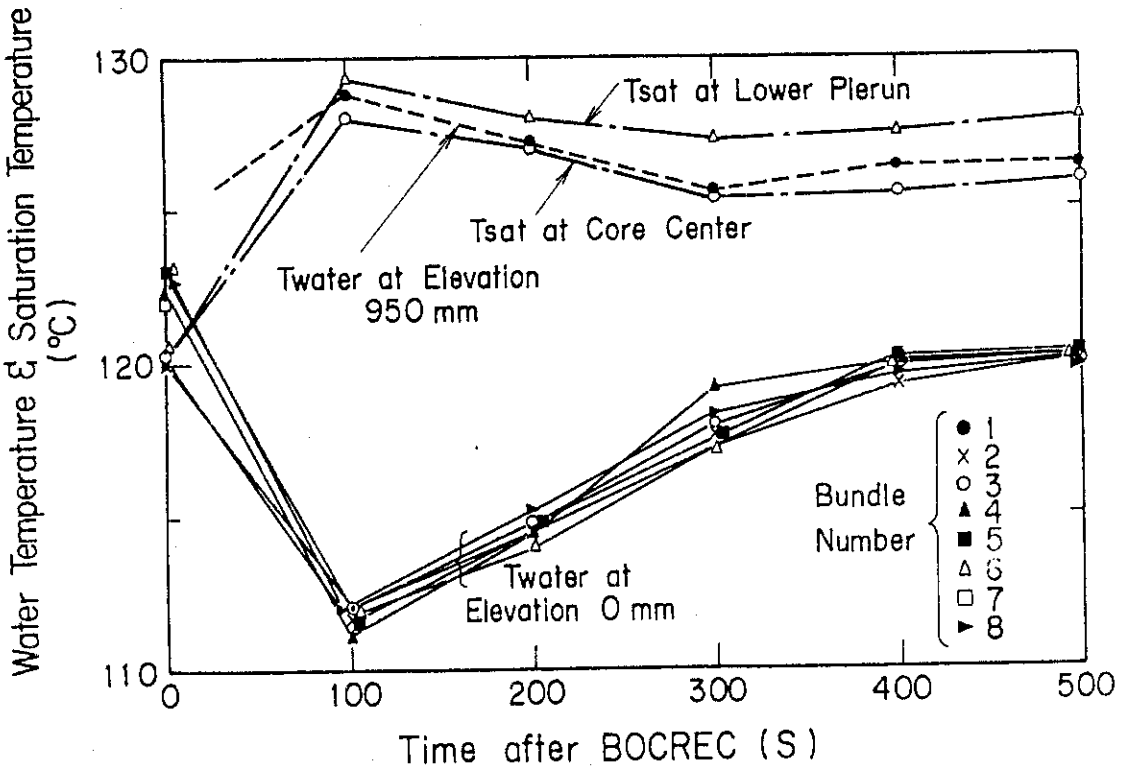

Fig.6.5 Transients of ECC Water Subcooling at Core Inlet for Test S1-01.

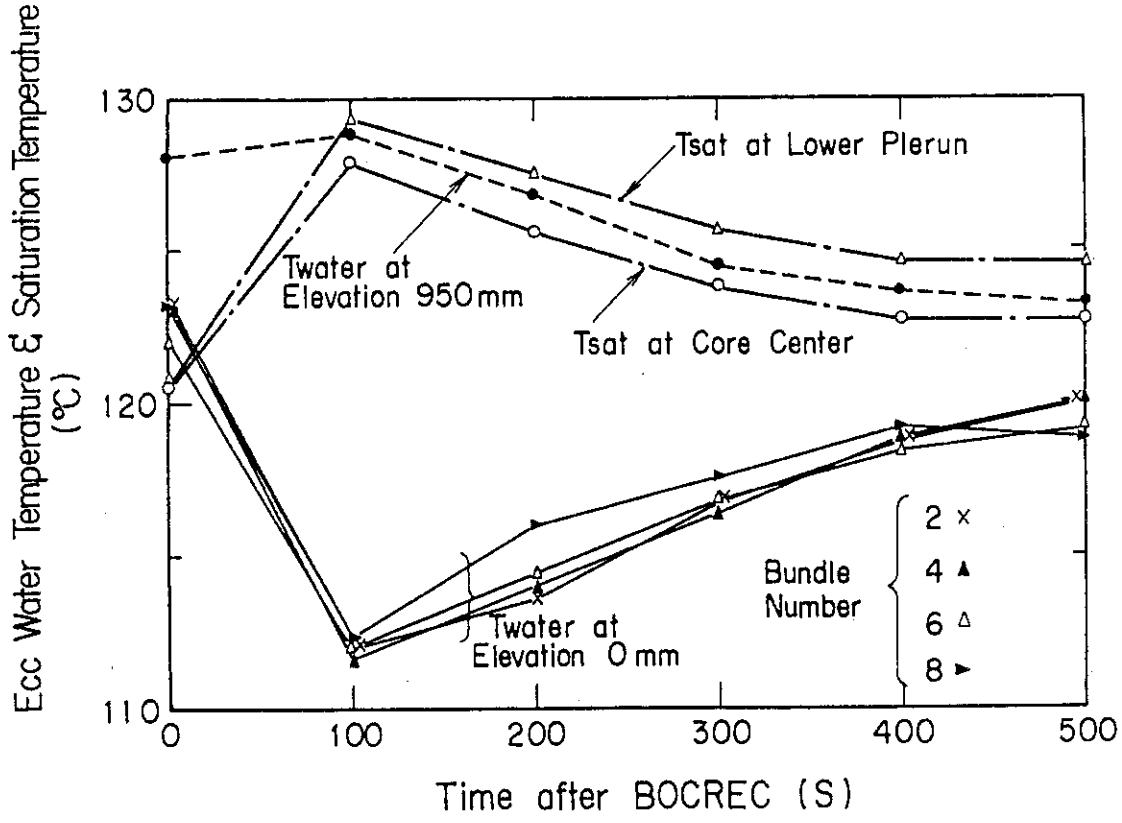

Fig.6.6 Transients of ECC Water Subcooling at Core Inlet for Test S1-03.

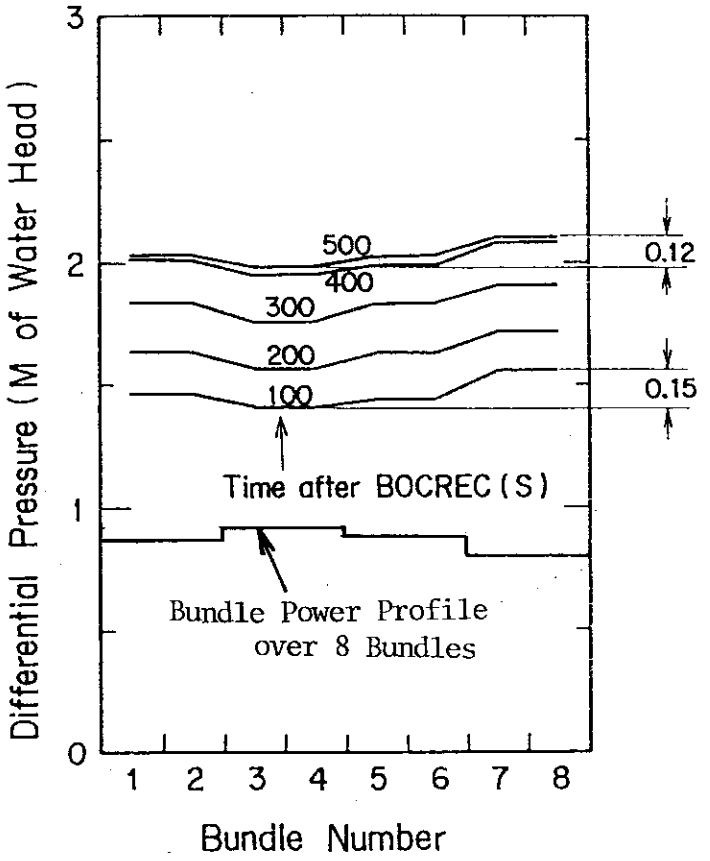

Fig.6.7 Illustration of Core Full Height Differential Pressure Profile over 8 Bundles for Test Condition of S1-01 Based on Assumption of No Fluid Communication between Bundles (100, 200, 300, 400 and 500 sec after BOCREC).

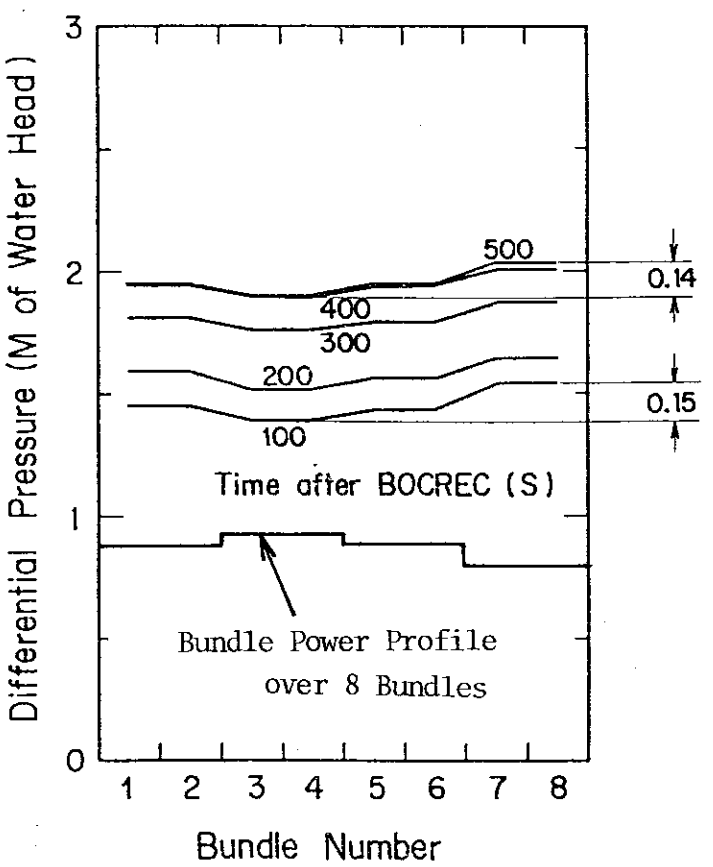

Fig.6.8 Illustration of Core Full Height Differential Pressure Profile over 8 Bundles for Test Condition of S1-03 Based on Assumption of No Fluid Communication between Bundles (100, 200, 300, 400 and 500 sec after BOCREC).

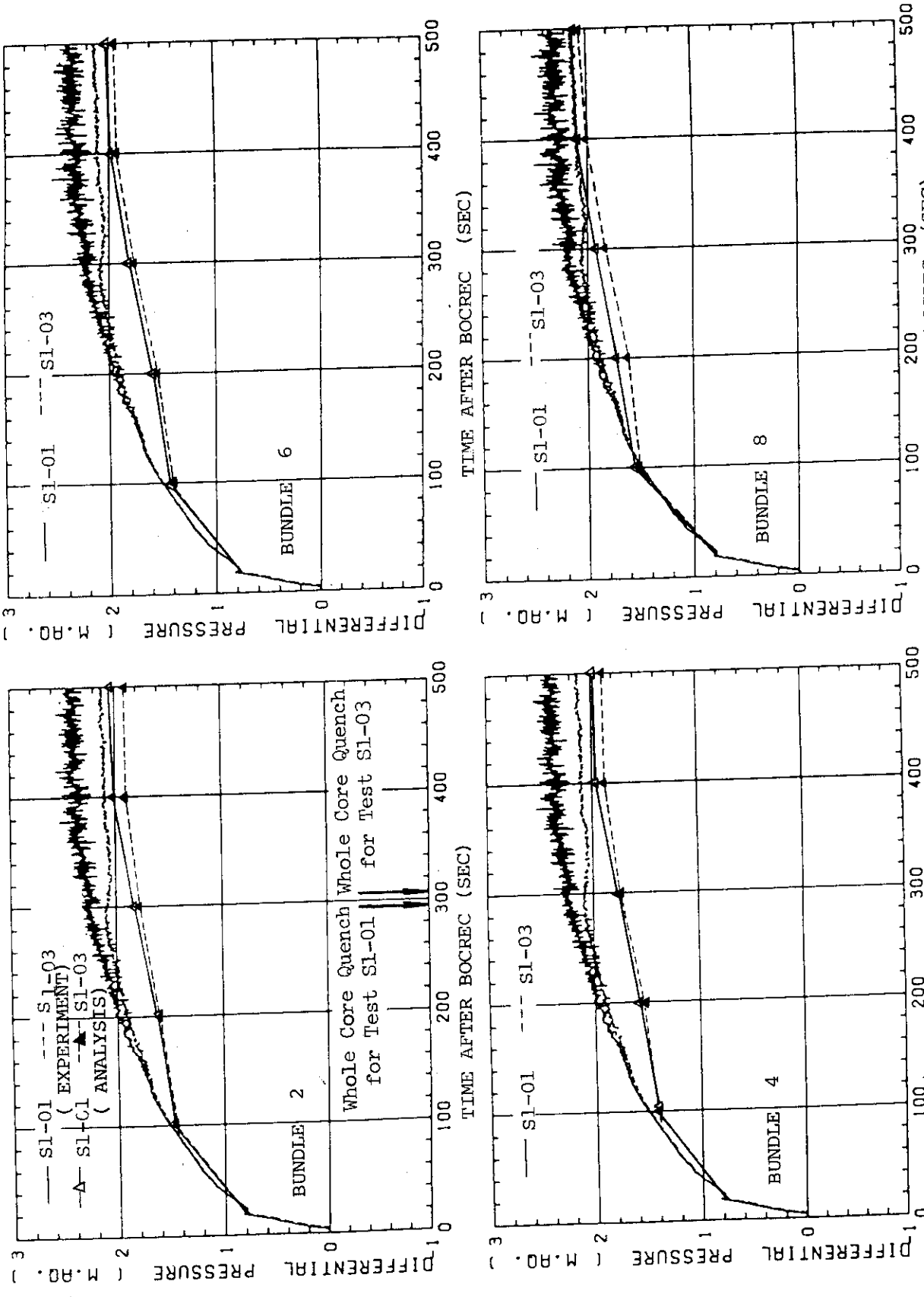

Fig.6.9 Comparison of Core Full Height Differential Pressure Transients between the Tests and the Analytical Results Based on the Assumption of No Fluid Communication between Bundles (Bundles 2, 4, 6 and 8).

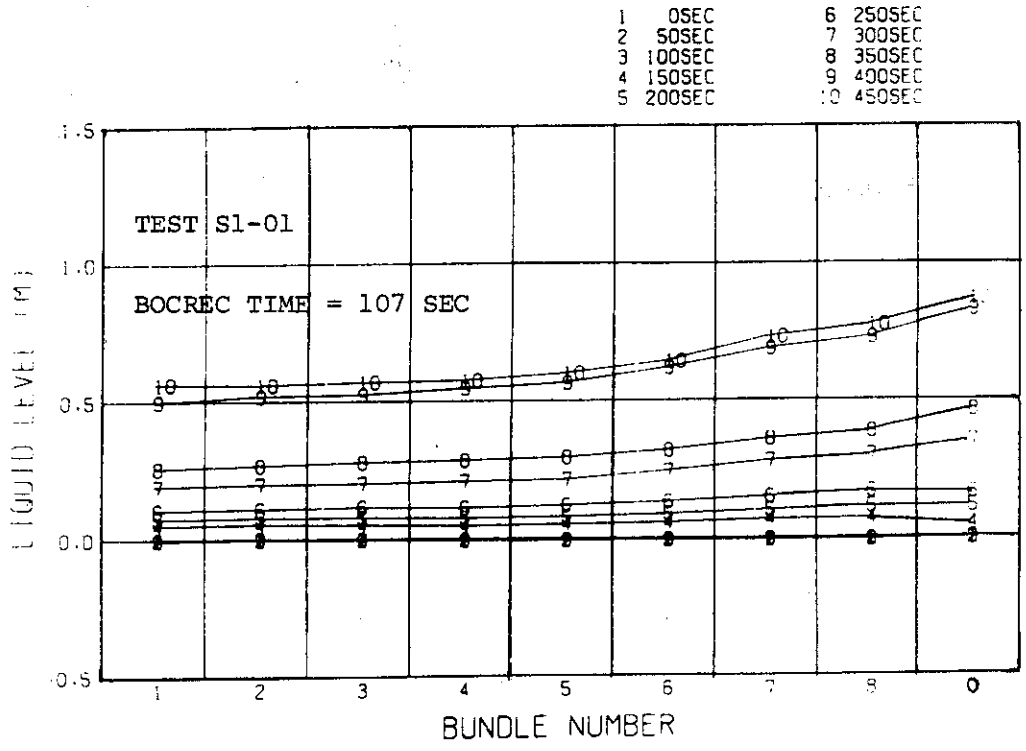

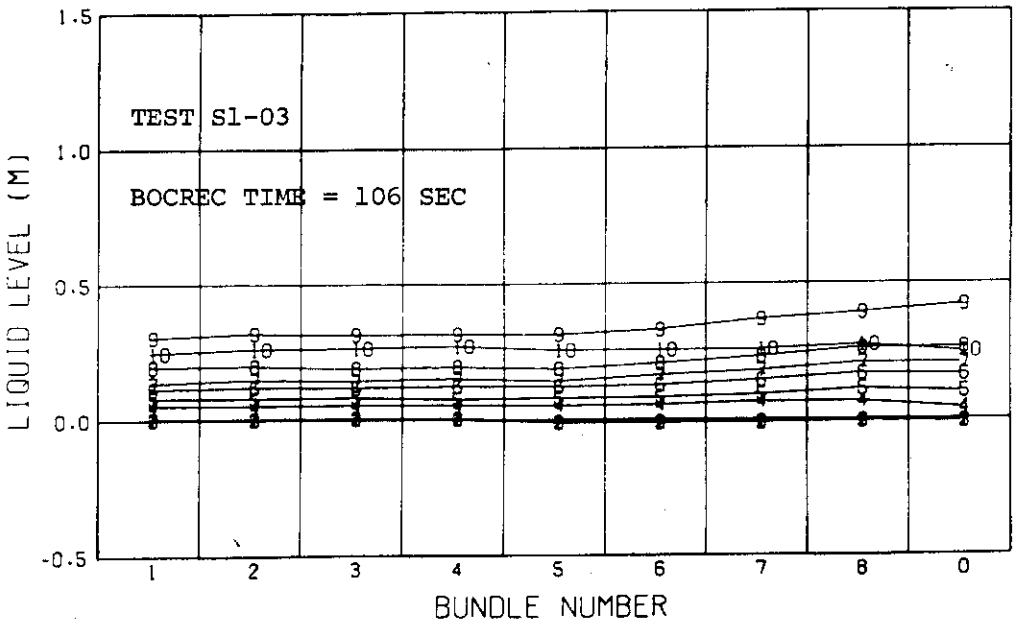

LIQUID LEVEL DISTRIBUTION ABOVE UCSP

Fig.6.10 Comparison of Liquid Level Distribution above UCSP for Tests S1-01 and S1-03.

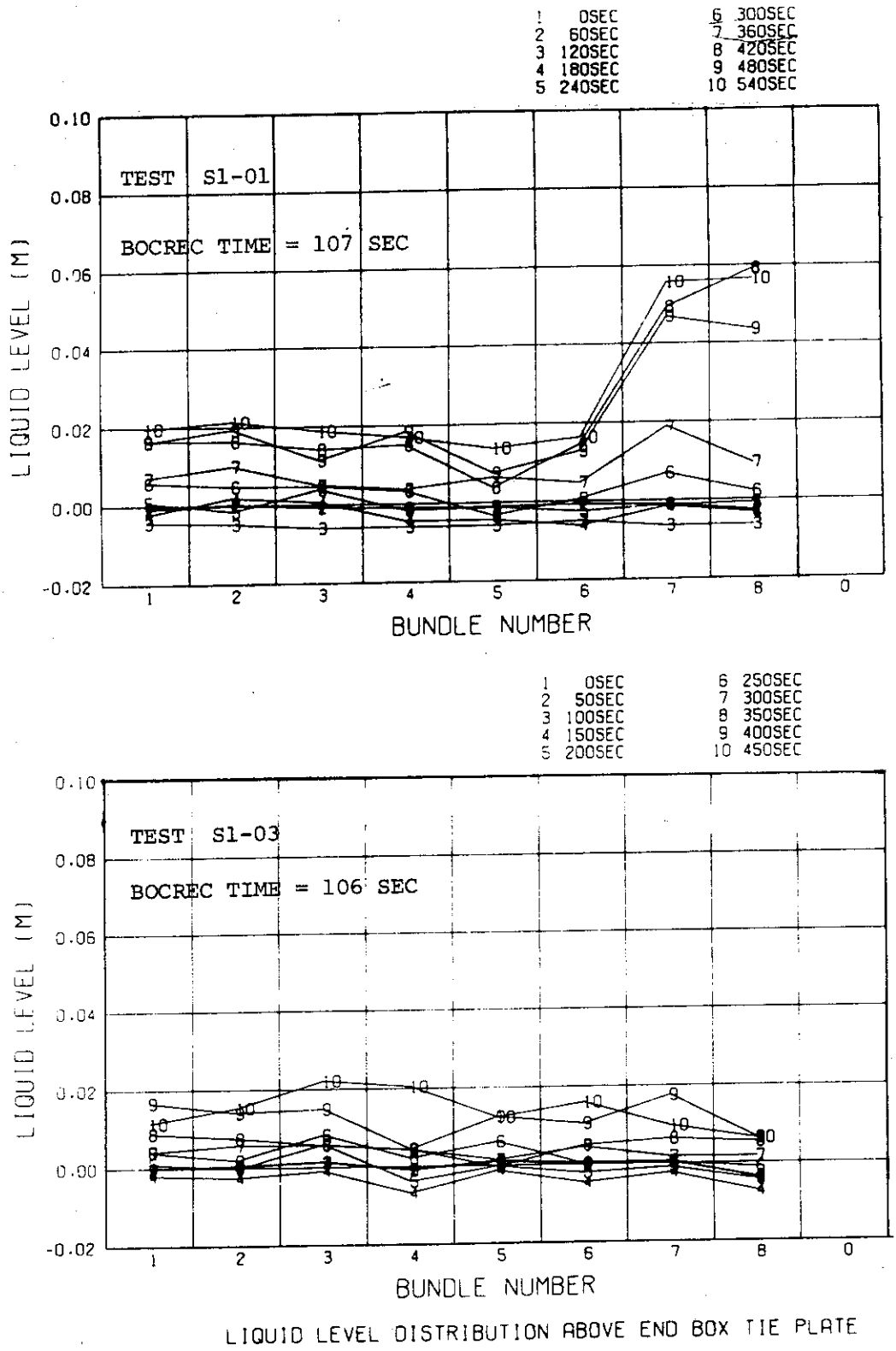

Fig.6.11 Comparison of Liquid Level Distribution above End Box Tie Plate for Tests S1-01 and S1-03.

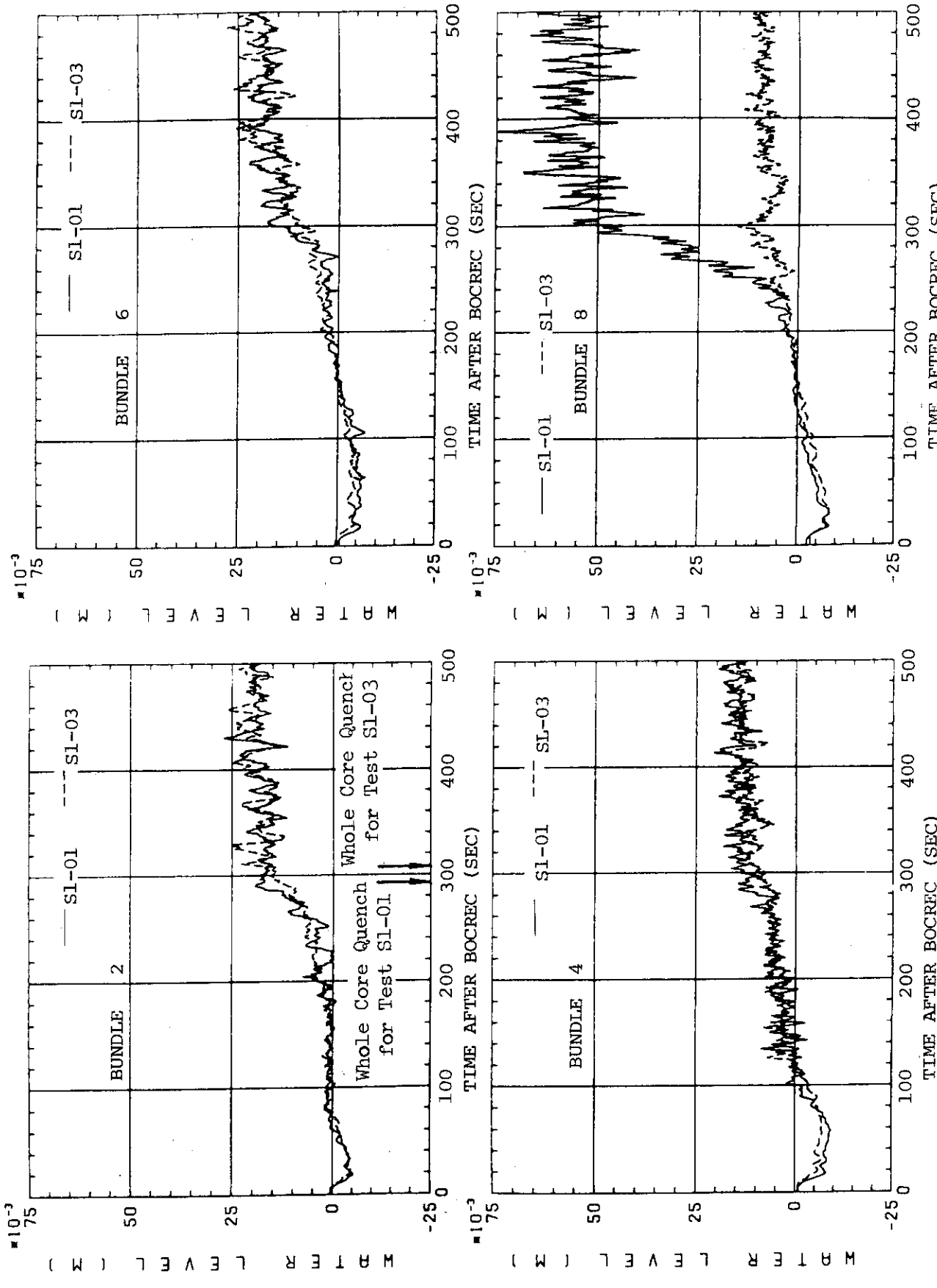

Fig.6.12 Comparison of Liquid Level Transients above End Box Tie Plate for Tests S1-01 and S1-03 (Bundles 2, 4, 6 and 8).

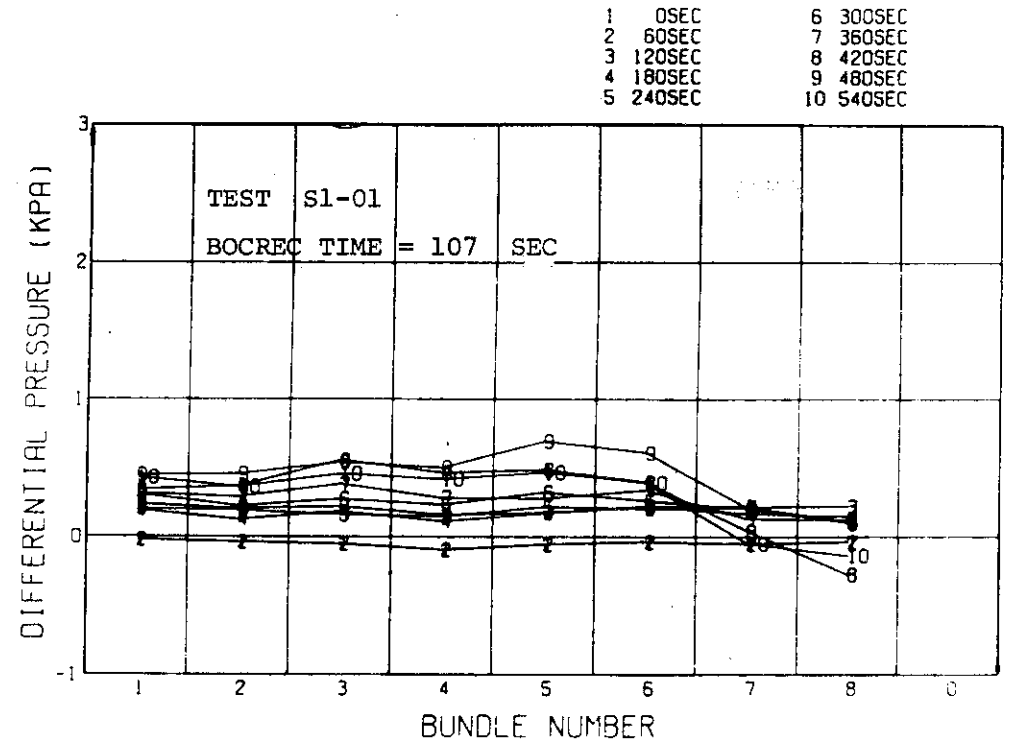

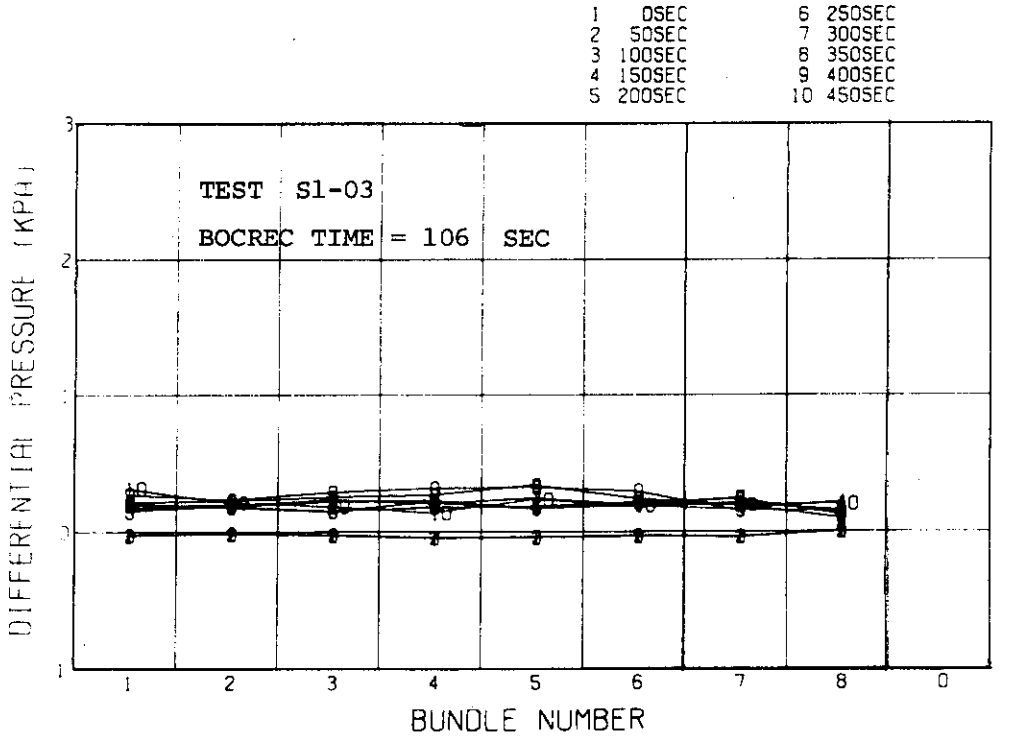

HORIZONTAL DISTRIBUTION OF DIFFERENTIAL PRESSURE ACROSS END BOX TIE PLATE

Fig.6.13 Comparison of Horizontal Distribution of Differential Pressure across End Box Tie Plate for Tests S1-01 and S1-03.

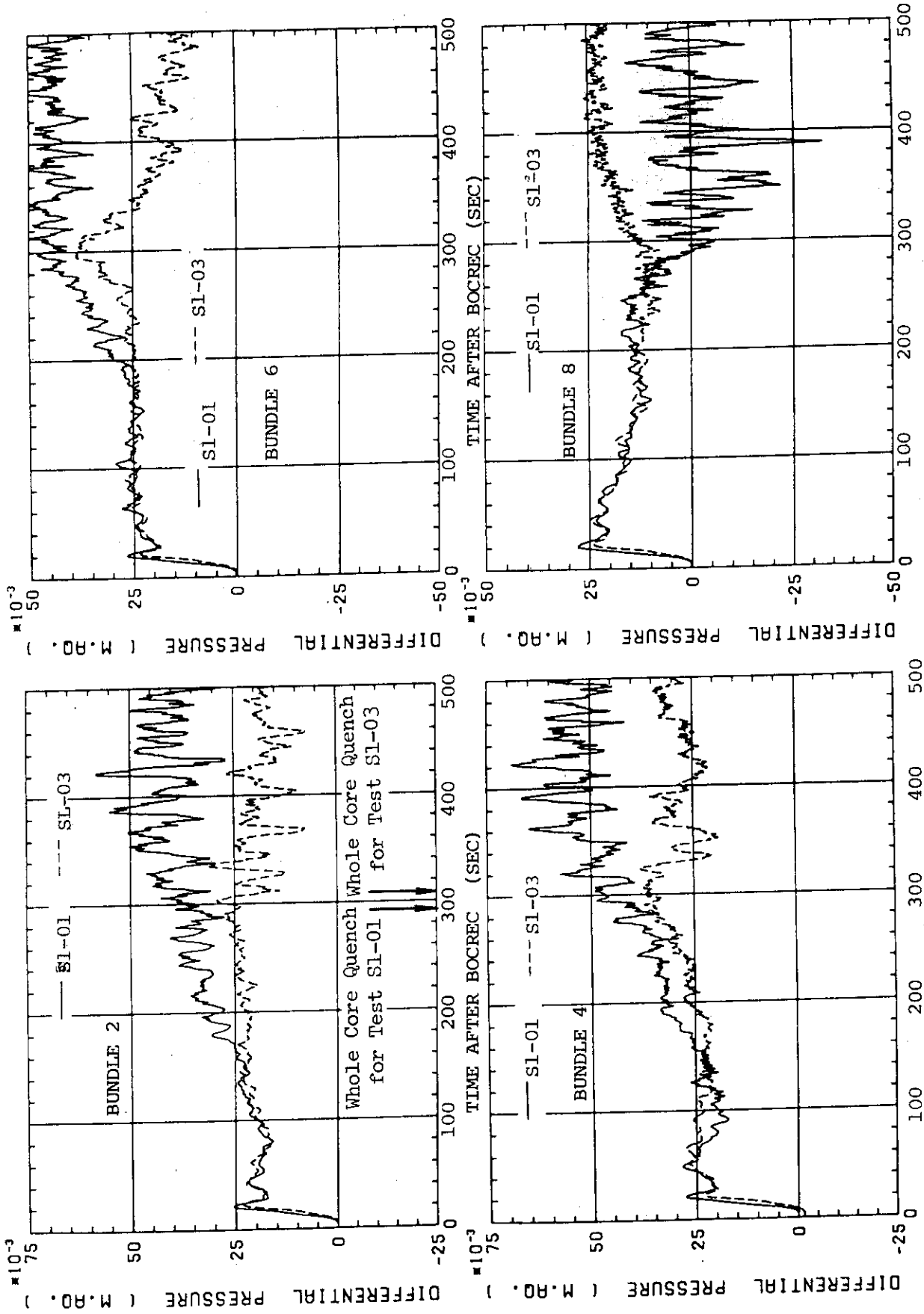

Fig.6.14 Comparison of Differential Pressure Transients across End Box Tie Plate for Tests S1-01 and S1-03 (Bundles 2, 4, 6 and 8).

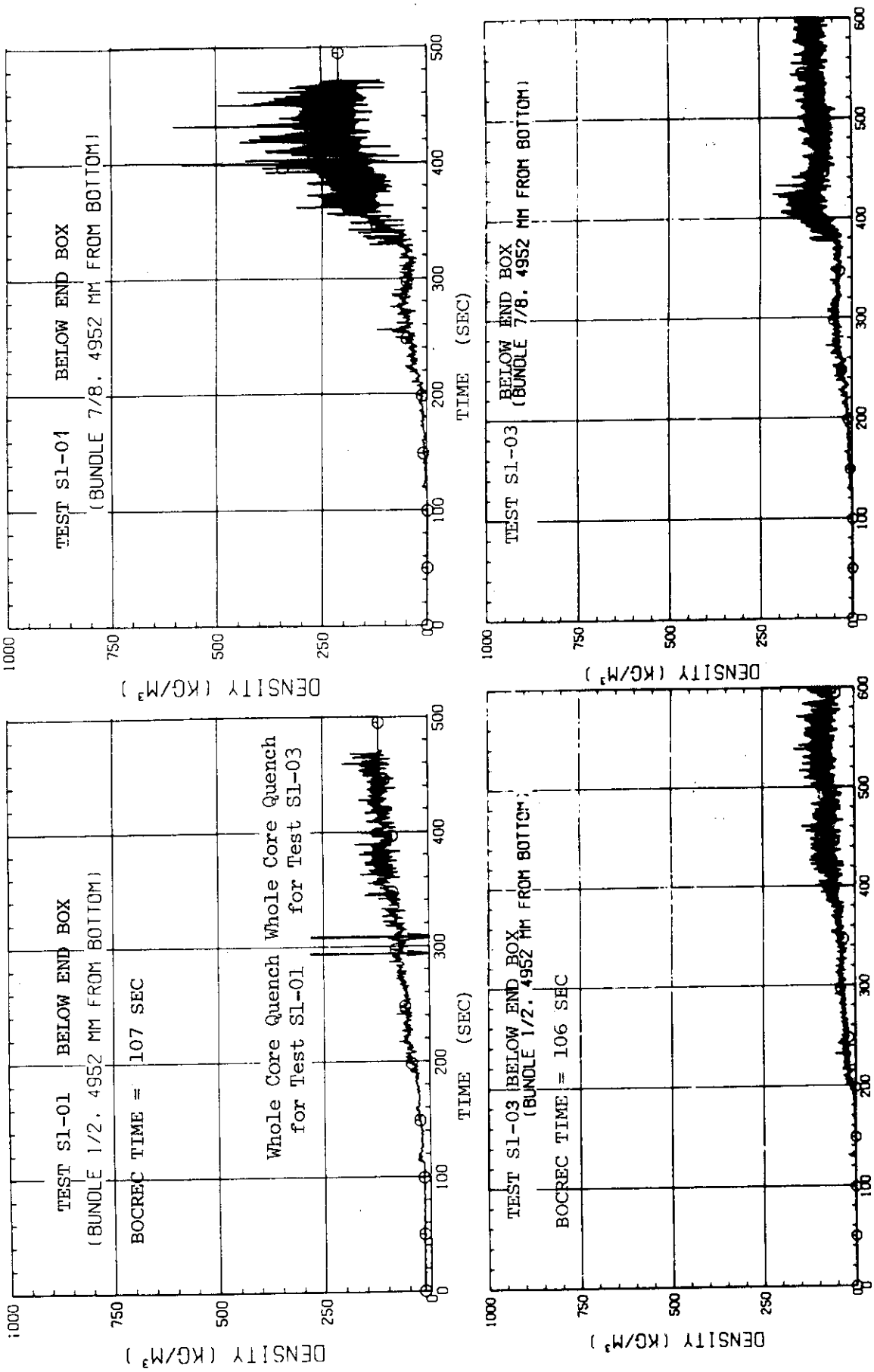

Fig.6.15 Comparison of Fluid Density Transients for Tests S1-01 and S1-03 at Elevation 4952 mm above the Bottom of the Heated Length of Heater.

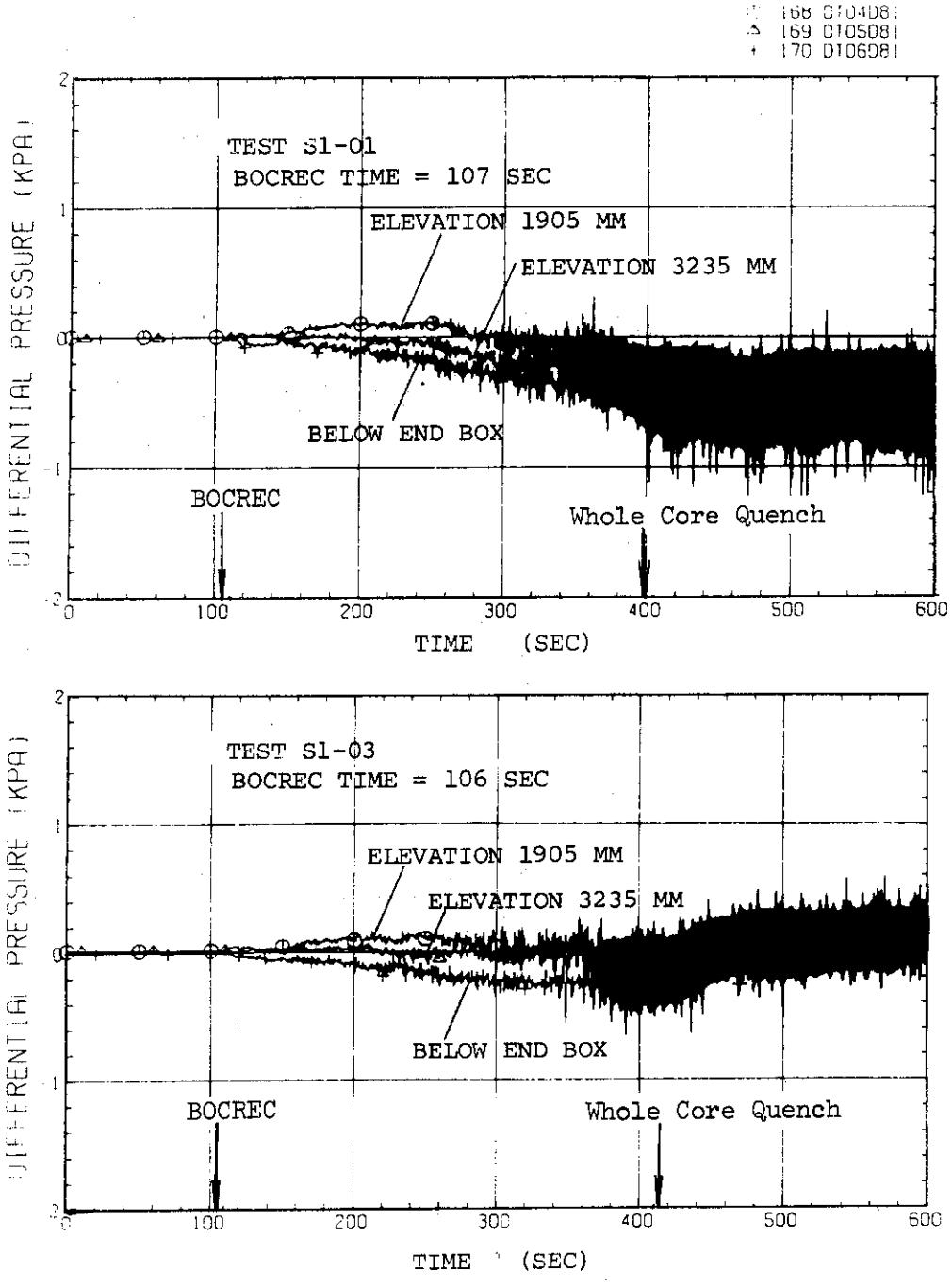

Fig.6.16 Comparison of Horizontal Differential Pressure Transients between Bundle 5 and Bundle 8, for Tests S1-01 and S1-03. (below Spacer 4, below Spacer 6 and below End Box)

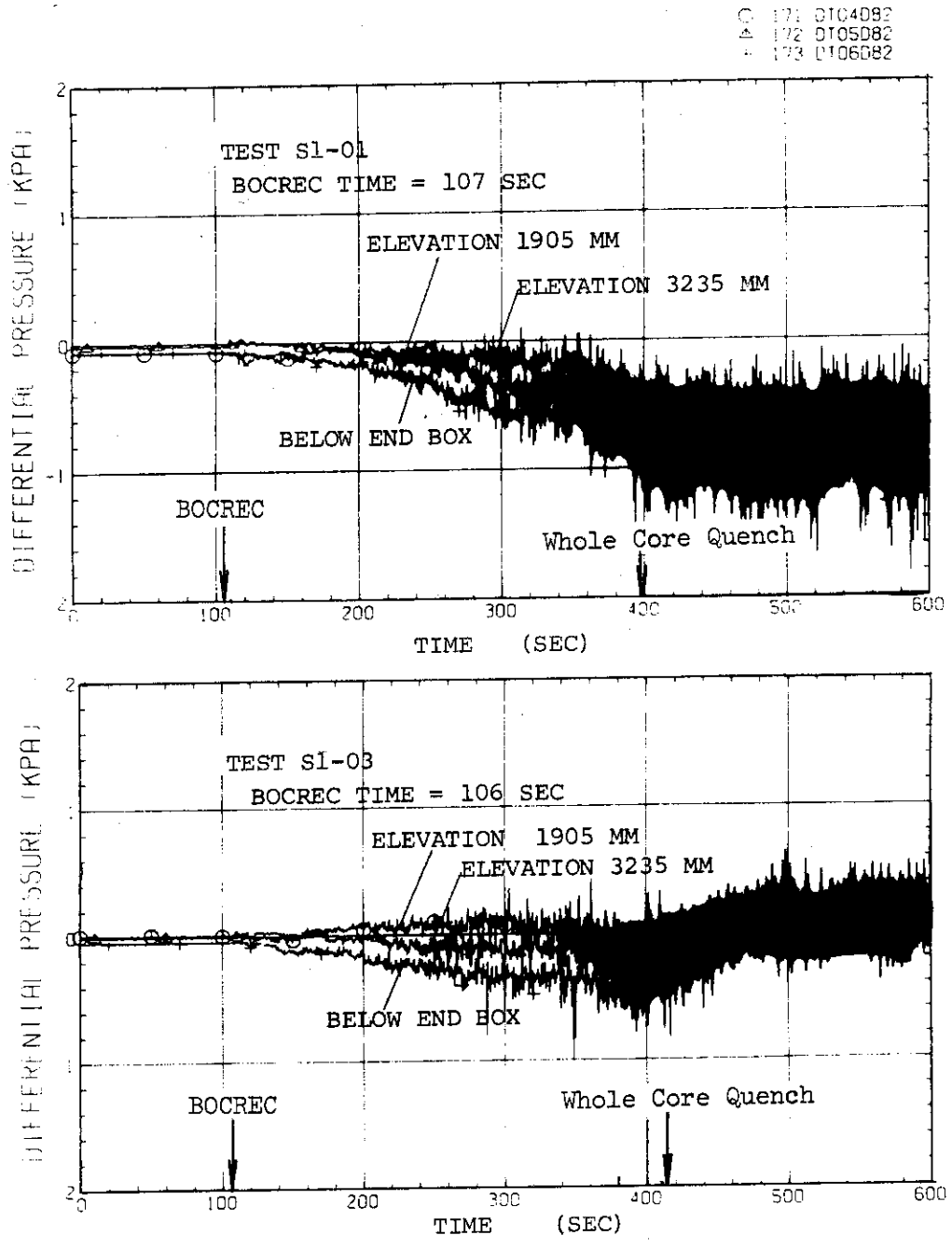

Fig.6.17 Comparison of Horizontal Pressure Transients between Bundle 1 and Bundle 8 for Tests S1-01 and S1-03 (below Spacer 4, below Spacer 6 and below End Box).

7. Conclusions

Effects of water accumulation on the upper core support plate on reflooding phenomena were investigated, comparing the data of Test S1-03 with upper plenum water extraction and those of Test S1-01 without the upper plenum water extraction. These two tests were performed under the condition of forced-feed flooding.

Major conclusions are as follows:

(1) Overall Hydrodynamic Behavior in the System

i) Carryover water flow rate through the hot leg decreases by water extraction from the bottom of the upper plenum to smaller steam velocity in the hot leg and smaller water accumulation in the upper plenum.

ii) The smaller steam velocity in the hot leg results not from the decreased steam flow rate but from the increased effective flow area due to decreased water built-up in the hot leg.

(2) Core Thermal Behavior and Heat Transfer

i) No significant effects of magnitude in water accumulation in the upper plenum on core thermal behavior can be seen in the lower and middle part of the core where quench propagates upward only.

ii) On the other hand, top quench observed in the upper part of the core is delayed due to the smaller fall back of water from the upper plenum into the core when water accumulation in the upper plenum is smaller.

iii) In the case of smaller water accumulation in the upper plenum, quench time becomes a little longer than the base case, although heat transfer coefficient is nearly the same.

(3) Two-Dimensional Hydrodynamic Behavior in Pressure Vessel

i) Water extraction from upper plenum results in not only smaller differential pressure across the core full height but also more uniform radial distribution of the differential pressure, due to smaller fall back effects of water.

ii) Radial distributions of water level on the end box tie plates, differential pressure across the end box tie plates, fluid density in the core and pressure in the core become more uniform as well as differential pressure across the core full height due to water extraction from the upper plenu. This is caused by smaller and uniform water distribution in the upper plenum suggesting that

fall back characteristics of water in the large core are different from those of the counter-current flow limitation (CCFL) observed in a pipe or a narrow rod bundle.

iii) Water extraction from the upper plenum evidently reduces or prevents from water fall back into the peripheral rod bundles of the core.

Acknowledgements

The authors are much indepted to Dr. M. Nozawa, Deputy Director General of Tokai Research Establishment, JAERI, Dr. S. Katsuragi, Director of Nuclear Safety Research Center, Dr. M. Hirata and Dr. K. Hirano, Director and Deputy Director of Department of Nuclear Safety Research, respectively, and Dr. Y. Murao, General Manager of Reactor Safety Laboratory 2, for their guidance and encouragement for this program.

The authors would like to express their appreciation to the CCTF analysis group, Messrs. T. Iguchi and J. Sugimoto, Dr. H. Akimoto and Mr. T. Ohkubo for their useful discussions, to Messrs. T. Wakabayashi and Y. Niitsuma for their contribution in the instrumentation, to Messrs. Y. Fukaya, N. Suzuki, T. Oyama, J. Matsumoto, T. Nishikizawa, K. Komori, and H. Sonobe of Safety Facility Engineering Service Section for their excellent operation of the test facility and to Mr. D. H. Miyasaki, resident engineer from USNRC, for his devoted help.

References

(1) K. Hirano and Y. Murao, Large Scale Reflood Test, J. At. Energy Soc. Japan 22, 10, 681 (in Japanese), (1980).

(2) Y. Murao, et al., REFLA-1D/MODE 1 : A Computer Program for Reflood Thermo-hydrodynamic Analysis during PWR-LOCA (Users' Manual), JAERI-M 9286 (1981).

(3) D. Liles, et al., TRAC-PD2, An Advanced Best-Estimate Computer Program for Pressurized Water Reactor Loss-of-Coolant Accident Analysis, LANL Report, LA-8709-MS, NUREG/CR-2054 (1981).

(4) Y. Murao, et al., CCTF CORE I Test Results, JAERI-M 82-073 (1982).

(5) H. Adachi, et al., SCTF CORE-I Test Results (System Pressure Effects on Reflooding Phenomena), JAERI-M 82-075 (1982).

(6) M. Osakabe and Y. Sudo, Heat Transfer Calculation of Simulated Heater Rods throughout Reflood Phase in Postulated PWR-LOCA, to be published in J. Nucl. Sci. Technol. 18, 6, (1983).

(7) M. Sobajima, Recent Development of Two-Phase Flow Instrumentation Related with Light Water Reactor Safety Research, J. At. Energy Soci. Japan 23, 11, 820 (in Japanese) (1981).

Acknowledgements

The authors are much indepted to Dr. M. Nozawa, Deputy Director General of Tokai Research Establishment, JAERI, Dr. S. Katsuragi, Director of Nuclear Safety Research Center, Dr. M. Hirata and Dr. K. Hirano, Director and Deputy Director of Department of Nuclear Safety Research, respectively, and Dr. Y. Murao, General Manager of Reactor Safety Laboratory 2, for their guidance and encouragement for this program.

The authors would like to express their appreciation to the CCTF analysis group, Messrs. T. Iguchi and J. Sugimoto, Dr. H. Akimoto and Mr. T. Ohkubo for their useful discussions, to Messrs. T. Wakabayashi and Y. Niitsuma for their contribution in the instrumentation, to Messrs. Y. Fukaya, N. Suzuki, T. Oyama, J. Matsumoto, T. Nishikizawa, K. Komori, and H. Sonobe of Safety Facility Engineering Service Section for their excellent operation of the test facility and to Mr. D. H. Miyasaki, resident engineer from USNRC, for his devoted help.

References

(1) K. Hirano and Y. Murao, Large Scale Reflood Test, J. At. Energy Soc. Japan 22, 10, 681 (in Japanese), (1980).

(2) Y. Murao, et al., REFLA-1D/MODE 1 : A Computer Program for Reflood Thermo-hydrodynamic Analysis during PWR-LOCA (Users' Manual), JAERI-M 9286 (1981).

(3) D. Liles, et al., TRAC-PD2, An Advanced Best-Estimate Computer Program for Pressurized Water Reactor Loss-of-Coolant Accident Analysis, LANL Report, LA-8709-MS, NUREG/CR-2054 (1981).

(4) Y. Murao, et al., CCTF CORE I Test Results, JAERI-M 82-073 (1982).

(5) H. Adachi, et al., SCTF CORE-I Test Results (System Pressure Effects on Reflooding Phenomena), JAERI-M 82-075 (1982).

(6) M. Osakabe and Y. Sudo, Heat Transfer Calculation of Simulated Heater Rods throughout Reflood Phase in Postulated PWR-LOCA, to be published in J. Nucl. Sci. Technol. 18, 6, (1983).

(7) M. Sobajima, Recent Development of Two-Phase Flow Instrumentation Related with Light Water Reactor Safety Research, J. At. Energy Soci. Japan 23, 11, 820 (in Japanese) (1981).

(8) L. A. Bromley, et al., Chem. Eng. Progr., 46, 5, 221 (1950).
(9) J. P. Cuningham and H. C. Yeh., Trans. ANS, 17, 369 (1973).
(10) M. Naitoh, et al., J. Nucl. Sci. Technol., 15, 11, 806 (1978).

Appendix Selected Data for Test S1-03

Table A TEMPERATURE PROFILE TABLE RUN 509

TAG-ID.	INITIAL TEMPERATURE (K-DEG)	TURNAROUND TIME (SEC)	TURNAROUND TEMPERATURE (K-DEG)	QUENCH TIME (SEC)	QUENCH TEMPERATURE (K-DEG)
TE0111C	422.2	106.5	540.3	110.5	521.4
TE0211C	455.2	109.5	707.5	138.5	597.5
TE0311C	486.1	115.5	841.6	178.0	613.4
TE0411C	511.6	116.0	909.9	225.0	596.3
TE0511C	521.7	134.5	960.1	269.0	635.0
TE0611C	520.3	135.0	976.8	286.5	657.1
TE0711C	500.8	138.0	954.1	330.0	624.3
TE0811C	488.0	129.0	872.8	366.5	563.7
TE0911C	409.9	179.0	752.4	386.5	561.2
TE1011C	394.6	126.5	552.6	127.5	551.9
TE0121C	421.9	106.0	541.7	110.5	526.6
TE0221C	451.6	109.5	718.1	139.0	605.7
TE0321C	483.6	114.0	846.3	179.5	615.7
TE0421C	509.8	119.5	922.8	233.0	586.3
TE0521C	519.1	132.0	955.3	277.0	613.4
TE0621C	520.3	140.5	988.1	295.0	640.6
TE0721C	505.2	157.5	965.4	341.0	604.7
TE0821C	497.4	147.5	893.9	377.0	563.4
TE0921C	488.9	160.0	797.6	399.0	545.9
TE1021C	432.1	139.5	597.2	246.5	506.6
TE0131C	412.8	106.5	540.9	109.0	531.0
TE0231C	435.0	109.0	698.8	135.5	606.9
TE0331C	478.0	114.0	875.4	177.5	636.9
TE0431C	510.7	123.5	928.9	234.0	587.2
TE0531C	523.2	133.5	994.9	276.0	661.2
TE0631C	520.6	134.0	1000.0	305.0	627.2
TE0731C	500.8	152.0	983.6	346.5	612.2
TE0831C	490.8	136.5	910.7	381.5	567.5
TE0931C	478.3	172.0	812.5	399.0	551.2
TE1031C	414.4	155.5	589.7	280.0	473.2
TE0141C	420.6	106.5	555.6	110.5	542.3
TE0241C	450.3	109.5	737.0	143.0	610.3
TE0341C	481.7	111.0	867.2	186.5	610.0
TE0441C	507.2	117.5	960.3	238.0	599.3
TE0541C	520.3	136.0	984.8	279.5	648.8
TE0641C	517.9	136.0	997.9	301.0	648.5
TE0741C	499.7	156.0	994.9	347.5	626.9
TE0841C	495.0	138.5	910.1	384.0	572.2
TE0941C	493.0	191.0	828.9	406.5	552.8
TE1041C	468.9	155.0	648.2	350.5	517.0

Table A TEMPERATURE PROFILE TABLE (CONT.)

TAG-ID.	INITIAL TEMPERATURE (K-DEG)	TURNAROUND TIME (SEC)	TURNAROUND TEMPERATURE (K-DEG)	QUENCH TIME (SEC)	QUENCH TEMPERATURE (K-DEG)
TE0151C	420.6	106.0	549.3	111.0	532.7
TE0251C	453.2	109.5	730.2	142.5	601.8
TE0351C	485.7	111.0	864.7	185.5	611.8
TE0451C	512.1	118.0	947.2	239.5	582.7
TE0551C	522.0	136.0	980.0	281.0	621.8
TE0651C	524.3	136.0	1003.0	295.0	654.0
TE0751C	509.8	142.0	979.3	339.5	620.5
TE0851C	504.0	141.5	914.2	378.5	566.8
TE0951C	496.7	143.5	837.7	397.5	564.6
TE1051C	463.8	137.0	631.5	294.5	501.9
TE0161C	423.2	106.0	550.3	111.0	533.2
TE0261C	458.7	109.5	736.4	140.0	600.9
TE0361C	492.9	111.5	867.1	183.0	612.4
TE0461C	512.7	116.0	947.7	233.0	582.1
TE0561C	523.1	131.0	987.1	274.0	637.1
TE0661C	525.7	136.0	1005.0	298.0	646.9
TE0761C	510.9	142.0	1006.0	346.5	622.4
TE0861C	505.7	136.5	927.1	385.5	572.7
TE0961C	498.5	142.0	831.2	407.0	559.3
TE1061C	469.5	142.5	639.9	352.5	510.3
TE0171C	422.6	106.5	536.0	109.5	527.6
TE0271C	456.5	110.0	720.5	139.0	602.6
TE0371C	491.5	111.5	837.6	181.0	604.2
TE0471C	518.0	117.5	918.7	233.5	582.9
TE0571C	525.0	134.5	914.6	272.5	598.9
TE0671C	525.0	138.5	959.5	295.5	627.9
TE0771C	507.3	137.0	939.9	339.5	601.0
TE0871C	499.5	132.5	865.2	378.0	544.5
TE0971C	482.8	159.0	770.7	398.5	545.7
TE1071C	406.2	133.0	552.0	134.5	551.4
TE0181C	415.5	106.5	525.0	107.5	524.7
TE0281C	452.4	110.5	689.2	136.0	593.6
TE0381C	484.0	114.5	815.9	177.5	604.5
TE0481C	502.4	117.5	888.7	228.5	578.9
TE0581C	512.5	135.5	933.5	269.0	615.4
TE0681C	515.1	135.0	945.8	276.5	671.1
TE0781C	494.3	148.5	939.9	321.0	644.4
TE0881C	491.8	136.0	858.7	361.0	565.7
TE0981C	488.7	142.0	773.0	381.0	583.8
TE1081C	449.9	135.5	591.5	263.0	528.4

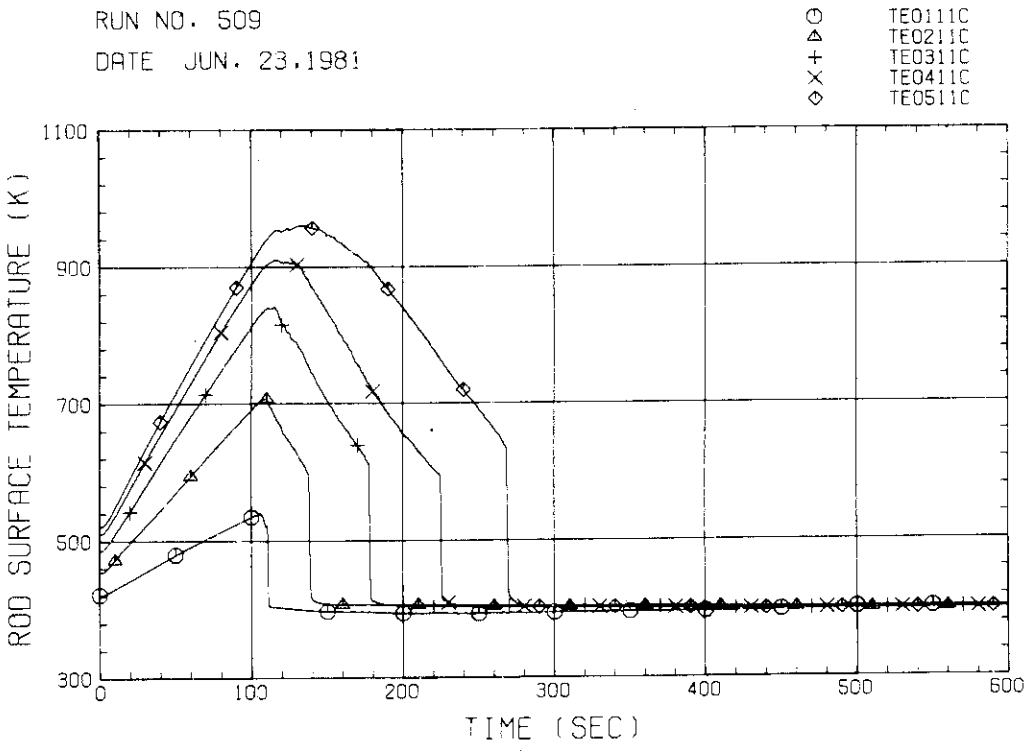

Fig.A.1 HEATER ROD TEMPERATURE
(BUNDLE 1-1C, LOWER HALF)

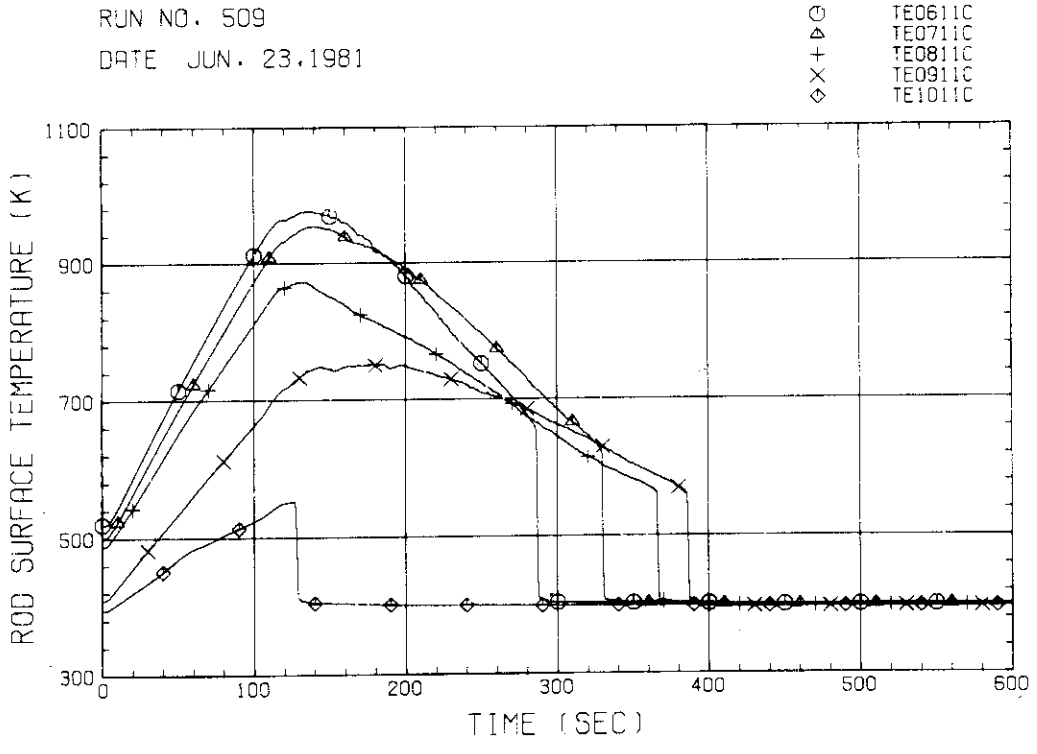

Fig.A.2 HEATER ROD TEMPERATURE
(BUNDLE 1-1C, UPPER HALF)

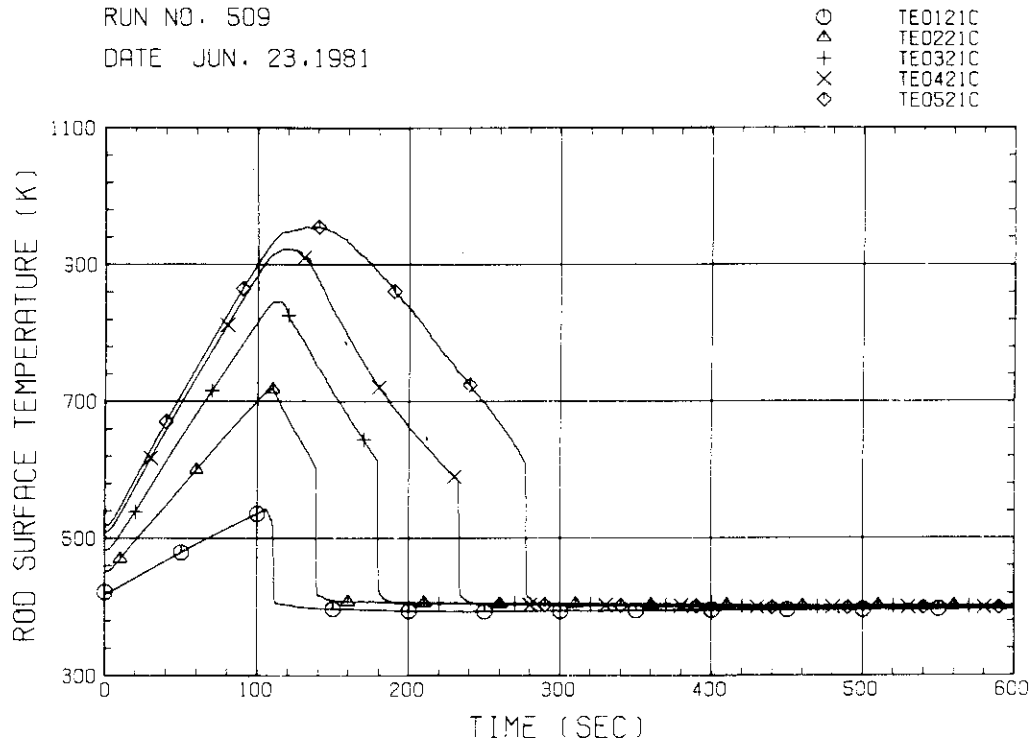

Fig.A.3 HEATER ROD TEMPERATURE (BUNDLE 2-1C, LOWER HALF)

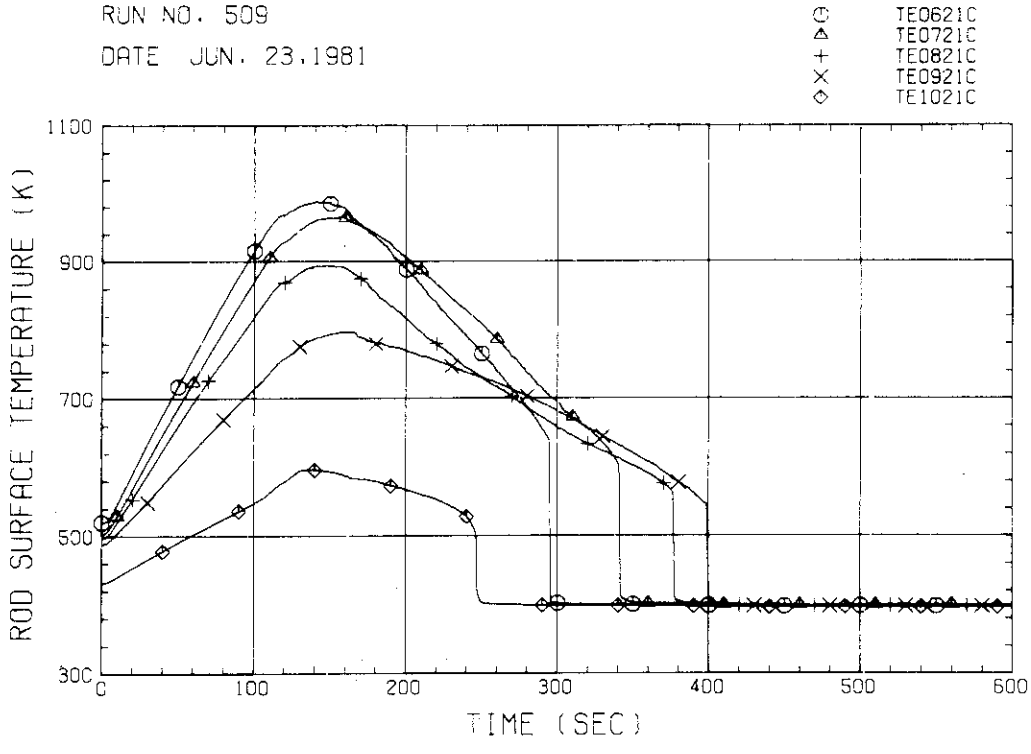

Fig.A.4 HEATER ROD TEMPERATURE (BUNDLE 2-1C, UPPER HALF)

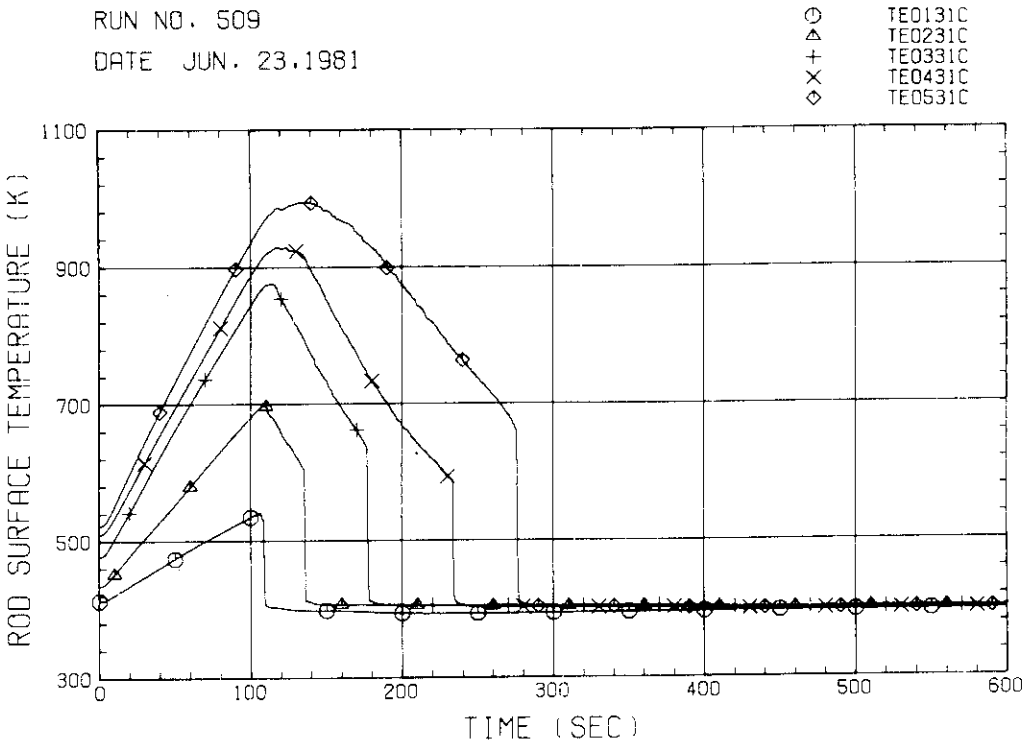

Fig.A.5 HEATER ROD TEMPERATURE (BUNDLE 3-1C, LOWER HALF)

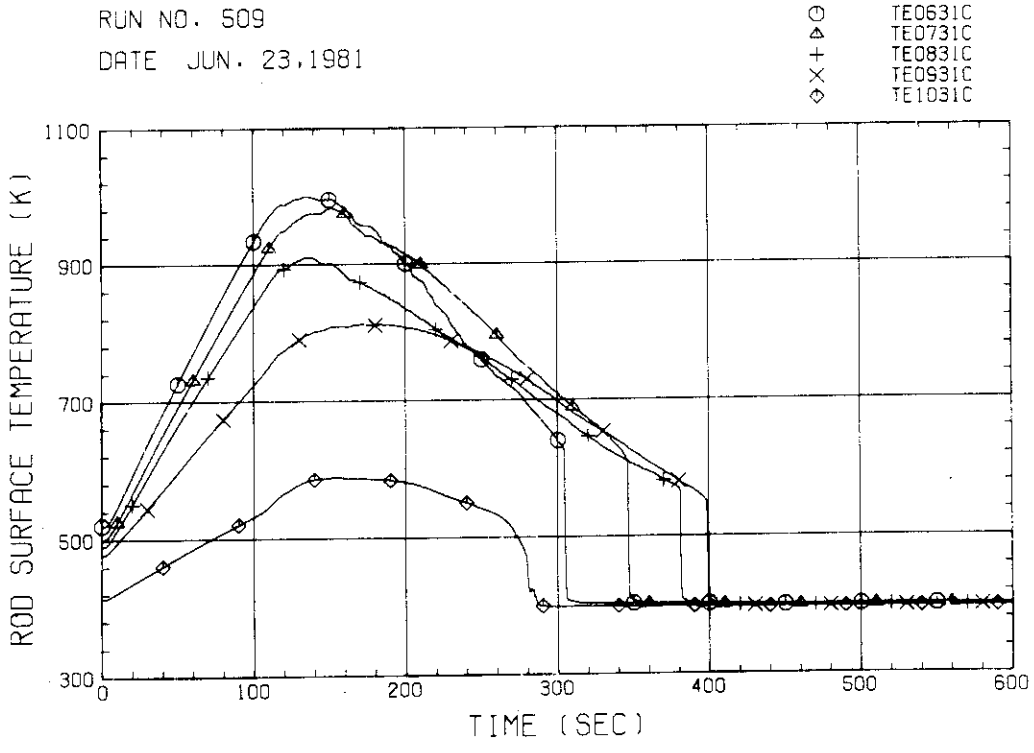

Fig.A.6 HEATER ROD TEMPERATURE (BUNDLE 3-1C, UPPER HALF)

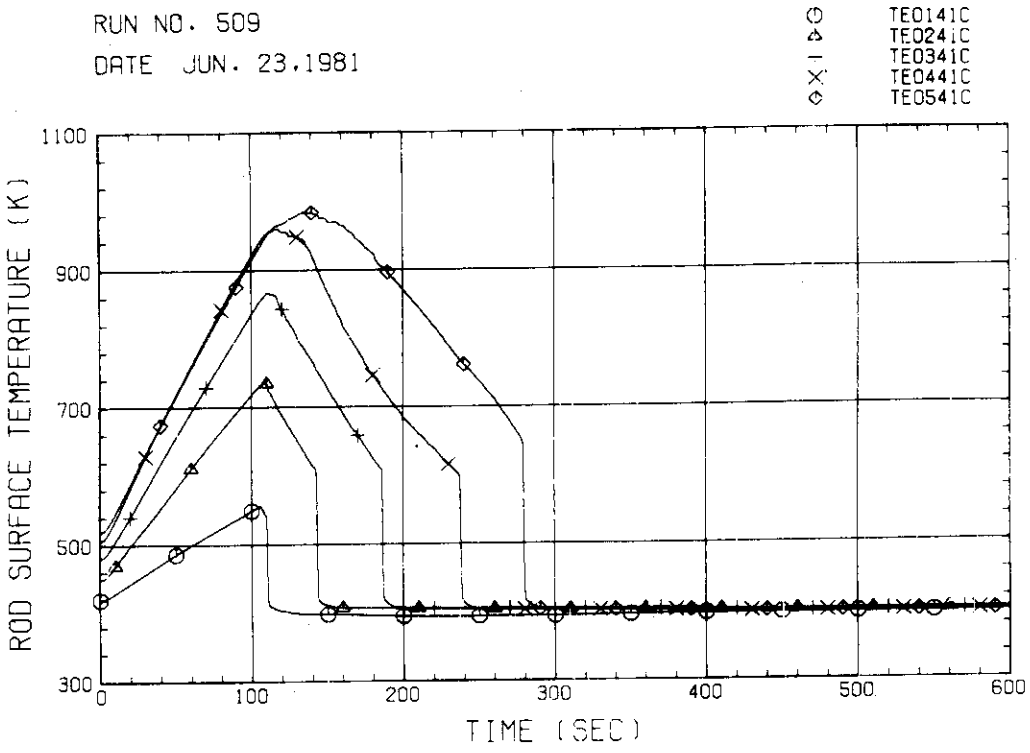

Fig.A.7 HEATER ROD TEMPERATURE (BUNDLE 4-1C, LOWER HALF)

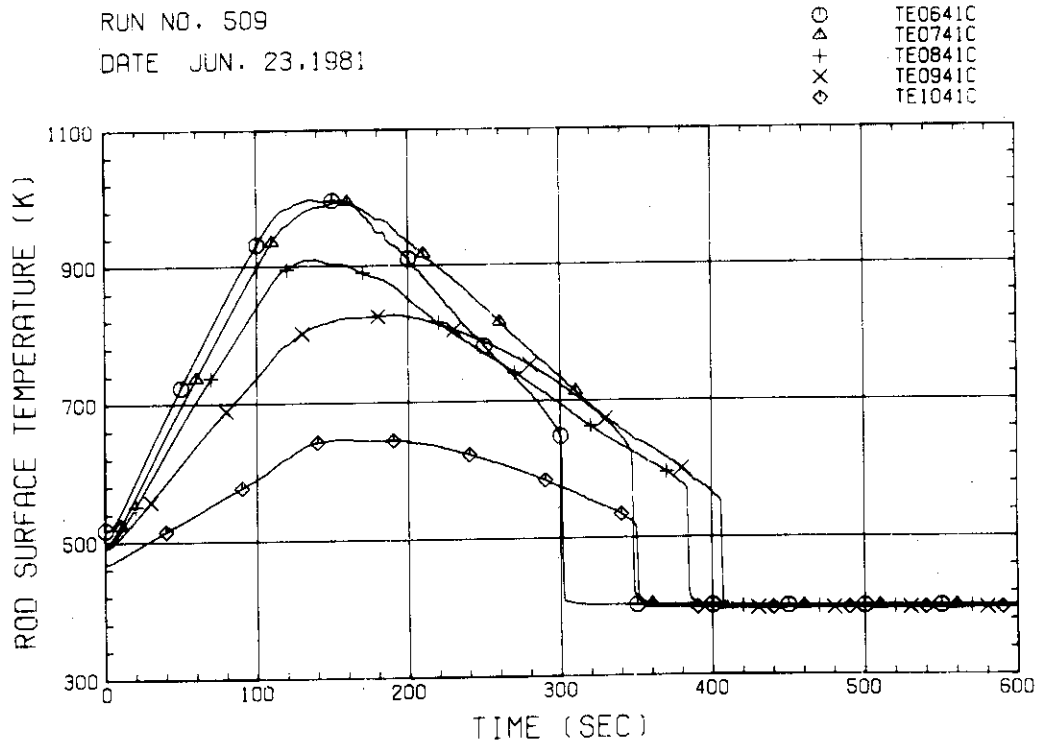

Fig.A.8 HEATER ROD TEMPERATURE (BUNDLE 4-1C, UPPER HALF)

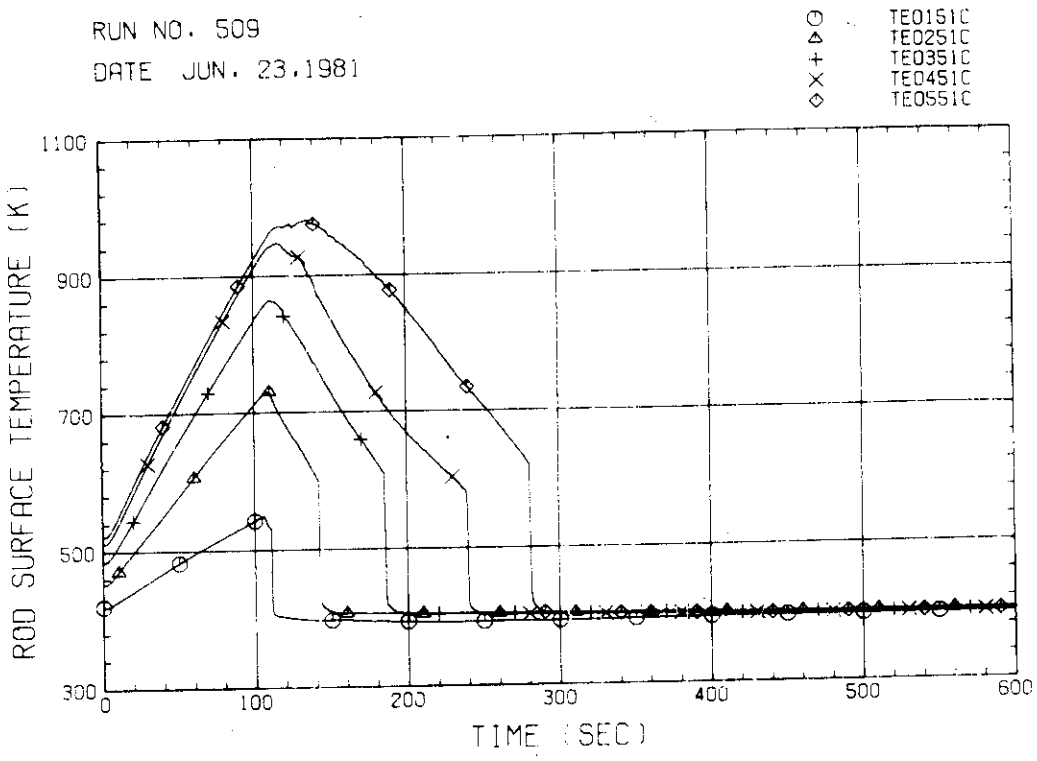

Fig.A.9 HEATER ROD TEMPERATURE (BUNDLE 5-1C, LOWER HALF)

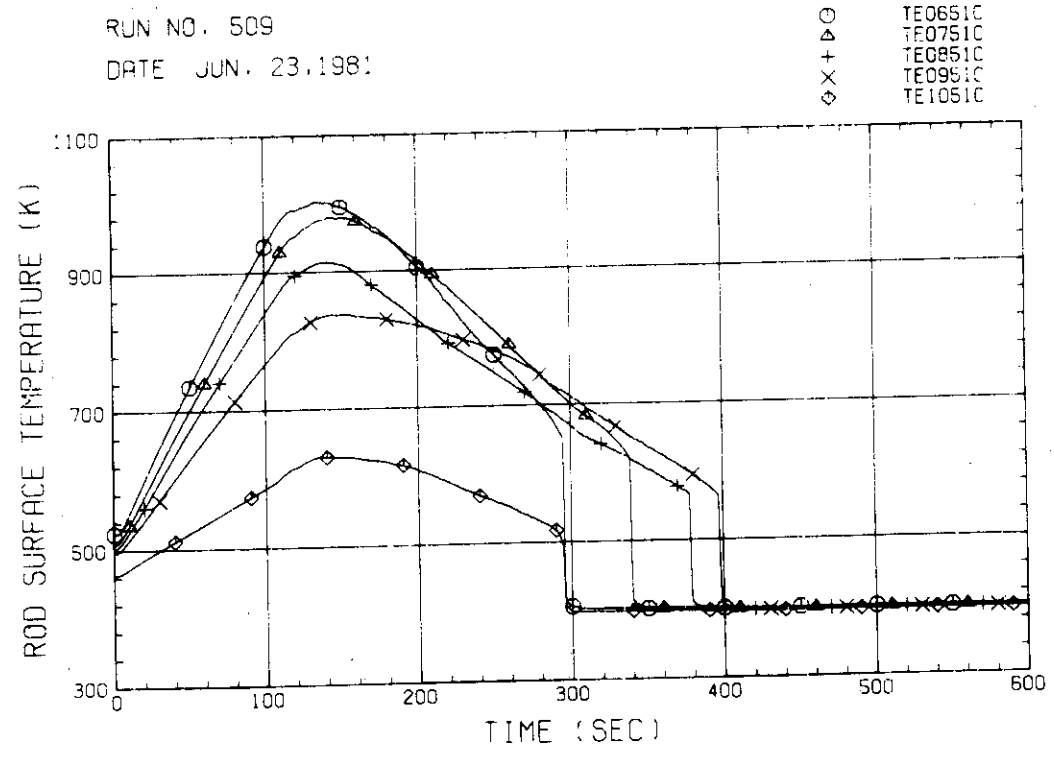

Fig.A.10 HEATER ROD TEMPERATURE (BUNDLE 5-1C, UPPER HALF)

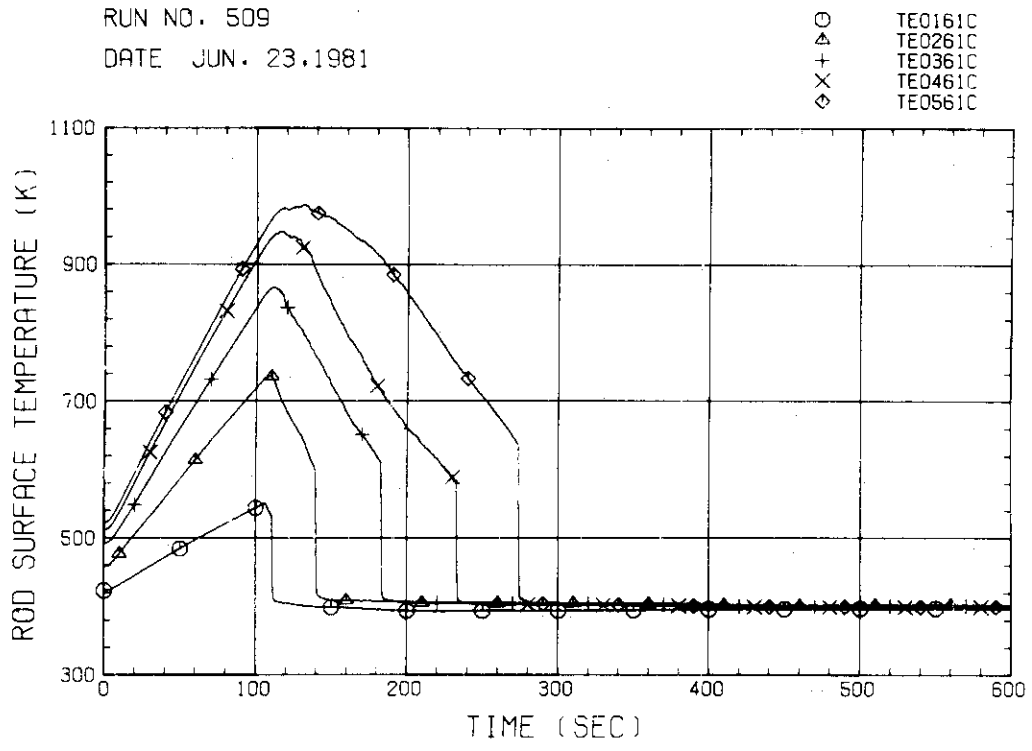

Fig.A.11 HEATER ROD TEMPERATURE (BUNDLE 6-1C, LOWER HALF)

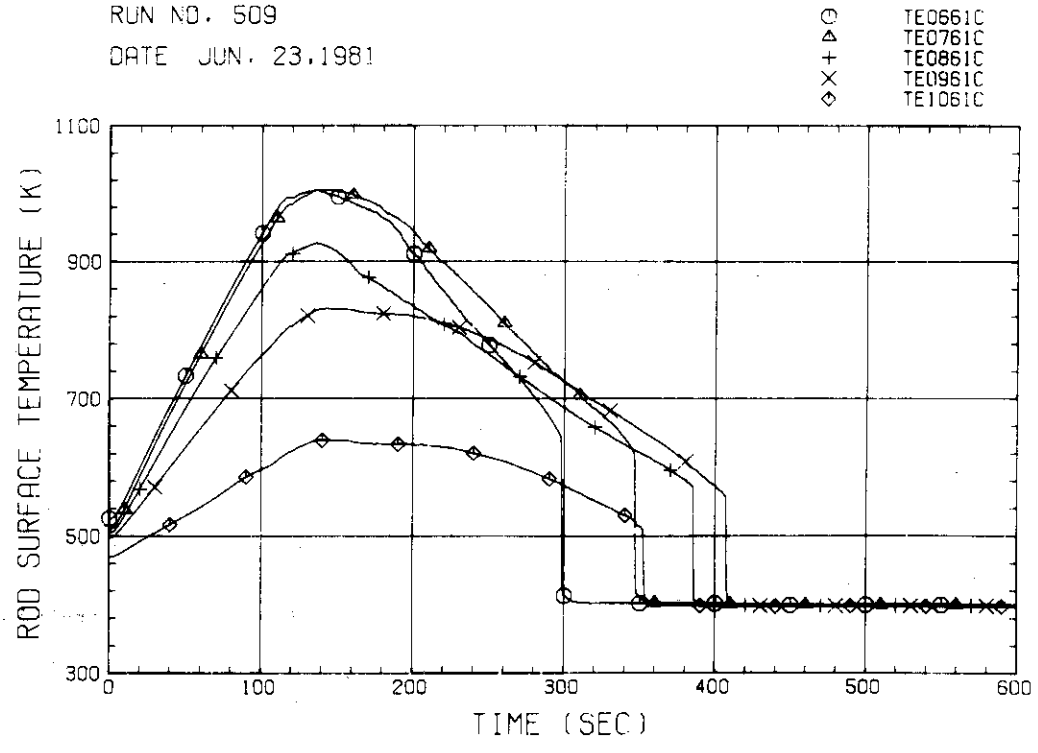

Fig.A.12 HEATER ROD TEMPERATURE (BUNDLE 6-1C, UPPER HALF)

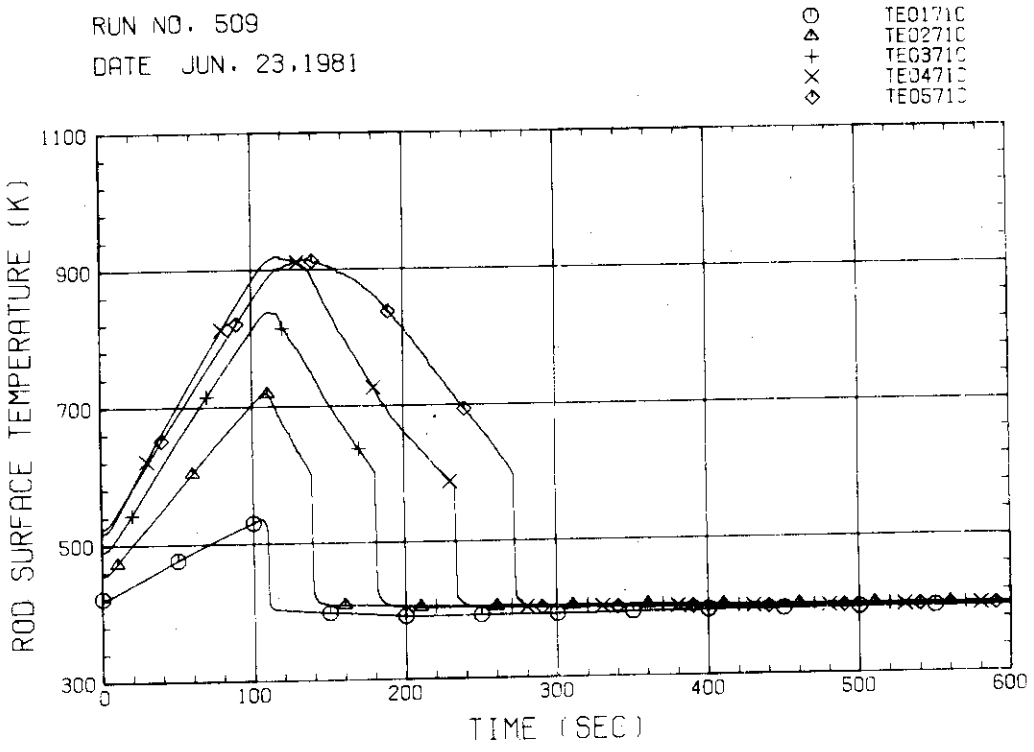

Fig.A.13 HEATER ROD TEMPERATURE (BUNDLE 7-1C, LOWER HALF)

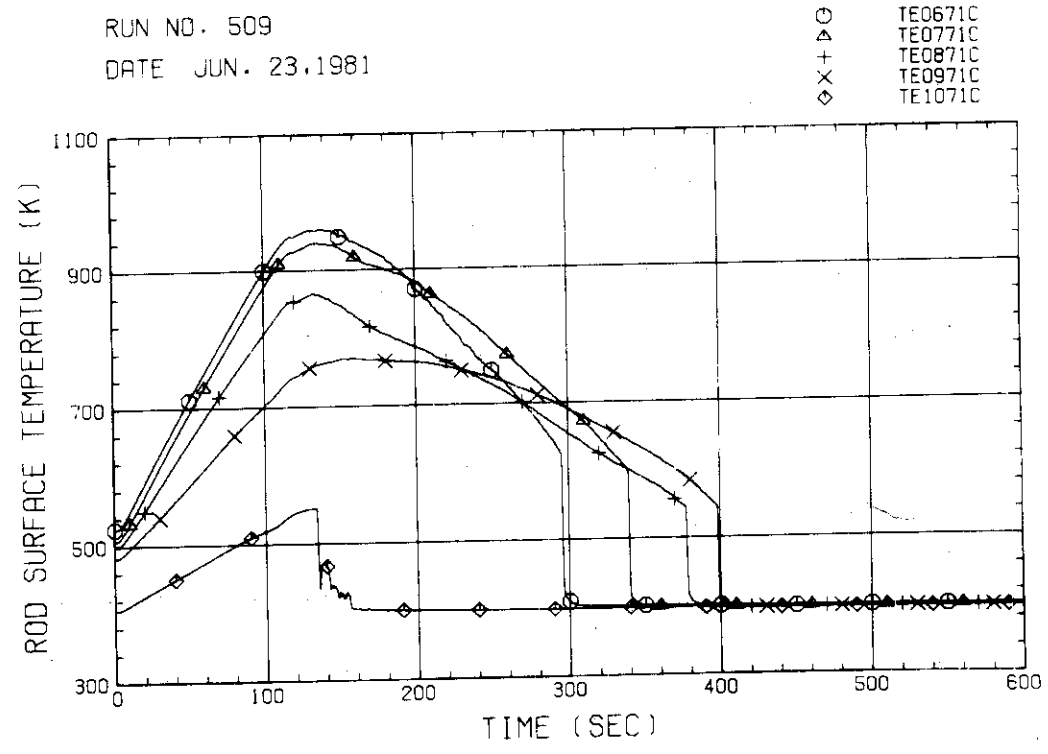

Fig.A.14 HEATER ROD TEMPERATURE (BUNDLE 7-1C, UPPER HALF)

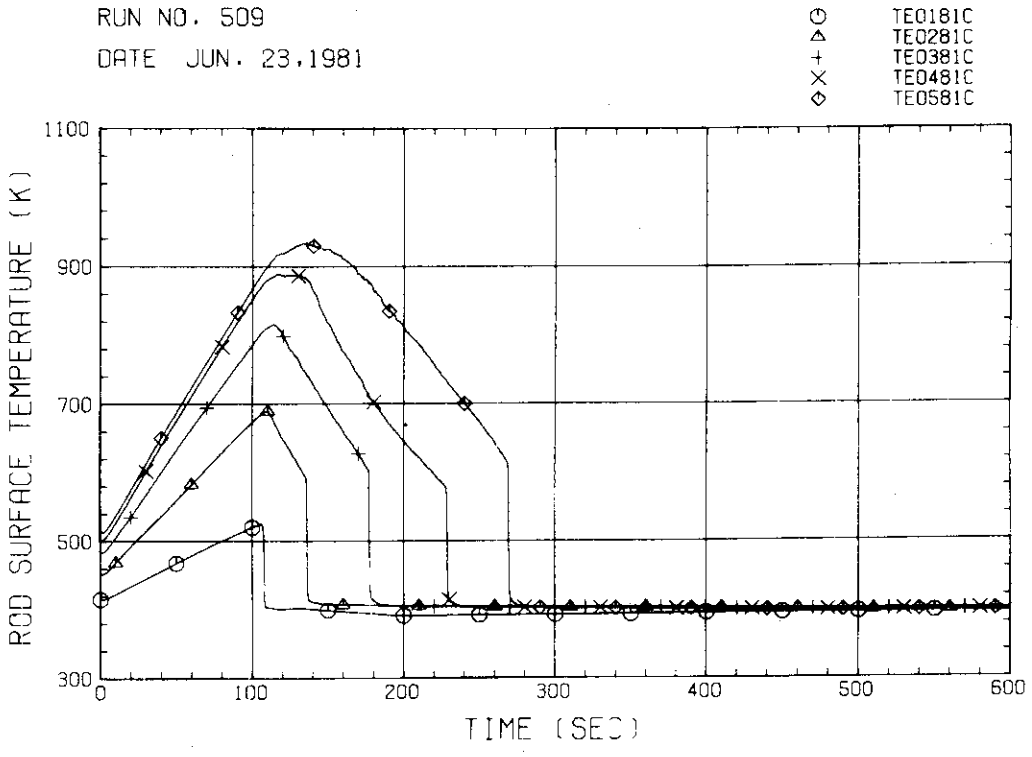

Fig.A.15 HEATER ROD TEMPERATURE
(BUNDLE 8-1C, LOWER HALF)

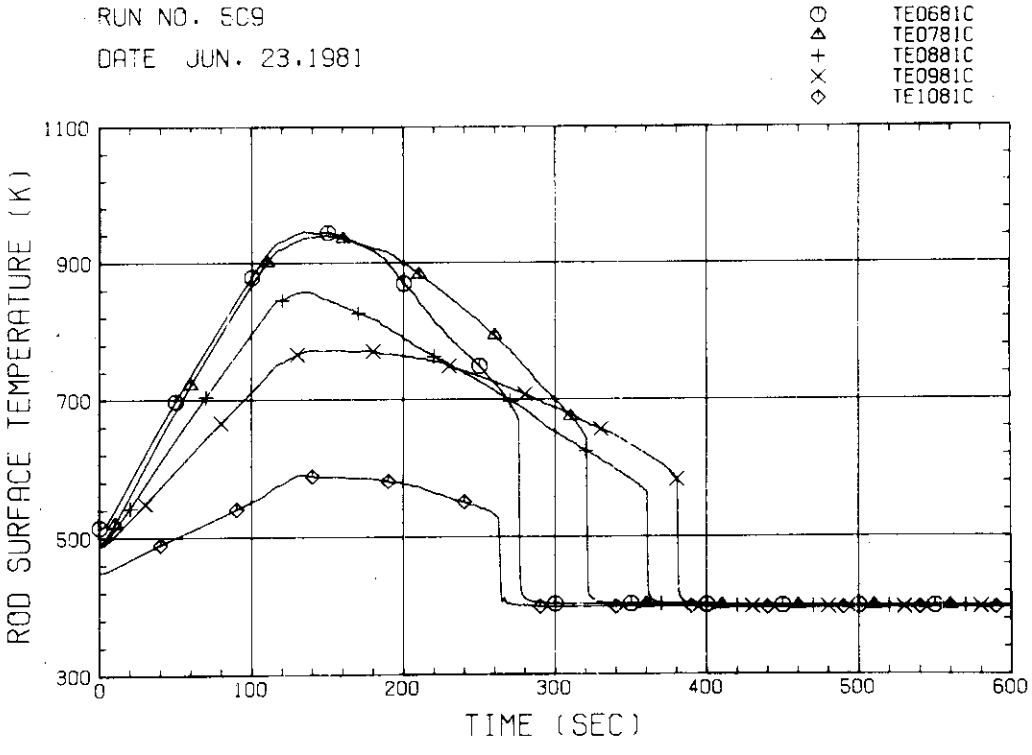

Fig.A.16 HEATER ROD TEMPERATURE
(BUNDLE 8-1C, UPPER HALF)